Nanowire photoelectrochemistry

Jiao Deng[1], Yude Su[2,§], Dong Liu[3], Peidong Yang[2,4,5,6,*], Bin Liu[3,*], Chong Liu[1,*]

[1] Department of Chemistry and Biochemistry, University of California, Los Angeles, Los Angeles, CA 90095, USA

[2] Department of Chemistry, University of California, Berkeley, Berkeley, CA 94720, USA

[3] School of Chemical and Biomedical Engineering, Nanyang Technological University, Singapore 637459, Singapore

[4] Materials Sciences Division, Lawrence Berkeley National Laboratory, Berkeley, CA 94720, USA

[5] Department of Materials Science and Engineering, University of California, Berkeley, CA 94720, USA

[6] Kavli Energy NanoScience Institute, Berkeley, CA 94720, USA

[*] To whom correspondence may be addressed. Email: pyang@berkeley.edu (P. Y.); liubin@ntu.edu.sg (B. L.); chongliu@chem.ucla.edu (C.L.).

Abstract

Recent applications of photoelectrochemistry at the semiconductor/liquid interface provide a renewable route of mimicking natural photosynthesis and yielding chemicals from sunlight, water, and air. Nanowires, defined as one-dimensional nanostructures, exhibit multiple unique features for photoelectrochemical applications and promise better performance as compared to their bulk counterparts. This review aims to provide a summary for the use of semiconductor nanowires in photoelectrochemistry. After a tutorial-type introduction of nanowires and photoelectrochemistry, the summary strives to provide answers to the following questions: 1) How can we interface semiconductor nanowires with other building blocks for enhanced photoelectrochemical responses? 2) How are nanowires utilized for photoelectrochemical half reactions? 3) What are the techniques that allow us to obtain fundamental insights of photoelectrochemistry at single-nanowire level? 4) What are the design strategies for an integrated nanosystem that mimics a closed cycle in artificial photosynthesis? We postulate that this summary will help the readers to evaluate the features of nanowires for photoelectrochemical applications. A comprehensive understanding of nanowires in photoelectrochemistry will promote the sustainable development of solar-powered chemical plants that will benefit our society in the long run.

Table of contents *Page*

1. Introduction

Energy and environmental sustainability, originated at large from the reliance of fossil fuels in our society, are two of the major challenges that our humanity is facing. The sunlight irradiating the Earth's surface provides immense energy, roughly 10^5 terawatts (TW), which far exceeds the 20~40 TW of global power consumption expected by 2050.[1-5] Therefore, efficient utilization of solar energy provides a renewable route to alleviate the energy and environmental issues associated from the extensive use of traditional fossil fuels.[1,6] However, as solar energy is intermittent,[1,2] efficient conversion and storage of solar energy is a critical component in a sustainable energy future. Since the photoelectric effect discovered by Edmond Becquerel,[7] researchers have made much progress in the capture and conversion of solar energy into valuable and important assets.[8-11] In addition to the photovoltaic (PV) effect that converts sunlight into electricity,[8,11] the photoelectrochemical (PEC) effect, the light-initiated charge separation and subsequent redox reaction at the semiconductor/liquid interface (Figure 1), provides an important pathway that directly stores solar energy in chemical bonds, particularly in the form of chemical fuels including hydrocarbons and dihydrogen.[1-3,10] PEC effect is capable to address the issue of intermittence in sunlight, facilitate the transportation of the "fixed" solar energy, and provide backup power during the supply interruption of electricity.[12] However, in order to achieve an efficient and economical solar conversion by PEC technology, a variety of factors has to be considered and optimized simultaneously: light absorption, separation and transportation of photo-generated charge carriers, carriers extraction for chemical reactions, component integration into an integrated system, as well as the cost of scalable module manufacturing. While a successful PEC-based artificial photosynthetic approach invites the participation from different disciplines, one of the concepts that introduces additional degrees of freedom in system optimization is nanomaterials and particularly a one-dimensional nanowire morphology,[13-16] thanks to the beneficial properties that have been demonstrated from recent literature.[4,15,17]

In this review, we aim to summarize the research of nanowires that utilizes PEC effects to store solar energy into chemical bonds, which was proposed as early as 2002.[18] Other important PEC-

related technologies, for example the dye-sensitized solar cells (DSSCs) that convert solar energy into electricity other than chemicals, are not discussed in detail here and alternative reviews are suggested.[19,20] Our narration starts from an introduction that includes the concept of nanowires, the principles of photoelectrochemistry, the figure-of-merits for the performance of a PEC device, and the potential benefits in PEC applications with the use of nanowires. As an efficient and effective PEC device requires the integration and optimization of multiple components, the second part of our review will focus on different strategies of interfacing semiconductor nanowires with other building blocks that may be needed in artificial photosynthesis. We propose to illustrate how the nanowire morphology can benefit the integration of multiple components in the system. These successful integrations will lead to the discussion of nanowire photoelectrodes in the third part of this review, which will be categorized based on the half reactions that are involved in a solar-to-chemical process. Such an application-oriented discussion is proposed to provide the readers a comprehensive landscape of current developments in nanowire photoelectrochemistry. The fourth part of this review will focus on the studies at single-nanowire level for PEC applications, which yields insights of photoelectrochemistry at microscopic scale. Last, we will discuss current progress of applying semiconductor nanowires to construct an integrated nanosystem for an artificial photosynthetic process. As compared to the cases that only a half-reaction is concerned, the integrated nanosystem demands a distinguishably different design principle for optimal performance, which will be illustrated in this section. Overall, we postulate that this review will help the readers to evaluate the features of nanowire photoelectrochemistry. A comprehensive understanding of nanowires in photoelectrochemistry will promote the sustainable development of solar-powered chemical plants that will benefit our society in the long run.

1.1 Concept of nanowires and nanomaterials

Nanowire is a type of nanostructure that possesses aspect ratio large than one. Since the 1990s, there have been increasing interests in investigating nanowires. A significant amount of understanding about nanowires has been obtained, thanks to their tunable physical and chemical properties.[14,21-26] Compared to their bulk counterparts, nanowires exhibit distinct characteristics

and subsequently advantages in many practical applications.[14,22,23] First, it is possible to fine-tune the radial dimensions of nanowires and render the nanowire diameters comparable or smaller than the characteristic lengths for various applications, including the wavelength of photons, the mean free path of phonons, and the diffusion lengths of photoexcited carriers.[25,27] Such a unique feature leads the observed changes of physical properties in nanowires, which have been reported in different sub-disciplines of physics and chemistry.[19,24,26] In addition, nanowire morphology possesses large surface-to-volume ratios and subsequently abundant active sites, which is beneficial for chemical reactions.[22] The large surface area also renders nanowires a suitable platform to interface with biological moieties, yielding inorganic | biological nanohybrids with functionalities unfound in the individual components.[14,22] Thanks to such favorable properties that nanowire morphology exhibits, a myriad of synthetic and fabrication techniques have been developed for the preparation of nanowires with high fidelity and targeted functionality.[21-23,28] Collectively, the concept of nanowire morphology have introduced many different applications in optoelectronics,[24,29-31] energy,[19,20,32] catalysis,[3,17,18] and biotechnology.[33-35]

1.2 Principle of photoelectrochemistry

Photoelectrochemistry is an optoelectronic effect that occurs at the interface of a semiconductor material and the liquid electrolyte (Figure 1a). Detailed information of the photoelectrochemistry per se have been discussed extensively in previous literature[8,16,36] and only general description is provided here. When a semiconductor is in contact with liquid electrolyte, the differences of Fermi levels between the semiconductor and electrolyte will lead to the band bending at the interface as well as the establishment of a built-in electric field.[8,36] Under photon irradiation, additional electron-hole pairs (e^-/h^+) are generated and spatial separation of these photo-excited carriers takes place thanks to the presence of the built-in electric field as well as the relatively high mobility of these carriers. Among these electron-hole pairs, the photoexcited minority carriers move towards the semiconductor/electrolyte interface, while the majority carriers travel through the bulk of semiconductor. A redox half-reaction that would not happen in the absence of photon irradiation is initiated, thanks to the accumulation of photo-excited minority

carriers. In the case of *n*-type semiconductor, termed as a photoanode, a upward band-bending leads to the accumulation of photo-generated holes for a oxidative half-reaction, while a downward bending occurs in a *p*-type semiconductor (a photocathode) with the accumulation of photo-generated electrons for a reductive half-reaction (Figure 1a). In practice, two sorts of configurations are possible depending on the fate of these photo-generated majority carriers: 1) a photoelectrode in which the bulk of the semiconductor is connected to an external electric circuit and the majority carriers from photoexcitation contribute to a measurable photocurrent; 2) a particulate form in which no external electric circuit is present and the majority carriers eventually transport to the semiconductor/electrolyte interface for another redox half-reaction, usually with the presence of a sacrificial chemicals termed as electron/hole scavengers. Both configurations are viable for a solar-driven chemical production with their own unique pros and cons. The particulate variant is considered to be of lower cost comparably, thanks to the simplicity in its design as well as the low operational expenditure that may incur in a photo-reactor.[37,38] On the other hand, photoelectrodes enjoy a possibly more effective charge-separation under solar irradiation, as well as the output of a photocurrent that allows for a more flexible design of the overall system. As the oxidation and reduction occur on separate electrodes in the configuration of photoelectrode, the backward reactions between the products of oxidation and reduction, termed as back reactions, are mitigated. This implies that the photoelectrode configuration may have a more straightforward design principle as only one of the half-reactions needs to be considered at a time.[38]

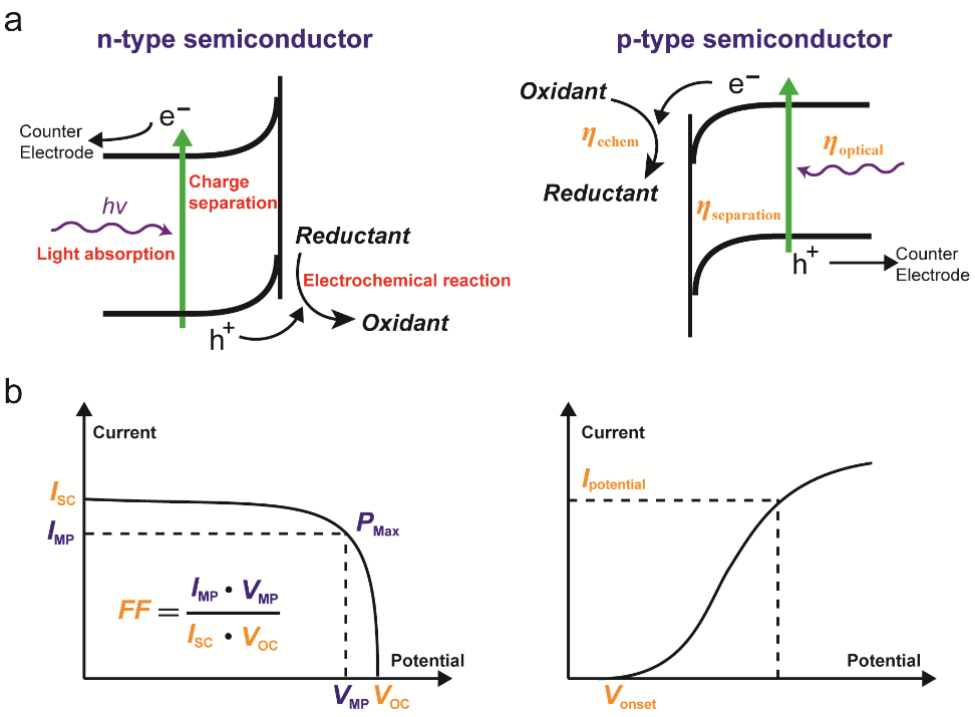

Figure 1. (a) Principles of PEC cells for both *n*-type semiconductor (left) and *p*-type semiconductor (right). The $\eta_{optical}$, $\eta_{separation}$, and η_{echem} stand for the efficiencies of light absorption, charge separation and transport to the semiconductor/electrolyte interface, and electrochemical transformation in PEC basic processes. (b) Evaluation of a PEC device. (left) the same way as a solar cell that open-circuit voltage (V_{oc}), short-circuit current (I_{sc}), and fill factor (FF) are concerned, while P_{Max}, I_{MP} and V_{MP} stand for maximum power, current at P_{Max} and voltage at P_{Max}. (right) resembling the way in traditional three-electrode electrochemistry that onset potential (V_{onset}), and current density at one given overpotential ($I_{potential}$) are typical measured parameter.

1.3 Evaluation of photoelectrochemical performance

As one important potential application of photoelectrochemistry is the solar-to-chemical conversion, specific methodologies are needed in order to evaluate the performance of a specific PEC system. Owing to the differences of device configurations that are mentioned in the previous section, two different scenarios should be considered in the context of evaluating the PEC performance.[12] In the first scenario, a single photoelectrode is poised at a certain electrochemical potential and a flux of photons is provided to the semiconductor. Light illumination leads to a measurable photocurrent, analogous as the case of a solar cell, with the simultaneous occurrence of a redox half-reaction. The performance evaluation of photoelectrode bears much similarity as

the method for solar cells, with the use of open-circuit voltage (V_{oc}), short-circuit current (I_{sc}) and fill factor (*FF*) as the figure-of-merits (left panel in Figure 1b). Additionally, two different quantum efficiencies are applied for performance evaluation: the incident photon-to-current conversion efficiency (IPCE) and the absorbed photon-to-current conversion efficiency (APCE). Here V_{oc} is defined as the voltage measured across the electrodes when there is infinite load in the circuit; I_{sc} is defined as the current measured directly across the electrodes in the absence of any load in the circuit, *FF* is defined as the ratio of maximum obtainable power to the product of the V_{oc} and I_{sc}; IPCE is defined as the number of photogenerated charge carriers contributing to the photocurrent per incident photon; APCE is defined as the number of photogenerated charge carriers contributing to the photocurrent per absorbed photon, which is termed the internal quantum efficiency. In the testing, a traditional three-electrode setup of electrochemistry is applied, and the thermodynamic potential of the proposed half-reaction is considered as the zero point of voltage when calculating the V_{oc} and I_{sc}. In practice, a few additional parameters are commonly reported in addition to the ones mentioned above. This includes the term of onset potential (V_{onset}), defined as the semi-quantitative electrochemical potential at which the "onset" of photocurrent is apparent as compared to the *I-V* characteristic in the dark. Even though V_{oc} is technically more rigorously defined, V_{onset} has gained more popularity in the study of photoelectrochemistry, as there is always some non-zero background current in the PEC testing which hardly satisfies the requirement of V_{oc}. Another important parameter that is frequently used is the current density at one given electrochemical potential ($I_{potential}$) (right panel in Figure 1b). As the solar flux from the sun is finite, it is important to report the current density that the PEC device can produce under a standardized condition, such as AM1.5 G simulated sunlight with a light intensity of 100 mW/cm^2.[12] Last, as a specific redox half-reaction is typically proposed in company with the observation of photocurrent, it is important to report the selectivity of the proposed half-reaction, termed as Faradaic efficiency (*FE*) which is defined as the percentage of total photocurrent that goes into the given product, especially when multiple possible reactions are all feasible and the information of reaction selectivity is highly demanded. In the second scenario of PEC

investigations, a complete cycle of oxidation and reduction is of interests or it is impossible to separate the PEC performance in a single half-reaction, such as the case of particulate system mentioned above. Here, the overall energy efficiency (*EE*), defined as the total Gibbs free energy gain normalized by the total energy of incident photons in the absence of any external electric energy input, should be reported in lieu of the one reported in the configuration of a photoelectrode. Specifically, when the PEC system is used for the proton reduction to produce hydrogen, the solar to hydrogen conversion efficiency (SHCE) which is defined as the ratio of the chemical energy stored in hydrogen to the solar energy input should be reported. This implies that the generation of both oxidation and reduction products should be quantified, no electric voltage is provided in the operation, and the redox potential of both oxidation and redox should be considered.

The reported performances of PEC devices are good indicators of the materials properties for the semiconductors used. For example, a typical parameter that is reported is the apparent quantum efficiency of the incident photons (η_{PEC}), which can be determined from the IPCE experiment. It has been reported : $\eta_{PEC} = \eta_{optical} \times \eta_{separation} \times \eta_{echem}$,[39] which states that the value of η_{PEC} is the product of three efficiencies that are related to different aspects of the PEC process: the efficiency of light absorption from the incident photons at a certain wavelength ($\eta_{optical}$), the efficiency of photo-excited minority carriers to have charge separation in the semiconductors and transport to the semiconductor/electrolyte interface (the charge collection efficiency, $\eta_{separation}$), as well as the efficiency of accumulated minority to perform half-reactions at the interface instead of other surface-initiated recombination events (η_{echem}). Such a relationship of η_{PEC} illustrates the intricacy of device optimization, which calls for additional degrees of freedom in developing PEC technologies for artificial photosynthesis. We postulate that the nanowire morphology is one of the possibilities that can advance artificial photosynthesis.

1.4 Potential benefits of nanowires in photoelectrochemistry

When introducing nanowire morphology to photoelectrochemistry and more generally artificial photosynthesis, one of the most critical questions is what sort of benefits that nanowire morphology can introduce as compared to its bulk counterparts. The benefits discussed here are

not just limited to the nanowire morphology. Other structures that, including nanorods,[40] nanotubes,[41] nanopillars,[42] pyramids,[43,44] and nanoholes,[45] share physical and chemical characteristics and will subsequently display similar PEC behaviors. Therefore, the above-stated benefits also apply to those nanostructures that may not be directly considered as nanowires and our discussion here is a good guide for people interested in utilizing other nanostructures for PEC applications. In addition, while aligned nanowire array with uniform and controllable morphology is a model system for understanding the fundamental principles and establishing a proof-of-concept for applications, the potential benefits of nanowire in PEC applications are not necessarily restricted to the aligned array and include configurations such as interconnected networks[46] and layered meshes.[47,48] Below we provide a list of properties of nanowires that might be beneficial, with appropriate design, to the development of artificial photosynthesis (Figure 2):

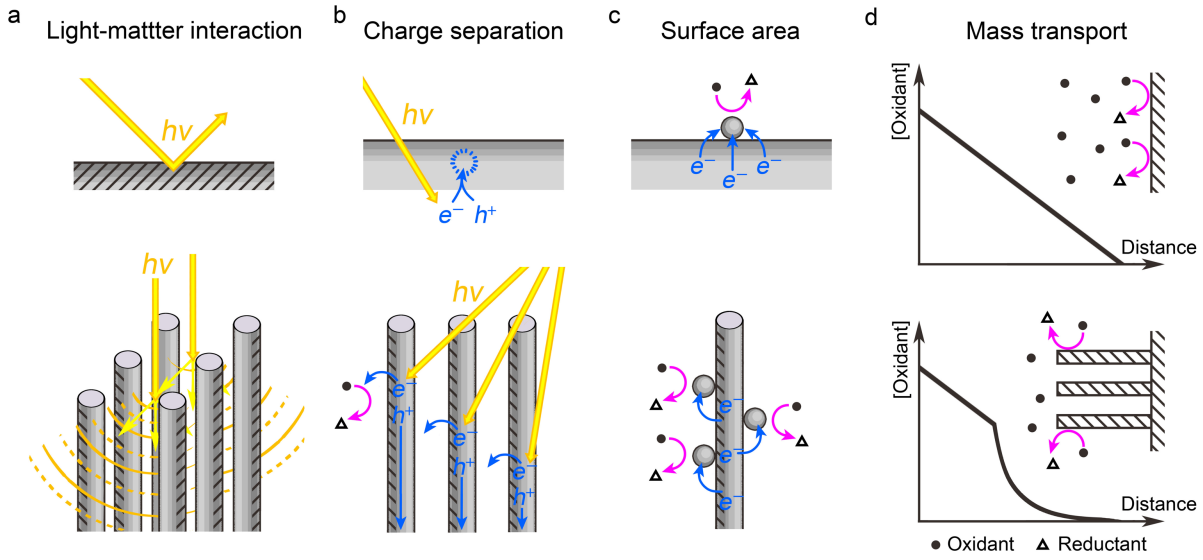

Figure 2. Merits of the nanowire geometry (bottom) for PEC in comparison to the planar counterpart (top): a) Light-trapping effect facilitates the nanowires to absorb more light than planar architectures; b) Efficient charge separation lowers the recombination of photogenerated carriers and reduces the purity requirement of materials. c) High surface area enhances the charge collection efficiency, reduces the TOF demand of electrocatalysts, and decreases the catalyst loadings. d) Control of mass transport establishes a local environment with deficient oxidants to favor several anaerobic processes.

Light-trapping for better photon absorption (Figure 2a). Nanowire, especially oriented nanowire array, is a platform that provides a gradient of refractive index at the interface between the liquid and semiconductors. This renders nanowire array remarkably suitable as an anti-reflection layer,[49,50] which suppresses reflection and enhances non-directional scattering of incident light. Such a phenomenon, dubbed as the light-trapping effect, allows nanowire to exhibit much higher equivalent absorption coefficients across a broad range of spectrum as compared to a planar architecture of semiconductors. Additionally, for crystalline nanowires, the well-faceted shape of the nanowire morphology creates unique optical modes that will further enhance the absorption of incident photons at resonance wavelengths.[51] Therefore, nanowire materials are much better light-absorbers as compared to planar or bulk materials, thanks to their favorable optical properties. Such a potential benefit will lower the cost of material preparation, especially in the case of indirect semiconductors such as silicon (Si) that demands hundreds of micrometers for appreciable absorption in the red part of the solar spectrum for a planar electrode.

Enhanced efficacy of charge separation (Figure 2b). Nanowire geometry can orthogonalize the directionality of light absorption and the process of charge separation. In typical scenarios, the incident photons are illuminated from an angle normal to the surface of semiconductor electrode or material. For a bulk material or photoelectrode, this implies that photo-generated minority carriers are required to travel the same distance as the equivalent absorption depth of the incident photons. However, for many indirect semiconductor light-absorbers that are of interest to the community, their minority carrier diffusion length and the width of band-bending region is much shorter than absorption depth of the incident photons. This will lead to significant amount of recombination of photo-excited carriers, a suboptimal value of $\eta_{\text{separation}}$ and subsequently lower energy efficiencies. In contrast, nanowires allow the photogenerated minority carriers to travel a much shorter distance to the materials/liquid interface, therefore significantly increase the value of $\eta_{\text{separation}}$.[12,52] Such a decoupling between light absorption and charge separation on nanowire materials is proposed to increase the overall quantum efficiency and energy efficiency of PEC

processes, at the same time may also increase the tolerance of impurities in the semiconductor materials.

Increased reaction turnover thanks to its large surface area (Figure 2c). A redox half-reaction at a sufficiently high rate of turnover is required at the semiconductor/electrolyte interface for an efficient solar-to-chemical process. While different reactions may have their own intrinsic reactivities, nanowire morphology provides a surface area that is much larger than its bulk or planar counterparts, thereby offers more active sites for the solar-driven reactions. The high surface area of nanowires will reduce the required overpotentials and flux density for the charge transfer of half-reactions, therefore boost η_{echem} by outcompeting the possibility of surface-associated recombination and increase the values of *FF*, V_{onset}, and the eventual energy efficiency.[40,53] One should note that such a contribution from nanowire morphology for PEC applications are distinguishably different from the cases of PV studies, since large junction area in solar cells is considered to reduce V_{oc} by diluting the photon flux, as well as reduce *FF* by introducing more surface recombination.[52,54] Moreover, nanowire of large surface area is a suitable platform to accommodate catalysts onto the semiconductor's surface and deliver additional functionality to the solar-to-chemical process. This is particularly beneficial for the use of earth-abundant building blocks, as an increased loading amount of these building blocks can help to reduce the required reactivity for the loaded catalysts and therefore help to achieve similar performance without the use of precious metals.

Controlled mass transport within the nanowire array (Figure 2d). Nanowire array electrode can be considered as a special form of porous electrodes, which has been intensively studied in the past.[55,56] One of the unique features of porous electrode is that the mass transport of redox species within the electrode is highly predictable and tunable. With inappropriate design, such an issue of mass transport can be a bane other than a blessing. Inadequate mass transport of redox-active species for the proposed half-reaction requires additional free energy as driving force thereby lowers the energy efficiency of a nanowire PEC device. However, we propose that the use of nanowire array and its controllable mass transport can also be beneficial for some specific

applications when we aim to interface semiconductor light absorbers with functional building blocks for artificial photosynthesis. One possible scenario is that the building block that the nanowire is interfacing has a restrictive requirement about the local environment. Many organometallic and microbial catalysts are highly sensitive to dioxygen (O_2), yet a practical application of artificial photosynthesis inevitably requires an oxygenic environment. It is postulated that the nanowire array indeed can provide a local O_2-free environment in air, thanks to its control of mass transport for redox active species including O_2.[34,57] Such a property allows nanowire arrays to embrace a broader range of building blocks and provide added flexibility when designing an integrated system.

Benefits for device integration. The nanowire morphology is suitable to be integrated into a functional device in the context of constructing a solar-powered chemical plant. Thanks to its large aspect ratio and the mechanical flexibility, nanowires can be readily processed through a variety of engineering techniques, including roll printing, drop casting and spin coating.[14] The rapid advance of synthetic methods for nanowires, especially low-temperature, solution-based approaches, promise a scalable production of nanowire materials with affordable cost for large-scale manufacturing, especially for the particulate configuration of photocatalysis. Moreover, as we have mentioned above, the large surface area of the nanowire morphology also invites versatile integration of nanowires with other building blocks in artificial photosynthesis. Here one specific benefit of nanowires is its capability to mimic the microscopic structure and functionality of the natural artificial photosynthetic system, which will be discussed in depth later in this review.

In a typical system of nanowires, more than one of the above listed benefits may exist for the PEC applications. We summarized recent literature and provided a survey of the benefits that are claimed by researchers, along with the materials system and the corresponding chemical reactions of interests (Table 1). As shown in Table 1, most studies focus on the first three aspects of nanowires in PEC applications. This suggests that the first three benefits discussed above are more relevant or directly applicable, while it does leave more leg rooms for future studies to exploit the under-utilized features of nanowires in PEC applications.

Table 1. Benefits of nanowire for a variety of PEC half-reactions. [a]

Nanowire	Reaction	Benefits of nanowire			
		Better photon absorption	Enhanced charge separation	Large surface area	Mass transport control
TiO_2	OER	58	59 60	60	_ [b]
ZnO	OER	–	61	–	–
α-F_2O_3	OER	62	62	–	–
α-F_2O_3/Si	OER	63	63	–	–
WO_3/$BiVO_4$	OER	64	64	–	–
Ta_3N_5	OER	65	65	65	–
Si/Ta_3N_5	OER	66	–	66	–
$BiVO_4$	Organics oxidation	–	–	67	67
$BiVO_4$	Biomass oxidation	68	68	–	–
Si	HER	69	–	69 70 71 72	–
InP	HER	42	42 73	–	–
GaP	HER	74	74	–	–
Cu_2O	HER	75	76 75	76 75	–
Si	CO_2 reduction	77 78 79	80 77 78 79	34 81 80	34
GaN	CO_2 reduction	82	82 83 84	83	–
CuO/Cu_2O	CO_2 reduction	–	85	85	–
Si	N_2 reduction	86	–	86	–
GaN	N_2 reduction	–	87	87	–
Bi_5O_7Br	N_2 reduction	41	–	41	–
CdS	N_2 reduction	88	88	–	–

[a] Numbers represent the corresponding references with benefits of nanowires are displayed. [b] Not specified in the summarized cases.

1.5 Design considerations for nanowire photoelectrochemistry

As alluded before, the above-mentioned potential benefits of nanowire morphology may not be readily translatable in the absence of a well-thought design strategy and a meticulous control of materials' properties. The development of nanowires for PEC devices requires precise design and control over a variety of materials' selection and properties.[39,52,89-91] In the following discussion we aim to provide some thoughts over the properties that need to be taken into account, commonly intertwined to each other, for the sake of maximizing the potential benefits of nanowires for PEC applications.

Overall, the nanowire dimensionality is one of the most critical factors for the whole PEC processes. First, the optical effect of light-trapping requires a careful control of the nanowire dimensionality as well as the accommodation of other optoelectronic properties for the targeted materials. It is necessary to consider the specific wavelength range that nanowires are expected to deliver their benefits, before any synthesis or fabrication work takes place.[90] It was found that absorption behavior in different light wavelength ranges can change along with the diameter variation.[92] Because of the resonant enhancement effect, Si nanowires of small diameters, usually smaller than 200 nm, exhibits strong absorption of short UV-visible light in the wavelength range of 300 nm to 500 nm. When the diameters of wires are increased up to 1400 nm, the short wavelength light absorption becomes less effective and the absorption in long wavelength light range of 500 nm to 900 nm will be enhanced.[92] The influence of length and filling ratio of Si nanowire on light absorption ability has been simulated.[93] By using longer nanowire, the absorption of long-wavelength photons was improved to alleviate the small extinction coefficients of Si at the corresponding wavelengths. With the same nanowire length, larger filling ratio shows a larger absorbance for long-wavelength near-infrared photons, while smaller filling ratio absorb more light in the UV-Vis regime.[93] Additionally, while long nanowires of small diameters may benefit light absorption, the benefits of optical absorption may promote detrimental surface recombination, which have been illustrated in detail for Si nanowires.[90] Similar trade-off is also present when we aim to maximize the value of $\eta_{\text{separation}}$ by fine-tuning the diameter and doping level in nanowires. A case study of gallium phosphide (GaP) nanowires found that the average diameter of GaP nanowire and the doping concentration of Zn had remarkable effects on the PEC performance.[91] For undoped GaP nanowire of small diameter (~25 nm), the radius of the nanowire is smaller than the width of the built-in depletion region at the semiconductor/electrolyte interface. Therefore the magnitude of band-bending was smaller than the case of bulk materials (Figure 3a), leading to lower values of measured photovoltage and photocurrent.[39,89] In comparison, GaP nanowires of larger diameter (~90 nm) with moderate concentration of Zn dopant mitigated this issue by providing a larger diameter as well as a smaller width of band bending,[89] which eventually

yielded larger values of $\eta_{separation}$ and photocurrent density.[89,91] However, excessively high concentration of Zn dopant in GaP nanowires was detrimental, as the high concentration of dopants increased recombination within the semicondcutor.[91] Similar argument was observed for Si nanowires.[89] At a lower dopant density level (N_D = 4.8 × 10^{15} cm^{-3}), photoelectrode of *n*-Si nanowire showed a similar V_{oc} but a lower light-saturated photocurrent density in comparison to planar photoelectrode (Figure 3b). At a higher dopant density level (N_D = 7.8 × 10^{17} cm^{-3}), the light-saturated photocurrent density was higher for nanowire photoelectrode, but the V_{oc} is smaller than that of the planar photoelectrode (Figure 3b). In addition, the measured quantum yield was also found to be strongly dependent on the properties of underlying Si substrate when the penetration depths of incident photons could be longer than the length of Si nanowire.[89] This illustrates the importance of appropriate experimental design in order to extract fundamental insights for nanowire-based photoelectrochemistry.

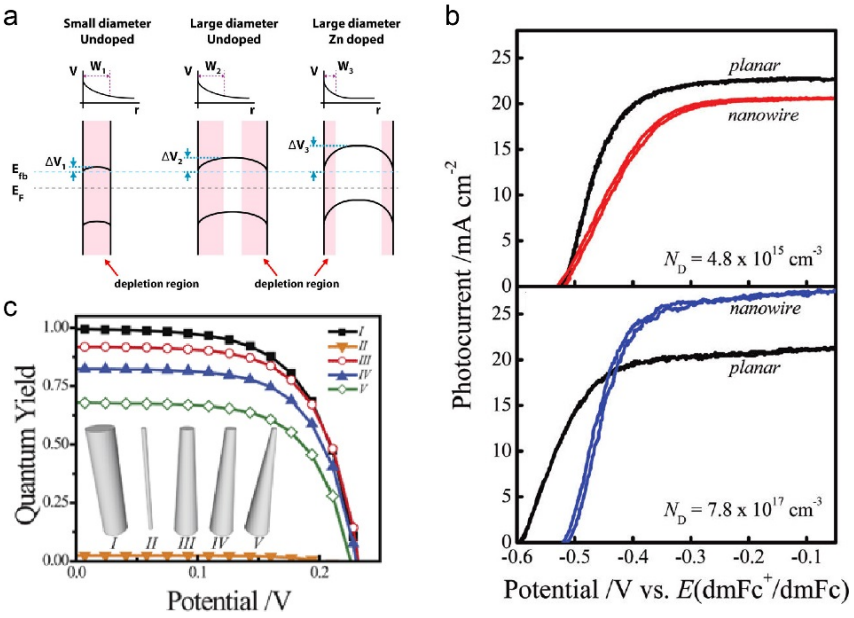

Figure 3. (a) Schematic illustration of the electrostatics of a GaP nanowire in electrolyte, exhibiting nanowire of small diameter suffers small band-bending, large diameter alleviates this issue, while it was not completely solved until Zn was introduced. Reprinted with permission from ref[91]. Copyright 2012 American Chemical Society. (b) Steady-state photocurrent-potential responses for planar and nanowire Si photoelectrodes: top) dopant density N_D = 4.8 × 10^{15} cm^{-3}, and bottom) dopant density N_D = 7.8 × 10^{17} cm^{-3}. Reprinted with permission from ref[89]. Copyright 2010 American Chemical Society. (c) Comparison of the simulated current-voltage photoresponse

under AM 1.5 (direct + circumsolar) illumination from five different high aspect ratio morphologies (*I-V*). Reprinted with permission from ref[39]. Copyright 2012 The Royal Society of Chemistry.

Interestingly, experimentally the measured performance of nanowire-based PEC process can be quite sensitive to the exact morphology of the prepared nanowires. One factor that may be less frequently considered is the diameter uniformity along the nanowires. By studying five Si photoelectrode architectures with two thin cylindrical nanowires and three tapered cylindrical nanowires, it was observed that at short-circuit condition the quantum yields of tapered nanowires is much smaller than the one of cylindrical nanowires (Figure 3c).[39] It was proposed that the deleterious charge transfer at the surface within tapered nanowires lead to the significant majority-carrier losses to give lower quantum yields.[39]

A quantitative analysis for identifying the controlling factors in nanowire PEC was conducted by a computational simulation with a focus on the charge carrier separation process.[39] The model considers a cylindrical nanowire photoelectrode under low-level injection, *i.e.* illumination levels where the concentration of only one charge carrier type changes appreciably. There are four principle processes relevant in the charge carrier recombination: in the bulk (1), in the depletion region (2), at surface traps (3), and through heterogeneous charge transfer (4). The solar energy conversion properties can be dictated by any individual, combination, or sum total of these processes in a real thin nanowire photoelectrode.[39] For properly doped thin *n*-type Si nanowire with trap states located uniformly throughout the material and minimal surface defects, the dominant recombination could happen in the bulk or the depletion region. By considering that the diffusion length (L_p) of a charge carrier is a function of both the mobility and lifetime (equation (*i*)), the open-circuit photovoltage (V_{oc}) could be estimated by equation (*ii*) when depletion region recombination is limiting. For a planar *n*-type Si photoelectrode with exact the same bulk and surface optoelectronic properties, the bulk recombination controls the V_{oc} with the analytic expression shown in equation (*iii*).[39]

$$L_p = \sqrt{\frac{k_B T}{q} \mu_p \tau_p} \; (i)$$

$$V_{\text{oc,nanowire}} = \frac{2k_B T}{q} \ln\left(\frac{J_{ph}}{q n_i Z(r_0, w) D_p / 2 r_{dr,max} L_p^2}\right) (ii)$$

$$V_{\text{oc,planar}} = \frac{k_B T}{q} \ln\left(\frac{J_{ph} L_p N_D}{q D_p n_i^2}\right) \; (iii)$$

k_B, Boltzmann's constant; T, temperature; q, unsigned charge of electron; μ_p, hole mobility; τ_p, hole lifetime; J_{ph}, photocurrent induced by illumination; n_i, intrinsic carrier concentration; $Z(r_0, w)$, effective recombination area as defined by explicit integral over the effective radius (r_0) and edge of the depletion region (w); D_p, hole diffusion constant; $r_{dr,max}$, radial position of maximum recombination rate in the depletion region; N_D, dopant concentration.[39]

In *n*-type Si nanowire, an increase in the attainable V_{oc} of 0.24 V per decade increase in L_p was predicted, but a slope of 0.06 V per decade change in L_p was obtained in planar *n*-type Si photoelectrode. A direct comparison of the V_{oc} between thin nanowire and planar photoelectrode is not rigorously applicable under all conditions even exact the same optoelectronic properties are given.[39] Such different V_{oc} also indicates the charge carrier generation in thin nanowire and planar photoelectrode is different. The charge carrier generation always occurs in or immediately adjacent to the depletion region in thin nanowire, while far away from the depletion region in planar photoelectrode. In addition, the shape of the photocurrent-potential response is very sensitive to the surface recombination velocity (S) from 1 to 10^6 cm s^{-1} for planar photoelectrode. Large values of S will lower the overall energy conversion efficiency by diminution of V_{oc}. In contrast, such features of the photoresponses for *n*-type Si nanowire shows insensitivity to the values of S.[39] Overall, the model described here provides the foundation for a quantitative evaluation of the benefits of nanowires for PEC applications as compared to its planar counterpart, when appropriate optical electronic properties of the materials are known or presumed.

Photo-stability is another important parameter when developing nanowire for PEC applications. The high surface area of nanowires relative to their bulk counterparts usually introduce abundant

surface defects as carrier trapping centers. This could lead to the pinning of surface Fermi level and a resultant band bending with a reduced photovoltage and subsequently reduced PEC efficiency.[94-96] These uncontrolled surface processes can also induce photocorrosion, a decrease of electric conductivity, and degradation of nanowire materials.[96] Coupling catalysts with nanowires will facilitate the charge transfer and a timely consumption of photo-generated carriers to help improve the photo-stability, as will be discussed in section 2.3. The passivation of the nanowire surface is another effective method to boost device efficiency and stability.[70,96-103] In the case of Si and III-V semiconductor materials, thin-film of amorphous oxide such as TiO_2 are very successful in impeding the surface corrosion while allowing the passage of high densities of photocurrents.[70,98,99,101,103] These oxide layers are also reported to increase the adhesion of the deposited metal catalysts and prevent aggregation on Si's surface.[98] Additionally, treating electrode surface with 1,2-ethanedithiol is reported to improve the separation and lifetimes of photo-excited charge carriers thanks to the suppression of surface oxygen-containing dangling bonds.[96] Advanced strategies to expand the scope of surface passivation for a broader range of semiconductor nanowires will definitely benefit the application of nanowires in PEC applications.

In general, the nanowire morphology does not automatically guarantee a better PEC performance as compared to its bulk counterparts, nor it means that we can neglect the intrinsic properties of the semiconductor materials that were utilized. In order to optimize a nanowire PEC device, the three important efficiencies discussed in section 1.3, $\eta_{optical}$, $\eta_{separation}$ and η_{echem}, must be considered and a suitable design strategy should be applied. In the rest of this review, we examine the current literature and provide additional thoughts towards an effective PEC device of nanowires.

2. Functionalized semiconductor nanowires for photoelectrochemistry

2.1 A survey of building blocks in photoelectrochemistry

To maximize the overall solar-to-energy efficiency, each step in the PEC process, including the light absorption, charge separation and transportation, and electrochemical reaction, should be

optimized.[12,39,104] A semiconductor alone usually may not possess the suitable properties for all of these steps, which calls for the integration of other building blocks in artificial photosynthesis with the use of nanowire morphology.[12,52,89] One type of the building blocks that may be needed is additional light-absorbers, often dubbed as light co-absorbers or photosensitizers, which can maximize the absorption of incident photons (Figure 4a). Wide band-gap semiconductors such as TiO_2 only absorb ultraviolet light that is only 4% of the solar spectrum, which is not sufficient for high energy efficiency.[105,106] For semiconductors of indirect band-gaps such as hematite Fe_2O_3, the nature of their low absorption coefficients posts as a major challenge for higher efficiency.[105,106] The introduction of co-absorbers will help to address the challenges mentioned above. Another type of useful building blocks are catalytic species, termed as catalysts, that will accelerate the charge transfer at the interface between semiconductors and electrolyte (Figure 4b). An efficient PEC device relies on the efficient charge transfer of the accumulated minority carriers without significant recombination.[39] Yet many of half-reactions that are of interest to artificial photosynthesis, such as water splitting or the reduction of CO_2, are multi-electron multi-proton reactions whose intrinsic reactivity may not high on the semiconductors' surface. This requires the deposition of catalysts on the semiconductors' surface to lower the kinetic barrier of electrochemical reactions and maintain a large value of η_{echem} leading to lower the efficiency of charge separation and transport to the semiconductor/electrolyte interface ($\eta_{separation}$).[107] The following sessions describe the advances in the integration of nanowires with both light-absorbers and catalysts. To assist the discussion, we provide a few tables that summarize some recent advances (Tables 2 to 5). In these tables, we not only provide the information associated with the semiconductor nanowires and loaded co-absorbers and catalysts, but also list the chemical reactions that are involved and their corresponding PEC performances.

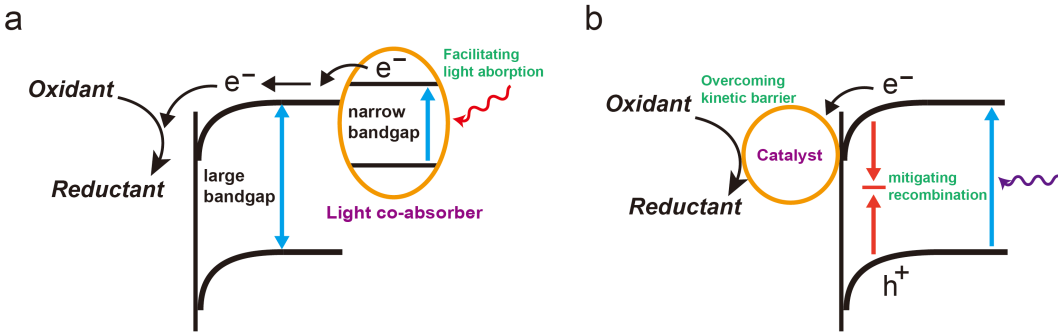

Figure 4. (a) Schematic of light co-absorber with narrow bandgap to facilitate the light absorption for benefiting the efficiency of light absorption ($\eta_{optical}$). (b) Schematic of catalyst to provide sites for trapping the photogenerated carriers and mitigating their recombination, favoring the efficiency of charge separation and transport to the semiconductor/electrolyte interface ($\eta_{separation}$). At the same time, catalyst could help to overcome the kinetic barrier, enhancing the efficiency of electrochemical transformation (η_{echem}).

2.2 Coupling nanowires with light co-absorbers

Benefiting from the unique one-dimensional (1D) structure, the light trapping ability of semiconductor nanowires can be significantly enhanced via multiple scattering. But light absorption is ultimately determined by the bandgap of semiconductor materials. Some commonly studied semiconductor materials for PEC applications, like TiO_2 and ZnO, can only absorb UV portions of the solar light. In light of this, co-absorbers are generally used to widen the light absorption spectrum in semiconductor nanowire PEC cells. Multifarious photo-responsive co-absorbers have been applied in the PEC systems, including organometallic dyes, plasmonic metal nanoparticles and narrow bandgap semiconductor nanoparticles.

2.2.1 Surface bound molecules and complexes

To fully utilize solar energy, visible light that accounts for ~50% of the entire solar photons needs to be efficiently harvested. Dye molecules can serve as the center of light absorption in visible solar spectrum. Ruthenium complex was employed as a photosensitizer in dye-sensitized solar cells in 1991.[108] Anchored onto a semiconductor, dye molecules can effectively absorb visible photons and transfer photoexcited energetic charge carriers to the semiconductor to realize efficient charge separation. Yang with their colleagues *et al.* developed the first nanowire dye-

sensitized solar cell, which not only offers fast electron transport, but also can improve quantum efficiency in the red region of the solar spectrum.[20] Dye-sensitized configuration has been recently applied in photoelectrochemical catalysis.[109-113] There are four main components in a dye-sensitized photoelectrochemical catalysis system, *i.e.* visible light absorbing sensitizer, oxidation catalyst, reduction catalyst, and semiconductor electrode. Visible-light absorbing dye molecules can be adsorbed onto surface of semiconductor and facilitate separation of photogenerated carriers to drive catalytic reactions.[111] Efficient light absorption by sensitizers requires electrode with large surface area. Table 2 summarizes the surface-bonding dye molecules as light co-absorbers in nanowire photoelectrochemical systems, for example InGaN nanowire photoelectrode could achieve a much enhanced harness of deep-visible and near-infrared solar photons via sensitization of Merocyanine-540 dye (Figure 5a).[114] The nanowire based dye-sensitized systems shall offer great potentials for photoelectrochemical catalysis.

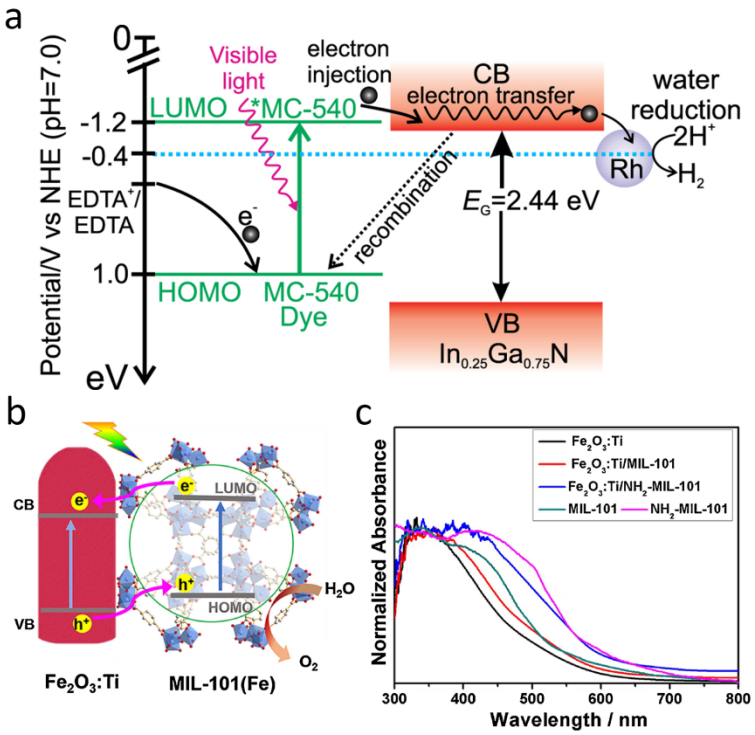

Figure 5. (a) Reaction mechanism of MC-540 dye-sensitized $In_{0.25}Ga_{0.75}N$/Rh nanowires. Reprinted with permission from ref[114]. Copyright 2015 IOP Publishing Ltd. (b) Schematic of band level positions and charge transfer path of Fe_2O_3:Ti and MIL-101(Fe) heterojunctions. (c) UV–vis

spectra of Fe_2O_3:Ti, MIL-101 and their heterojunctions. (b-c) Reprinted with the permission from ref[115]. Copyright 2018 Elsevier E.V.

Besides dye molecules, some metal-organic frameworks (MOFs) show excellent photoresponse to visible light resulting from organic ligands or metal centers. Moreover, ligand modification of MOFs could tune the gaps between highest occupied molecular orbital (HOMO) and lowest unoccupied molecular orbital (LUMO) to further change their optical properties.[116] As shown in Figure 5b and c, through ligand connection, MOFs can form heterojunction with semiconductor nanowires to promote light absorption and charge kinetics.[115] Liu *et al.* observed that photocurrent of nanowire photoanode could be improved by nearly 100% under visible light through sensitization with aminated MOFs.[116] By adjusting metal center and/or organic ligand as the light-absorbing center, various MOFs can be designed as promising photosensitizers in nanowire photoelectrochemical systems. Additionally, graphene quantum dots (QDs), in one aspect could be considered as a "molecular" photosensitizer, could be covalently bonded on the surface of nanowires via ligand modification, which are able to greatly enhance visible-light absorption of photoanodes.[117] Photosensitive polymers were also investigated as organic light absorbers and utilized in nanowire based photoelectrochemical cells.[118]

Table 2. Surface-bonding molecules as light co-absorbers in nanowire photoelectrochemical cells.

Co-absorber	Nanowire	Absorption wavelength	Reaction	Electrolyte	J (potential) [a] / IPCE [b] mA cm^{-2} / %	FE [c] %	EE [d] %	Ref.
Merocyanine-540 dye	InGaN	500-610 nm	HER	EDTA and acetonitrile	NA [e] / NA	NA	NA	114
NH_2-MIL-101 (Fe)	Fe_2O_3:Ti	365-700 nm	OER	1 M NaOH	2.27 (U_{RHE} = 1.23) / NA	NA	NA	115
NH_2-MIL-125	TiO_2	> 420 nm	OER	0.5 M Na_2SO_4	0.032 (U_{RHE} = 0.75) / NA	NA	NA	116
NH_2-Graphene QDs	ZnO	400-620 nm	OER	0.5 M Na_2SO_4	0.34 ($U_{Ag/AgCl}$ = 0.6) / ~0.5	NA	3.18	117
Polythiophene	TiO_2	300-420 nm	OER	0.5 M Na_2SO_4	0.24 ($U_{Ag/AgCl}$ = 0.6) / NA	NA	0.11	118

[a] J (potential), current density at one given potential. [b] IPCE, incident photon-to-current conversion efficiency. [c] FE, Faradaic efficiency. [d] EE, energy efficiency. [e] NA, value was not available or determinable from presented data.

2.2.2 Metal nanostructures

Plasmonic metal nanostructures show distinctive light absorption properties resulting from localized surface plasmon resonance effect. When incident photon frequency matches with the inherent frequency of collective oscillation of free electrons (on the surface of metal nanostructures) against the restoring force of positive nuclei, surface plasmon resonance is created,[119] which will give rise to intensive and highly localized electromagnetic field in metal nanostructures, manifesting as greatly enhanced light absorption at specific wavelength as shown in Figure 6a. The resonant wavelength and intensity are dependent on the nature of metal, together with the size and shape of the metal nanostructures. By manipulating composition, shape and size of plasmonic nanostructures, the plasmonic bands can be tuned from visible to near-IR region and thus it is possible to design multiple metallic nanostructures serving as light absorbers to harvest solar photons.[119] It has been demonstrated that Ag and Au nanoparticles can significantly improve light absorption and charge kinetics via plasmonic effect in nanowire PEC cells.[120-122] Following light absorption, electrons from the occupied states are stimulated above the Fermi level to transform into hot-electrons, which with adequate and suitable energies can be utilized for catalysis. Rapid hot-electron separation before charge recombination is the key to achieve high energy conversion efficiency.[123,124] Hot-electrons can be injected into semiconductors following a similar mechanism as dye sensitization. When attached to a semiconductor photoelectrode, plasmonic metal nanostructures absorb resonant photons and deliver the photo-excited electrons to the neighboring semiconductor for an increased optical response in a wide spectral range. Table 3 summarizes the metal nanostructures used as light-absorbers to improve light absorption in nanowire-based PEC systems. For example, in CdS-Au-TiO_2 sandwiched nanorod photoelectrode, Au nanoparticles act as the plasmonic photosensitizer to extend light absorption from visible to near-infrared (Figure 6b-c).[122] A roughly 30-time enhancement of reaction rate for water oxidation could be obtained after 1.0 wt% Au nanoparticles decorated on $BiFeO_3$ nanowires suspension system.[125] Despite such promising properties, current research has only witness a limited numbers of metallic plasmonic nanostructures used in PEC systems, with limited variations in composition, size and shape of the metallic nanostructures. This should be one of the aspects that should be addressed in

future research, in order to broaden the spectral response and increase the efficiency of charge separation for photo-excited hot-electrons. We posit that tuning the composition, size and shape of plasmonic nanostructures will increase the solar energy utilization efficiency in photoelectrochemistry.[119]

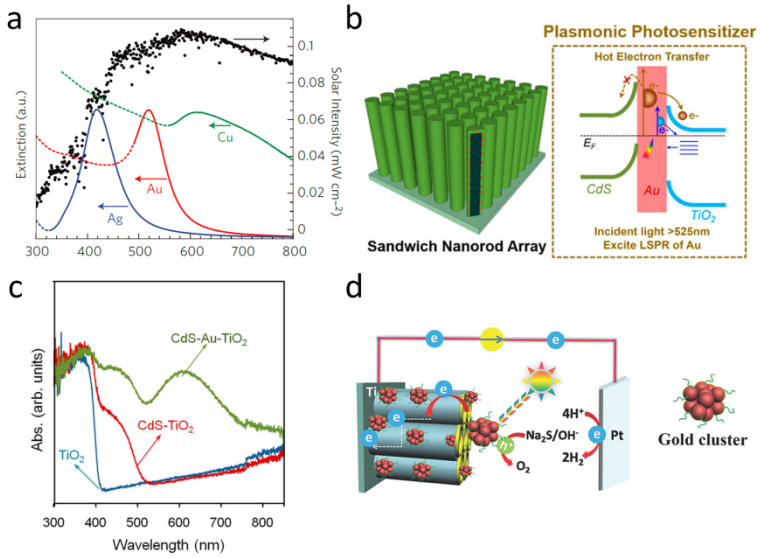

Figure 6. (a) Normalized extinction spectra of spherical Ag (38 ± 12 nm), Au (25 ± 5 nm) and Cu (133 ± 23 nm) nanoparticles and intensity of solar radiation (black dots). Reprinted with permission from ref[119]. Copyright 2011 Macmillan Publishers Limited. (b) Schematic of Au nanoparticles as plasmonic photosensitizer in CdS-Au-TiO_2 sandwiched nanorod photoelectrode. (c) UV−vis absorption spectra of CdS-TiO_2 nanorod arrays with and without Au nanoparticles. (b-c) Reproduced with permission from ref[122]. Copyright 2014 American Chemical Society. (d) Schematic illustration depicting the mechanism of Au_x sensitized photoelectrochemical cell under simulated solar light irradiation. Reproduced with permission from ref[126]. Copyright 2015 John Wiley & Sons, Inc.

Another interesting aspect of the light co-absorbers is the convergence between metallic nanostructures and molecular photosensitizer at sub-nanometer scale. When size of metal nanostructures reduces to sub-nanometers, these metal nanostructures, usually termed as metal (nano)clusters, exhibit well-defined optical responses that resembles more to the molecular photosensitizers. The properties of these nanoclusters change from metallic to semiconductive with well-defined HOMO-LUMO gaps. Serving as a photosensitizer, metal clusters can be

photoexcited under visible light illumination and thus generate electron-hole pairs. Liu *et al.* demonstrated that photogenerated electrons from Au_x clusters could be readily injected into the conduction band of TiO_2 to realize efficient charge separation (Figure 6d).[126] Metal nanocluster sensitization has already been applied in nanowire-based photoelectrochemical systems.[127]

Table 3. Metallic nanostructures as light co-absorbers in nanowire-based photoelectrochemical cells.

Co-absorber	Nanowire	Absorption wavelength	Reaction	Electrolyte	J (potential) [a] / IPCE [b] mA cm^{-2} / %	FE [c] %	EE [d] %	Ref.
Au nanoparticles	ZnO	> 420 nm	OER	0.5 M Na_2SO_4	0.3 ($U_{Ag/AgCl}$ = 1.0) / NA [e]	69	NA	[120]
$Ag@Ag_3(PO_4)_{1-x}$ nanoparticles	ZnO	300-590 nm	OER	0.5 M Na_2SO_4	3.1 (U_{Pt} = 0.6) / 60	NA	2	[121]
Au nanohole array	α-Fe_2O_3	300-675 nm	OER	1 M NaOH	~0.95 ($U_{Ag/AgCl}$ = 0.23) / 17.4	NA	NA	[62]
Au nanoparticles/ Au nanorods	TiO_2	300-800 nm	OER	1 M NaOH	NA / ~0.014	NA	NA	[128]
Au nanoparticles	Si@α-Fe_2O_3	350-1100 nm	OER	1 M NaOH / Na_3PO_4	2.60 (U_{Pt} = 0) / 12	NA	6	[129]
Ag nanoparticles	ZnO	400-800 nm	OER	0.5 M Na_2SO_4	1.8 ($U_{Ag/AgCl}$ = 0) / 3.9	NA	NA	[130]
Au interlayer	CdS	400-625 nm	Water splitting	0.2 M Na_2S/1 M Na_2SO_3	10.5 ($U_{Ag/AgCl}$ = 0) / ~30	NA	NA	[131]
Au@CdS nanoparticles	TiO_2	525-725 nm	Water splitting	0.35 M Na_2SO_3 / 0.25 M Na_2S	4.07 ($U_{Ag/AgCl}$ = 0) / 85	NA	2.8	[122]
$Ag@Ag_2S$ nanoparticles	Ti@TiO_2	300-650 nm	Water splitting	1 M NaOH	0.089 (U_{Pt} = 0.2) / NA	NA	NA	[132]
Au nanoparticles	3D ZnO	300-750 nm	OER	0.5 M Na_2SO_4	4.07 (U_{RHE} = 1) / ~5.5	NA	0.52	[133]
Ag nanoparticles	Si@PEDOT	350-875 nm	Water splitting	pH=1, H_2SO_4+ water /methanol	6.6 (U_{SCE} = 0) / 40	NA	2.86	[134]
$Au@SiO_2$ nanoparticles	Cu_2O	400-600 nm	HER	0.1 M Na_2SO_4	–29 (U_{RHE} = 0) / ~0.45	NA	NA	[135]
Au_x nanoclusters	TiO_2	200-600 nm	OER	0.1 M Na_2S	~0.15 ($U_{Ag/AgCl}$ = 0) / NA	NA	NA	[126]
Au nanoparticles	ZnO/ZnS core-shell	NA	OER	0.5 M Na_2SO_4	0.58 ($U_{Ag/AgCl}$ = 1) / NA	NA	0.21	[136]
Au_3Cu nanoparticles	Silicon	NA	CO_2 reduction	0.1 M $KHCO_3$	2.2 (U_{RHE} = –0.2) / NA	80	NA	[81]
Cu nanoparticles	GaN	NA	CO_2 reduction	0.5 M $KHCO_3$	44.9 ($U_{Ag/AgCl}$ = –1.5) / NA	19	NA	[137]

Ag nanoparticles	ZnO/CdS core-shell	375-550 nm	OER	0.25 M Na_2S / 0.35 M Na_2SO_3	~4 (U_{SCE} = 0) / ~22	NA	3.13	[138]
Au nanoparticles	ZnO/Al_2O_3 core-shell	NA	OER	0.5 M Na_2SO_4	0.512 ($U_{Ag/AgCl}$ = 1) / NA	NA	0.67	[139]
Au nanoparticles	3D TiO_2	400-700 nm	OER	1 M NaOH	2.69 (U_{SCE} = 0) / NA	NA	NA	[140]
Au_x nanoclusters	ZnO	300-450 nm	OER	0.5 M Na_2SO_4	~0.8 (U_{RHE} = 1.2) / NA	NA	NA	[127]
Au nanoparticles	$BiVO_4$/ZnO	400-550 nm	OER	pH=7.2, 0.5 M PBS	2.87 (U_{RHE} = 1.23) / 40	NA	NA	[141]
Au nanostars	TiO_2	400-800 nm	OER	1 M NaOH	0.95 (U_{NHE} = 1) / 0.4	NA	NA	[142]
Ni nanoparticles	H-TiO_2	300-500 nm	OER	1 M KOH	0.165 ($U_{Ag/AgCl}$ = 0.23) / 7.5	NA	NA	[143]
Ag nanoparticles	$NaNbO_3$	NA	OER	0.5 M NaOH	3.54 ($U_{Ag/AgCl}$ = 0.9) / NA	NA	NA	[144]
Au@SiO_2 nanoparticles	α-Fe_2O_3	NA	OER	0.5 M Na_2SO_4	~0.1 (U_{RHE} = 0.8) / ~0.03	NA	NA	[145]

[a] J (potential), current density at one given potential. [b] IPCE, incident photon-to-current conversion efficiency. [c] FE, Faradaic efficiency. [d] EE, energy efficiency. [e] NA, value was not available or determinable from presented data.

2.2.3 Semiconductor nanoparticles

Semiconductor-semiconductor junction offers another class of hybrid structures to enhance light absorption. Since the discovery of photosensitization effect in TiO_2 electrode during water electrolysis, the research of hybrid semiconductor systems for photo(electro)catalysis has made tremendous progresses.[38,146,147] In order to remedy the limited light absorption of single semiconductor material in photoelectrochemistry, semiconductor heterojunctions are constructed. Semiconductor-semiconductor junctions can be used to extend the light absorption range and at the same time improve the efficacy of electron-hole separation for the photo-generated carriers.[148] In virtue of the high aspect ratio of nanowires, semiconductor nanoparticles can be easily deposited on the surface of nanowires. Owing to their differences in the flat-band potentials and band structures, a variety of models for the band alignments with different terminologies, such as semiconductor sensitization, Type II, phase junction, and Z-scheme, can be established when semiconductor nanoparticles are interfaced with semiconductor nanowires.[148] If both semiconductor components are photo-excitable, semiconductor nanoparticles with suitable energy band can form favorable band alignments with the nanowires. Such a configuration can effectively broaden the spectral response of light absorption and promote charge separation. One example that

illustrates the above concept is the decoration of $ZnFe_2O_4$ (ZFO) nanoparticles on ZnO/CdS nanorods (Figure 7a-b).[149] Here the favorable band alignment among these semiconductors leads to effective light absorption as well as efficient charge separation, which provides a much higher photocurrent density under simulated sunlight. Additional examples for the use of semiconductor nanostructures as light absorbers in nanowire PEC systems can be found in Table 4.

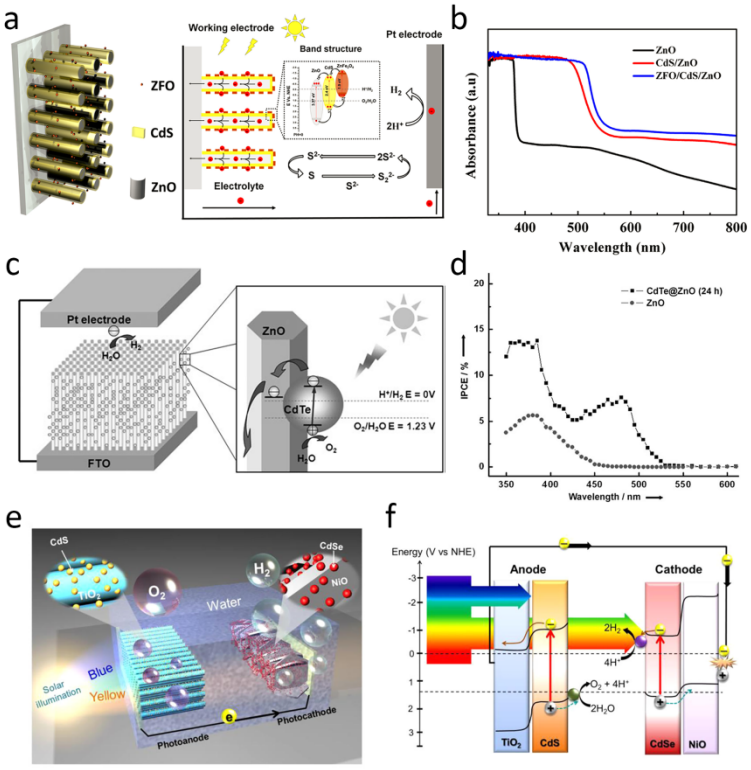

Figure 7. (a) Schematic of the ZFO/CdS/ZnO nanorod array photoanode. (b) UV–vis diffuse reflectance spectra of ZFO/CdS/ZnO photoanodes. (a-b) Reproduced with permission from ref[149]. Copyright 2016 Elsevier Ltd. (c) Schematic of ZnO nanowires decorated with CdTe QDs and the corresponding charge-transfer pathway. (d) IPCE spectra of pristine ZnO nanowire photoelectrode and CdTe QDs sensitized ZnO nanowire photoelectrode in the wavelength region of 350–600 nm at a potential of 0 V versus Ag/AgCl. (c-d) Reproduced with permission from ref[61]. Copyright 2010 John Wiley & Sons, Inc. (e) Cadmium chalcogenide QDs modified photoelectrolysis cell system constructed with CdS QDs-TiO_2 nanorod photoanode and CdSe QDs-NiO nanosheet photocathode. (f) Energy band diagram of the QDs sensitized unassisted photoelectrolysis cell. (e-f) Reproduced with permission from ref[150]. Copyright 2014 American Chemical Society.

On the other hand, when only one of the semiconductors in the PEC system is photo-excitable, photo-generated charge carriers may transfer to the unexcited semiconductor via a sensitization process. Chalcogenide semiconductor QDs possess tunable optical properties over a wide spectrum resulting from the quantum confinement effect, making these QDs promising for solar light harvesting.[151] For example, Chen *et al.* reported that CdS and CdSe QDs, acting like dye sensitizers, could be stimulated to generate electron-hole pairs under light irradiation as shown in Figure 7c.[61] Here photogenerated electrons could transfer to the conduction band of adjacent semiconductor nanowires for an enhanced efficiency of solar-driven catalysis such as water-splitting (Figure 7e-f).[61,150] Mi *et al.* reported that GaN nanowires loaded with doped InGaN segments can proceed efficient CO_2 reduction and water splitting reactions under solar illumination.[152,153] Here one additional benefits is the tunable band-gap of the loaded InGaN based on different synthetic recipes, which can absorb photons from the whole solar spectrum if needed.

Table 4. Semiconductor nanoparticles as light co-absorbers in nanowire photoelectrochemical cells.

Co-absorber	Nanowire	Absorption wavelength	Reaction	Electrolyte	J (potential) [a] / IPCE [b] mA cm^{-2} / %	FE [c] %	EE [d] %	Ref.
CdTe QDs	ZnO	350-550 nm	OER	0.5 M Na_2SO_4	2 ($U_{Ag/AgCl}$ = 1) / NA [e]	NA	1.83	61
CdS QDs/CdSe QDs	ZnO	310-650 nm	HER	0.25 M Na_2S / 0.35 M Na_2SO_3	12 ($U_{Ag/AgCl}$ = 0.4) / 45	NA	NA	154
CdSe QDs	TiO_2	350-600 nm	HER	0.25 M Na_2S / 0.35 M Na_2SO_3	2.75 ($U_{Ag/AgCl}$ = –0.4) / 6	NA	NA	151
CdS QDs	TiO_2	375-600 nm	OER	1 M Na_2S	5.778 ($U_{Ag/AgCl}$ = 0) / ~20	NA	NA	155
CdS QDs	TiO_2	350-550 nm	HER	0.25 M Na_2S / 0.35 M Na_2SO_3	7.2 (U_{RHE} = 0.5) / 76	NA	NA	156
CdS QDs	TiO_2	NA	Water splitting	0.25 M Na_2S / 0.35 M Na_2SO_3	0.2 ($U_{Ag/AgCl}$ = 0.5) / NA	NA	NA	157
CdS QDs / CdSe QDs	ZnO	300-750 nm	Water splitting	0.25 M Na_2S / 0.35 M Na_2SO_3	13.9 (U_{RHE} = 0.6) / ~80	100	NA	158
W:$BiVO_4$	WO_3	300-515 nm	OER	pH = 8, 0.5 M K_3PO_4	3.1 (U_{RHE} = 1.23) / ~60	79	NA	64
(W,Mo)-$BiVO_4$	WO_3	300-500 nm	OER	0.5 M K_2SO_4	5.35 (U_{RHE} = 1.23) / ~90	96.21	NA	159

CdS QDs / CdSe QDs	TiO_2	350-630 nm	Water splitting	0.5 M Na_2SO_4	0.19 ($U_{Ag/AgCl}$ = 0) / NA	95	0.17	[150]
Au@CdS nanoparticles	TiO_2	300-525 nm	Water splitting	0.35 M Na_2SO_3 / 0.25 M Na_2S	4.07 ($U_{Ag/AgCl}$ = 0) / 85	NA	2.8	[122]
Ag@Ag_2S nanoparticles	Ti@TiO_2	300-650 nm	Water splitting	1 M NaOH	0.089 (U_{Pt} = 0.2) / NA	NA	NA	[132]
CdSe QDs	TiO_2	300-800 nm	OER	1 M NaOH	~0.07 (U_{RHE} = 0.5) / 0.45	NA	NA	[160]
$CuInS_2$ QDs	TiO_2	350-700 nm	OER	0.5 M Na_2S, 2 M S, 0.2 M KCl	2.85 ($U_{Ag/AgCl}$ = 0) / 18	NA	NA	[161]
Au@CdS nanoparticles	ZnO	350-700 nm	HER	0.25 M Na_2S / 0.35 M Na_2SO_3	0.273 ($U_{Ag/AgCl}$ = 0) / 14.8	NA	NA	[162]
CdS QDs/Co-Pi	TiO_2	200-550 nm	OER	pH = 7, 0.1 M Na_3PO_4	0.69 ($U_{Ag/AgCl}$ = 0.6) / ~80	NA	0.48	[59]
Bi_2MoO_6 nanosheets	ZnO	visible light	OER	pH = 7, 0.2 M Na_2SO_4	0.11 (U_{SCE} = 0.6) / NA	NA	NA	[163]
Cu/ZnO nanosheets	GaN	NA	CO_2 reduction	0.5 M $KHCO_3$	10 (U_{RHE} = 0.6) / 5.12	NA	NA	[82]
rGO/NiFe-LDH	TiO_2	250-600 nm	OER	0.5 M Na_2SO_4	1.74 (U_{SCE} = 0.6) / 5.12	NA	0.58	[164]
$ZnFe_2O_4$ nanoparticles	ZnO/CdS	350-800 nm	OER	0.5 M Na_2S	3.88 ($U_{Ag/AgCl}$ = 0) / NA	NA	4.43	[149]
$ZnFe_2O_4$	TiO_2	300-600 nm	OER	1 M KOH	0.7 (U_{RHE} = 1.0) / NA	NA	0.31	[165]
g-C_3N_4 QDs	TiO_2	350-450 nm	OER	1 M KOH	3.40 (U_{RHE} = 0) / 75	NA	NA	[166]
Zeolite CPM-121	TiO_2	300-600 nm	OER	0.5 M Na_2SO_4	0.055 (U_{RHE} = 1.0) / NA	NA	NA	[167]
1T-MoS_2 nanosheets	TiO_2	220-800 nm	OER	0.5 M Na_2SO_4	2.4 ($U_{Ag/AgCl}$ = 1.2) / NA	NA	0.81	[168]

[a] J (potential), current density at one given potential. [b] IPCE, incident photon-to-current conversion efficiency. [c] FE, Faradaic efficiency. [d] EE, energy efficiency. [e] NA, value was not available or determinable from presented data.

2.3 Coupling nanowires with catalysts for chemical reactions

Different from the co-absorbers or sensitizers to facilitate the light absorption, catalysts are combined with nanowires to boost the half-reactions of oxidation and reduction and suppress the possible charge recombination and reverse reactions at the semiconductors' surface.[107] Generally, catalysts are considered to lower the activation energy of the catalytic reactions and facilitate the charge transfer of the photo-generated carriers. In addition, thanks to the timely consumption of photo-generated carriers, especially the holes, the catalysts could help to improve the photo-

stability of nanowires if that is an issue.[107] The catalysts are usually classified into three categories: molecular/cluster catalysts, inorganic materials, and biological entities (Table 5).

2.3.1 Molecular/cluster as catalysts

The molecular/cluster catalysts with earth-abundant elements always possess the advantages of definite and designable structures, tunable redox properties, and potential links to material surface,[169] rendering them suitable as catalysts for nanowires.[80,87,170-174] However, as these catalysts seem to be less stable under oxidative environment,[169] they are more often applied to photocathode rather than photoanode. At the photocathode, Si is the most popular semiconductor material that has so far been studied, thanks to its low band-gap (1.1 eV), high carrier mobility, long life-time of photo-excited carriers, and commercial availability.[9] One of the most common applications for Si nanowires as a photocathode is solar-powered proton reduction into dihydrogen.[9] An incomplete cubane-like Mo_3S_4 cluster has been coupled with Si nanopillar as photocathode to catalyze the hydrogen evolution reaction (HER) (Figure 8a-b).[170] Here the Mo_3S_4 cluster as the catalyst exhibited structural similarity to the building block commonly found in enzymatic co-factors, which are excellent HER catalysts. Under low intensity of light illumination, the onset of photocurrent shifted to more positive potential with the addition of Mo_3S_4 cluster as compared to that of the naked Si pillar. Moreover, the current density at the reversible hydrogen evolution potential reaches 9 mA cm^{-2}, which is the highest among the naked planar Si, Mo_3S_4 cluster modified planar Si, and naked Si pillar (Figure 8b). The authors claim that the current density can match the requirement of a PEC hydrogen production system with a solar-to-hydrogen efficiency in excess of 10%. Another study also investigated the effect of loading amount of molybdenum-sulfur (MS) cluster on the PEC performance over Si nanowire.[172] It is found that increasing the MS cluster content will positively shift the onset of photocurrent, while decreasing the limiting photocurrent. This is due to the partial overlapping of light absorption range between Si nanowire and MS cluster, reducing the incident photon utilization by Si nanowire.

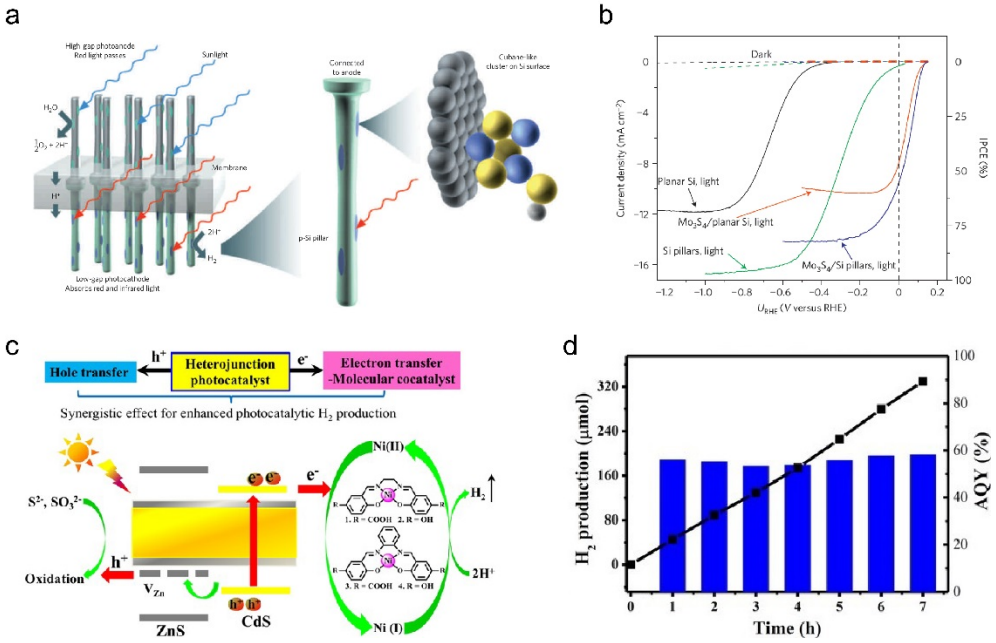

Figure 8. (a) Schematic of the tandem chemical solar cell. Pillars are embedded in a proton conducting membrane. The anode absorbed the blue part of the solar spectrum for oxidizing water into molecular oxygen and protons. The protons migrate through the membrane and are reduced at the cathode side by Mo_3S_4 clusters adsorbed on the Si pillars, which are excited by the red part of the spectrum. (b) Steady-state current density–voltage (left axis) and calculated IPCE (right axis) for planar and pillared Si with/without Mo_3S_4 clusters. The almost horizontal dashed lines denote the current measured in darkness. (a-b) Reprinted with permission from ref[170]. Copyright 2011 Nature Publishing Group. (c) Schematic illustration for the synergystic effect of the CdS/ZnS heterojunction and the water-soluble nickel–salen cocatalyst for enhanced photocatalytic H_2 production. (d) The time courses of H_2 production (black dot and line) and apparent quantum yield (AQY) (blue bar) over complex 3/CdS/ZnS nanorods photocatalyst. (c-d) Reprinted with permission from ref[171]. Copyright 2016 John Wiley & Sons, Inc.

In addition to the HER system, molecular/cluster catalysts can be coupled with nanowires for CO_2 reduction. Three kinds of Mn-based carbonyl bipyridyl complexes were tested as molecular catalysts on Si nanowires.[80] Towards the CO_2 reduction to CO happened in CH_3CN + 5% H_2O (v/v), all nanowire samples loaded with Mn-based complex exhibited higher performance over their planar counterparts in terms of the fill factor and energy efficiency for the device. Ru clusters as catalyst was also loaded on the surface of GaN nanowires to assist the reduction of N_2 under light illumination.[87] The GaN nanowires exhibited a much higher stability when loaded with ultra-small Ru sub-nanostructures at high loading density (*ca.* 10^{17} m^{-2}). The authors proposed that the

Schottky junction at the metal/semiconductor interface possess a barrier height of 0.94 eV, which can facilitate the transfer of photo-generated electrons from GaN nanowires into the Ru clusters. The Ru species accumulated with photo-excited electrons are supposed to promote the cleavage of N≡N bonds and achieve nitrogen fixation at low-temperature.

Molecular catalysts are also introduced to the systems that include semiconductor nanowires added with semiconductor light co-absorbers. The addition of both catalyst and co-absorbers provides a viable approach for device optimization, as shown in the case of core-shell CdS/ZnS nanorod heterojunctions loaded with nickel-salen molecular catalyst for solar-driven HER (Figure 8c).[171] The CdS/ZnS heterojunction facilitates the charge separation with possibly minimal charge recombination. The Ni^{II}/Ni^{I} redox couple in nickel-salen received the photo-generated carriers and performed catalytic proton reduction. The synergy between nickel-salen molecular catalyst and CdS/ZnS heterojunction results in a quantum efficiency up to 58.3% for hydrogen production during a 7-hr irradiation of visible light, as compared to the efficiency of 16.8% when the catalyst was not included (Figure 8d).

2.3.2 Inorganic materials as catalysts

Inorganic materials are the type of catalyst that has gained much when coupling with nanowires for PEC applications. Both photocathode and photoanode can employ various inorganic materials to boost the catalytic performance, thanks to their tunable structural and electronic properties, as well as the recent advances in inorganic electrochemical catalysis.[175,176] Precious metals such as Pt are still widely applied for many electrochemical reactions.[42,69-71,81,83,177,178] In the case of nanowire photocathode, Pt is the widely used catalyst for hydrogen evolution with Si, GaN and GaP semiconductor nanowires.[69-71,178] Due to the high cost of Pt, it is worthwhile to investigate the lower bounds of Pt loading on nanowires under the desirable charge flux for practical applications. A highly conformal coating of Pt nanoparticles with tunable sizes between 0.5 and 3 nm was loaded onto Si nanowire array by atomic layer deposition (ALD) to precisely control the mass loading.[70] When 1 cycle of Pt was deposited on Si nanowire's surface via ALD technique, a surface mass loading of ~10 ng cm^{-2} was achieved and finely distributed Pt nanoparticles smaller

than 1 nm were observed on the nanowire's surface. Despite such small loading amount of Pt, the deposited nanowire photocathodes still provided the necessary charge flux for solar-to-hydrogen conversion, therefore quantitatively determines the lower limits of Pt catalysts on high surface area nanowire photoelectrodes. This work presents a general approach for minimizing the cost of precious metal catalysts for efficient and affordable solar-to-fuel applications. Precious metals have also been combined with nanowires for solar-powered reduction of CO_2. Guided by the one-dimensional geometry of Si nanowires, well-dispersed assembly of Au_3Cu nanoparticles on their surfaces was realized.[81] The Si nanowires decorated with Au_3Cu nanoparticles exhibited high CO_2-to-CO selectivity of about 80% at –0.2 V vs reversible hydrogen electrode (RHE), and the selectivity towards HER has been largely suppressed. Thanks to the optimized spatial arrangement of Au_3Cu nanoparticles on the nanowire arrays, the overpotential for CO_2-to-CO conversion has been reduced by 120 mV as compared to that on planar counterpart. The Pt nanoparticles can also be utilized somewhat as catalyst to drive the CO_2 reduction. By loading Pt nanoparticles onto GaN nanowire arrays, not only the CO_2 reduction rate can be increased, but also the production selectivity can be switched from CO to CH_4. The photoreduction rate of CO_2 to CH_4 can reach ~14.8 μmol g_{cat}^{-1} h^{-1} when Pt nanoparticles were on the lateral *m*-plane surfaces of GaN nanowires, which is almost an order of magnitude higher than that measured on naked nanowire arrays with CO as the dominant product.[83]

In order to deviate from the disadvantages of high cost and low elemental abundance of precious metals, nanowires have been integrated with a large variety of earth-abundant catalysts, including transition metals,[77,82,137,179] metal oxide,[66,180] metal chalcogenides,[72,73,181-184] metal phosphides or phosphates,[185-188] metal nitrides,[189] metal borides,[190] metal hydroxides,[164,191] and metal-free materials.[192,193] Among the possible half-reactions that will be of interest to artificial photosynthesis, the reduction of CO_2 and N_2 as well as the oxidation of water demand more assistance with the introduction of catalysts due to their sluggish kinetics.[175,176] Moreover, sometimes two different sorts of inorganic materials, instead of one, were introduced with nanowires in the hope of obtaining certain synergistic effect among the nanowires and catalysts.

For example, InP nanopillars were integrated with TiO_2 thin film and Cu nanoparticles together (Figure 9a).[179] In this case, the Cu nanoparticles provides the active sites for the reduction of CO_2 into methanol. Yet interestingly, the coated TiO_2 layer not only provided a stable photocatalytic surface, but also is proposed to stabilize the CO_2^- intermediates on the O vacancy active sites and further increase the selectivity and yield of methanol transformed from CO_2 (Figure 9b). In another case, two-dimensional ZnO nanosheets and zero-dimensional Cu nanoparticles were both deposited onto GaN nanowires as dual catalysts to synergistically catalyze CO_2 and H_2O reduction to syngas with high efficiency (Figure 9c).[82] The CO/H_2 ratio in the syngas products could be tuned by the Cu-ZnO catalysts into a large range between 2:1 and 1:4 with a total Faradaic efficiency close to unity (Figure 9d). It was proposed that the complementary chemical properties between Cu and ZnO lead to unique reaction pathways that were not feasible when only one of these two catalysts were added.

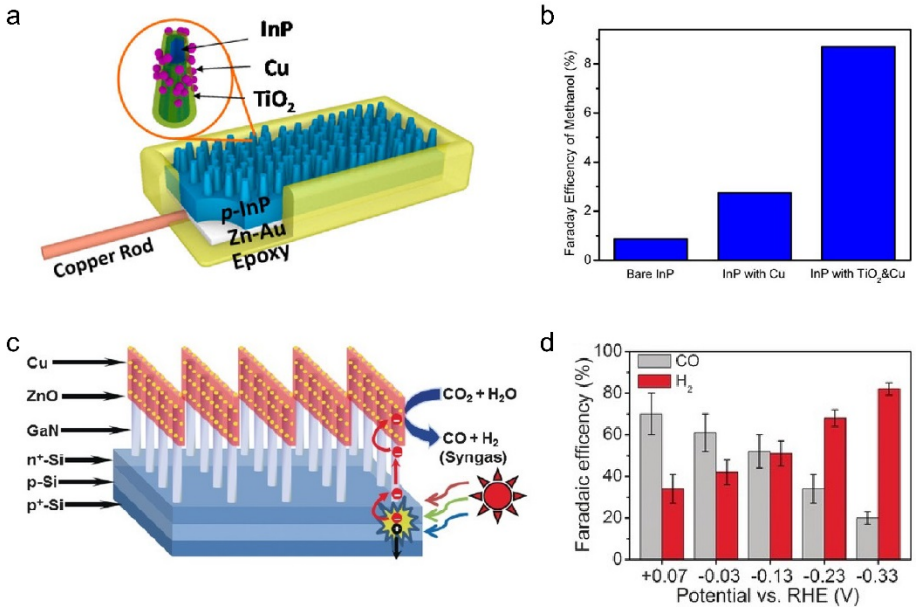

Figure 9. (a) Schematic diagram of TiO_2-passivated InP nanopillars with Cu cocatalyst nanoparticles. (b) Faraday efficiencies of methanol production for bare InP, InP/Cu, and InP/TiO_2/Cu. (a-b) Reprinted with permission from ref[179]. Copyright 2015 American Chemical Society. (c) Schematic for the design of Cu-ZnO/GaN/n^+-p Si photocathode to synergically catalyze CO_2 and H_2O reduction to syngas. (d) Faradaic efficiencies for CO (gray bars) and H_2 (red bars) of Cu-ZnO/GaN/ n^+-p Si photocathode as a function of potential. (c-d) Reprinted with permission from ref[82]. Copyright 2016 John Wiley & Sons, Inc.

Inorganic materials have been interfaced with nanowires for solar-powered wastewater treatment. The degradation of atrazine, a typical herbicide found in both surface and ground waters, was achieved with Pd_4S nanoparticles as the photocatalyst decorated with Bi_2S_3 nanorods.[183] Under visible light irradiation, Pd_4S nanoparticles facilitate the charge separation and the delivery of photo-generated carriers into Bi_2S_3 nanorods, which serve as active sites with the formation of hydroxyl radicals for organic decomposition. Pd-decorated Si nanowires was used as photocathode coupling for light-powered reduction of Cr(VI), a potent toxicant in water. 98.7% Cr(VI) was efficiently reduced under visible light illumination within 8 h, thanks to the use of Pd nanoparticles as the catalysts.[177]

Inorganic materials as catalysts were also frequently coupled with nanowires light-absorbers in the particulate configuration for photocatalytic reactions.[194-198] Pt nanoparticles have been deposited on CdS nanowires for the application of photocatalytic H_2 generation. The yielded Pt/CdS photocatalysts contained 0.3 wt% of Pt nanoparticle with the size of about 1 to 2 nm, and displayed promising photocatalytic activity with a 1.49 mmol h^{-1} rate of H_2 production rate and a quantum efficiency of 61.7%.[194] Two-dimensional MoS_2 were incorporated onto TiO_2 nanowire for photocatalytic HER under visible light. With a few layers of MoS_2 on porous nanowires of TiO_2, the core-shell hybrid structure was photocatalytically active with a H_2-generating rate of 16.7 mmol h^{-1} g^{-1}.[195] Last, $Zn_{0.5}Cd_{0.5}S$ nanorods as photocatalyst was decorated with CoP nanoparticle and exhibited a photocatalytic activity that was not only twenty times higher than that of pure $Zn_{0.5}Cd_{0.5}S$ sample, but also two times higher than the $Zn_{0.5}Cd_{0.5}S$ sample loaded with Pt.[196] The caveat here is to ensure a suitable loading amount of CoP so that the catalytic proton reduction was facilitated but the competitive light absorption from CoP was minimized.

2.3.3 Biological moieties as catalysts

Biological entities including enzymatic catalysts or whole cells often exhibit high selectivity towards a specific reaction process.[199] However, they displayed at most moderate solar-to-energy efficiency at about 0.5% to 2.0%, which is dwarfed by, the values up to 20% that can be achieved

by inorganic semiconductors.[199] We postulate that a inorganic-biological hybrid that combines semiconductor light-absorbers with biological catalysts can take the strengths of both and achieve an efficient and selective process of artificial photosynthesis.[33,199,200] The first step towards such an integration is to investigate the interactions between the inorganic and biological components at microscopic level. Si nanowire array was applied as real-time imaging platform at the single-cell level to study the interactions between Si nanowires and *Shewanella oneidensis* MR-1, a gram-negative facultative bacterium that was known to facilitate charge transfer with inorganic materials.[201] The presence of nanowire array was recognized by the *S. oneidensis* MR-1 and modified the swimming patterns of the microbes as well as the early-stage attachment between the nanowire and bacteria.[201] The physical interaction between bacterial and nanostructures was also sensitive to the parameters of local environment, including the ionic strength of the electrolyte and the gas pressure in the headspace. Researchers have studied the interactions between the nanowire array and the *Sporomusa ovata*,[202] a bioelectrochemically active bacterium that has been reported to fix CO_2 into acetic acid with the supply of electricity from an electrode.[203] At high ionic strength or hydrostatic pressure, *S. ovata* formed vertically aligned filamentous cells parallel to the nanowires. Such observation indicate that local environment with the presence of nanowire should be considered in order to interface nanowires with biocatalysts with good compatibility.

Integrating semiconductor nanowires with *S. ovata* lead to the a solar-powered device that reduce CO_2 into acetic acid with high selectivity (Figure 10a-b).[34] Here the nanowire morphology provided a large surface area to accommodate *S. ovata* as the catalyst. Under solar irradiation, the photo-generated carriers in Si was directly transferred to *S. ovata*, whose enzymes in the Wood-Ljungdahl pathway[204] take these carriers as reducing equivalents and fix CO_2 into acetic acid. This inorganic-biological hybrid system showed a low overpotential of CO_2 fixation ($\eta < 200$ mV), high Faradaic efficiency (up to 90%), and decent long-term stability (up to 200 h). The yielded acetate, at a titer of about 6 $g \cdot L^{-1}$, can be further upgraded by genetically engineered *Escherichia coli* for a number of value-added chemicals including *n*-butanol, polyhydroxybutyrate, and three different isoprenoid natural products (Figure 10c). In this study, there is one additional benefit for

the nanowire array. As *S. ovata* is strictly anaerobic bacteria that cannot tolerate ambient air, an integration between a planar photoelectrode and *S. ovata* cannot function in aerobic environment such as the air. As stated above, nanowire array as a porous electrode can control the mass transport of redox active species within the wire array. The nanowire array depleted the O_2 diffused from the air and create a local anaerobic environment suitable for *S. ovata*, which was not possible with planar photoelectrode. Thanks to such a locally anaerobic region in the nanowire array, the integrated system is capable to house *S. ovata* and facilitate the solar-powered device of CO_2 fixation in air. This demonstrates that a proper design with the use of nanowires can provide additional synergistic effect that may not be possible for individual components.

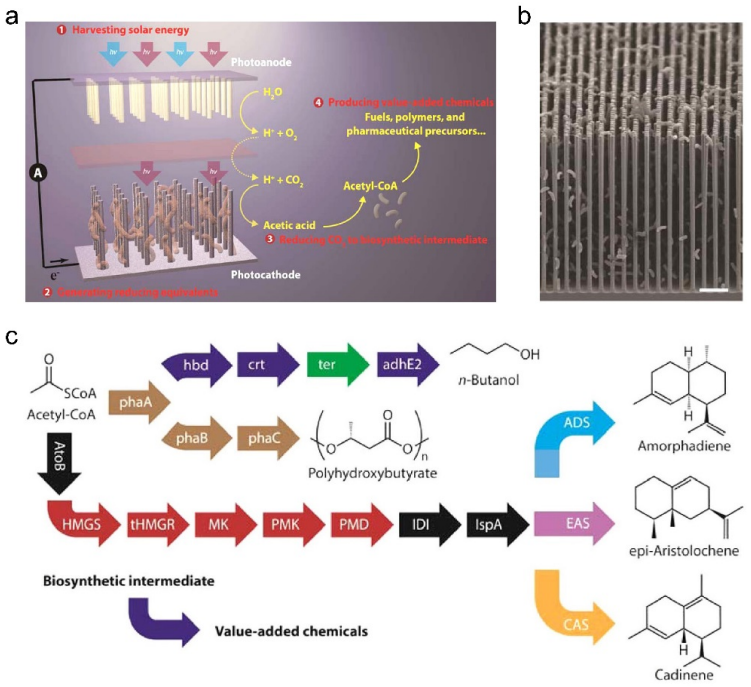

Figure 10. (a) Schematics of a general artificial photosynthetic approach combining the advantages of solid-state devices with living organisms. Such proposed approach for solar-powered CO_2 fixation includes four general components: (1) harvesting solar energy, (2) generating reducing equivalents, (3) reducing CO_2 to biosynthetic intermediates, and (4) producing value-added chemicals. (b) Cross-sectional SEM image of the three-dimensional network in the nanowire-bacteria hybrid. (c) Synthetic pathways for the production of a variety of value-added chemicals. The names of proteins are listed, and the colors differentiate their genetic origins. In addition to these described pathways, some of the acetyl-CoA are expected to be diverted into the

TCA cycle for redox balancing. (a-c) Reprinted with permission from ref[34]. Copyright 2015 American Chemical Society.

Besides the utilization of biological entities in inorganic-biological hybrid for enhancing the PEC efficiency of nanowire, the PEC process within nanowire could be used for probing and modulation of cellular interface and activity.[205-207] The potential benefits of nanowire discussed in section 1.4 could be applicable here. The light-trapping effect and enhanced charge separation efficacy of nanowire will promote the photoelectrochemical response, and the high surface area will permit the efficient guest loading and molecule capture.[205,206] By growing *H9c2* cardiac myoblasts on nitrogen-doped carbon nanodots (N-Cdots) coupled TiO_2 nanowires, a nanomaterial-cell platform was constructed for photoelectrochemical probing of physiological levels of H_2S messenger generated by living cells.[205] The proposed process is the existence of Cu^{2+} in electrolyte will quench the charge transfer pathway between N-Cdots and TiO_2 nanowires to decrease the photocurrent to the level of pristine TiO_2 nanowire (PEC-off state). Then, the excited *H9c2* cardiac myoblasts can produce H_2S to reduce the Cu^{2+} concentration by forming CuS, which will reinstate the transfer process of photogenerated charge and thereby increase the photocurrent to the "PEC-on" stage. The detection sensitivity of H_2S in the buffer can reach 10 nM.[205] Another study also adopted TiO_2 nanotubes for physiological level probing of H_2S.[206] The different process is Cd^{2+} was first adsorbed onto the TiO_2 nanotubes, and then the *HepG2* cells grown on nanotubes generated H_2S under stimulation to react with Cd^{2+} into CdS, which will increase the photocurrent of TiO_2 nanotubes by enhancing the light absorption.[206]

Table 5. Different kinds of catalysts coupled with semiconductor nanowires for various PEC reactions.

Catalyst	Nanowire	Absorption wavelength	Reaction	Electrolyte	J (potential) [a] / IPCE [b] mA cm^{-2} / %	FE [c] %	EE [d] %	Ref.
Mo_3S_4 cluster	Si	> 620 nm	HER	1 M $HClO_4$	9 (U_{RHE} = 0) / 93	NA [e]	10	[170]
Mn-based complex	Si	> 600 nm	CO_2 reduction	CH_3CN + 5% v/v H_2O	NA / NA	0.35	3	[80]
Pt nanoparticle	Si	NA	HER	0.5 M H_2SO_4	7 (U_{RHE} = 0) / NA	NA	NA	[70]

Au_3Cu nanoparticle	Si	740 nm	CO_2 reduction	0.1 M $KHCO_3$	2.75 (U_{RHE} = –0.2) / NA	80	NA	81
Ru film	InP	NA	HER	1 M $HClO_4$	37 (short circuit) / NA	NA	14	42
Sn nanoparticle	Si	NA	CO_2 reduction	0.1 M $KHCO_3$	NA / NA	40	NA	77
Cu nanoparticle	GaN/Si	NA	CO_2 reduction	0.5 M $KHCO_3$	44.9 ($U_{Ag/AgCl}$ = –1.5) / NA	19	NA	137
$NiRuO_x$	Si	NA	OER	(PH = 7.2) PBS	1.36 (U_{RHE} = 1.23) / NA	NA	NA	180
$CoTiO_x$	Ta_3N_5/Si	< 590 nm	OER	0.1 M KOH	2.6 (U_{RHE} = 1.23) / NA	NA	NA	66
MoS_2 layers	TiO_2/Si	NA	HER	0.5 M H_2SO_4	15 (U_{RHE} = 0) / NA	100	NA	72
MoS_3 nanoparticle	InP	NA	HER	1 M $HClO_4$	NA / NA	NA	6.4	73
$NiCoSe_x$	Si	NA	HER	0.5 M H_2SO_4	37.5 (U_{RHE} = 0) / NA	NA	NA	184
FeP	Si	NA	HER	(PH = 1) 0.5 M K_2SO_4	13.9 (short circuit) / NA	100	2.64	188
Co-P nanoparticle	Si	NA	HER	(PH = 1) 0.5 M K_2SO_4	18.2 (U_{RHE} = 0) / NA	NA	NA	185
$Ni_{12}P_5$ nanoparticle	Si	NA	HER	(PH = 1) 0.5 M K_2SO_4	21 (short circuit) / NA	NA	2.98	186
ZnFe-LDH nanosheet	TiO_2	NA	OER	0.5 M Na_2SO_4	1.51 (U_{RHE} = 1.23) / 4.86	100	NA	191
NiFe-LDH nanoplatelet	TiO_2	NA	OER	0.5 M Na_2SO_4	1.74 (U_{SCE} = 0.6) / 5.12	NA	0.58	164
CoB nanoparticle	Si	NA	HER	(PH = 7) PBS	19.5 (U_{RHE} = 0) / NA	95	2.46	190
N-doped graphene quantum sheet	Si	NA	CO_2 reduction	0.1 M TBAH in acetonitrile	7.07 (U_{Ag/Ag^+} = –2.5) / NA	95	NA	193
Bacterium *S. ovata*	Si	NA	CO_2 reduction	(PH = 6.3 ~ 6.7) brackish water solution	NA / NA	90	0.38	34

[a] J (potential), current density at one given potential. [b] IPCE, incident photon-to-current conversion efficiency. [c] FE, Faradaic efficiency. [d] EE, energy efficiency. [e] NA, value was not available or determinable from presented data.

3: Nanowires for the half reactions in photoelectrochemistry

The previous sections have provided the design strategy and examples of how to apply semiconductor nanowires for PEC applications as well as its integration of other building blocks, including light co-absorbers and catalysts, for efficient solar-to-chemical conversion. As discussed

above, the fundamental processes of photoelectrochemistry relies on the turnover of redox half-reactions at the semiconductor/electrolyte interface. Therefore, it seems necessary for us to describe the current applications of nanowires for various half-reactions mostly with the use of nanowire photoelectrode, which is the main focus of this section. We will first review the oxidative and then reductive sides of photoelectrochemistry. The readers are also guided to Table 2 to 5, in which the specific half-reactions that were studies are also listed. In addition to the synergistic benefits when integrating nanowires with other building blocks discussed in section 2, the claimed advantages from nanowire morphology in previous literature for different reactions are summarized in Table 1, consistent with our discussion in section 1.4. We posit that the previous and current sections provide two different yet complementary aspects of nanowires in photoelectrochemistry, which will yield a more comprehensive summary for this field.

3.1 Nanowire for oxidative photoelectrochemistry

3.1.1 Photoelectrochemical water oxidation

Water oxidation reaction is critical as it is the vital component of the overall water-splitting reaction that produces molecular hydrogen, which is a promising renewable energy solution to the global challenges in energy and environments. Water splitting occurs as: $2H_2O \rightarrow 2H_2 + O_2$, where the theoretical electrochemical potential (V_{eq}) is 1.23 V for the overall reaction. In practice, the operating voltage of water electrolysis (V_{op}) is determined by the dynamics of half reactions and the system configuration as:

$$V_{op} = V_{eq} + \eta_A + |\eta_C| + \eta_\Omega$$

where V_{eq} = 1.23 V; η_A and η_C are the overpotentials required to overcome the kinetical barrier at the anode and cathode for oxygen and hydrogen evolution reactions, respectively, and η_Ω is the overpotential to offset the loss of electric resistance in the system.[208] In many cases, the rate of a water-splitting process is limited at the anode because of the sluggish oxygen evolution reaction (OER),[209] which involves multiple electron transfer and surface adsorbed intermediates.[210] In recent years, based on *in-situ* spectroscopy techniques, water oxidation intermediates were

tentatively probed.[211-214] The OER in is generally considered following a four-step single-electron transfer reaction with three adsorbed intermediates: $OH_{(ad)}$, $O_{(ad)}$, and $OOH_{(ad)}$:

$$H_2O \xrightarrow{\Delta G_1} OH_{(ad)} + H^+ + e^-$$

$$OH_{(ad)} \xrightarrow{\Delta G_2} O_{(ad)} + H^+ + e^-$$

$$O_{(ad)} + H_2O \xrightarrow{\Delta G_3} OOH_{(ad)} + H^+ + e^-$$

$$OOH_{(ad)} \xrightarrow{\Delta G_4} O_2 + H^+ + e^-$$

The expression of these equations are specific for OER happens under acid condition. The maximum Gibbs reaction energy of the four primary reactions governs the overpotential of OER.[210] Valdés *et al.* showed that the OER activity largely depends on the binding strength of OER intermediates on the catalyst surface.[215] In principle, the adsorption energies of reactive intermediates are controlled by the surface electronic structure of calalyst.[208] By adjusting surface adsorption, it is rational to steer the four primary reactions to optimize the water oxidation reaction.[147,216]

Photogenerated holes from semiconductor can be utilized to oxide water to evolve oxygen. The first demonstration of a photoanode for water oxidation was made by Honda and Fujishima.[217] At an external bias of ~0.9 V vs. RHE under UV illumination, 1 mA cm^{-2} photocurrent density could be generated on undoped TiO_2 photoelectrode. For photoanode made of *n*-type semiconductor, water oxidation occurs at the interface between the photoanode and electrolyte.[38] When semiconductor photoelectrode is immersed into electrolyte, the Fermi level of semiconductor will equilibrate with the electrochemical potential of the redox pair, causing band bending. The built-in interfacial electric field in the space charge region can effectively promote charge separation for enhanced solar energy conversion efficiency. Photogenerated holes can be accumulated on the surface of *n*-type semiconductor under illumination to induce water oxidation reaction as shown in Figure 11a.[38] The potential difference of the anodic photogenerated holes and cathodic photogenerated electrons should be larger than 1.23 eV for overall water splitting to overcome the overpotentials in both electrodes.

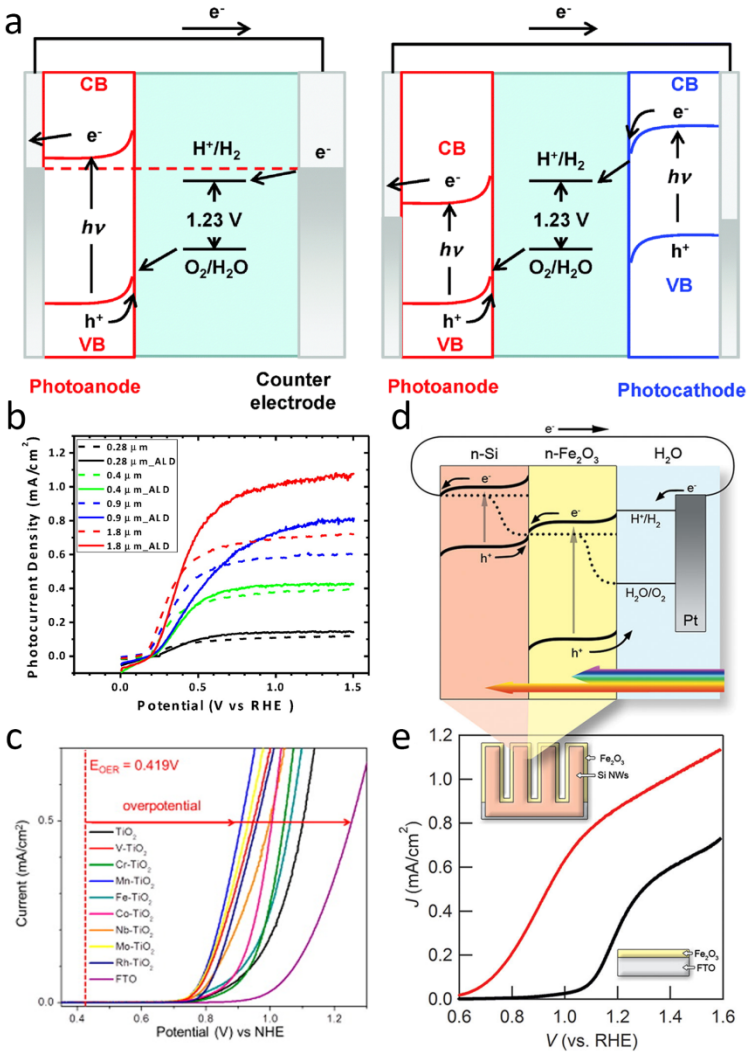

Figure 11. (a) Energy diagrams of photoelectrochemical water splitting cells with photoanode, and photoanode and photocathode in a tandem configuration. Reproduced with permission from ref[38]. Copyright 2014 The Royal Society of Chemistry. (b) Photocurrent densities of TiO_2 nanowire arrays of different lengths with and without 150 ALD TiO_2 cycles. Reprinted with permission from ref[60]. Copyright 2012 American Chemical Society. (c) OER overpotential of TiO_2 nanowires with/without transition metal doping in basic electrolyte. Reprinted with permission from ref[58]. Copyright 2013 American Chemical Society. (d-e) Energy band schematics and *J*–*V* plots under simulated solar illumination of the hematite/Si nanowire dual-absorber PEC cells. Reprinted with permission from ref[63]. Copyright 2012 American Chemical Society.

Nanowire morphology is important for an efficient PEC water oxidation process, since a high efficiency of water-splitting requires not only competent photoanode with suitable band structure,

but also eligible surface for adsorption and activation of reaction species. N-type transition metal oxides and nitrides such as TiO_2,[60,218] ZnO,[61,154] α-Fe_2O_3,[62] WO_3,[64] Ta_3N_5,[65] and *n*-type silicon[146] nanorod or nanowire arrays and their derivatives have been developed as photoanodes for water oxidation, which show decent performance in terms of charge transport and carrier collection. Owing to the one-dimensional morphological feature, nanowire photoanode is able to decouple the directionality of light absorption and charge transport, as stated in the section 1.4.[90,219] The photo-generated minority carriers in *n*-type nanowire could transfer to the surface via a short diffusion pathway along the radial direction to participate in the oxidation reaction with a significantly enhanced $\eta_{separation}$, while the morphology of nanowires affords an increased light absorption.[19] Additionally, the nanowire geometry could also provide sufficient sites for catalytic reactions. Jaramillo *et al.* demonstrated that the photoelectrochemical water oxidation performance of core-shell Si-Ta_3N_5 nanowire photoanode could be greatly improved as compared to the planar counterpart, owing to the enhanced light absorption and larger electrochemically active surface area in Si-Ta_3N_5 nanowires, which are beneficial for water oxidation reaction.[66] The integration of *n*-type silicon nanowire with Ta_3N_5 could shift the photocurrent onset to more negative potentials owing to an "improved" band alignment.[66] In another example, Ta_3N_5 nanowire photoanode displayed an enhanced OER photocurrent up to 3.2 fold at 1.23 V vs. RHE compared with its thin-film counterparts, thanks to its large surface active area, the short diffusion length of photoexcited holes, and the enhanced light absorption with suppressed reflection as discussed in section 1.4.[65] Moreover, WO_3/W:$BiVO_4$ nanowire photoanode achieved a OER photocurrent density of 3.1 mA cm^{-2} and an 60% IPCE at 300–450 nm, both at 1.23 V vs. RHE.[64] Such a decent photoelectrochemical performance is attributed to the higher value of charge separation efficiency ($\eta_{separation}$) and the efficient charge transfer at surface in WO_3/W:$BiVO_4$ nanowire photoanode.[64]

Besides the advantages brought by morphological features, surface properties of nanowires are also important in PEC cells as they directly influence charge recombination and chemical reaction kinetics. Hwang *et al.* reported that both the length and surface properties of TiO_2 nanowires had strong impacts on their PEC performances of water oxidation (Figure 11b).[60] Since here nanowire

photoanode acted as both the light absorbers and catalytic sites, it is important to find a balance between light harvesting and catalytic reaction to optimize the photoanode's performance. Additionally, the addition of catalyst should be considered when the kinetic of water oxidation could be the bottleneck. For example, hematite nanowires have advantages of visible light absorption, large abundance and low cost, but with high overpotential for water oxidation. Consequently, it is necessary to apply catalyst to improve kinetics of oxygen evolution on hematite.[147] As such, surface and interface engineering are indispensable as discussed in Section 2, in which catalysts play a crucial role at lowering the reaction barrier and improving charge separation efficiency. Moreover, the doping of hetero-atoms and the establishment of heterojunction in nanowire photoanode are commonly used to optimize surface properties, which can promote charge kinetics and facilitate surface reaction. Under visible light illumination (400–475 nm), an apparent quantum efficiency of the incident photons (η_{PEC}) of 12.3% was achieved for overall wireless water-splitting in neutral aqueous medium, with the use of core/shell Rh/Cr_2O_3 decorated double-band *p*-GaN/*p*-$In_{0.2}Ga_{0.8}N$ nanowire heterojunction photoelectrode.[153] Under concentrated sunlight, the establishment of GaN/InGaN heterojunction and the introduction of Rh/Cr_2O_3 catalysts led to a production rate of H_2 and O_2 as high as 3.46 mol h^{-1} g^{-1} and 1.69 mol h^{-1} g^{-1}, respectively.[153] For TiO_2 nanowire array photoanode, the coating of CdS later lead to distinctive shift of the photocurrent onset potential, from –0.297 V to –0.403 V vs. Ag/AgCl. Additional coating of cobalt phosphate OER catalyst could further shift the onset potential to –0.469 V vs. Ag/AgCl.[59] Here, it was proposed by the authors that the introduction of CdS layer leads to a negative shift of Fermi level, while the addition of cobalt phosphate catalysts suppressed charge recombination around the flat-band potential and subsequently improved the kinetics for OER.[59] Transition-metal dopants were demonstrated to be helpful in lowering overpotential of OER in rutile TiO_2 nanowires resulting from enhanced adsorption of OER intermediates (Figure 11c).[58] Wang *et al.* established a Z-scheme Si@α-Fe_2O_3 dual-absorber system, which could absorb photons in a wide spectrum and promote charge separation through band engineering (Figure 11d-e).[63] In this system, different doping levels of silicon nanowires at 10^{14}, 10^{16}, and 10^{18} cm^{-3} could

lead to onset potentials of 0.6, 0.8 and 0.9 vs. RHE, respectively.[63] The Si@α-Fe_2O_3 core-shell nanowire photoanode with appropriate band engineering exhibited the lowest turn-on potential among all reported hematite-based photoelectrochemical water splitting systems.[63]

3.1.2 Photoelectrochemical oxidation of organics and biomass conversion

Photo-generated holes can participate in other oxidative reactions beyond OER. Reactions of organic oxidation possess more favorable kinetics as compared to water oxidation.[220] The replacement of OER with oxidation of organic substrate not only can substantially lower the anodic potential for PEC hydrogen production, but also may serve as a potential approach toward chemical synthesis. Photo-oxidative degradation of organic compounds was developed decades ago, but there were minimal efforts to study the kinetic mechanism and enhance product selectivity.[221,222] Recently, Durrant *et al.* showed that methanol could be almost completely oxidized to formaldehyde on hematite photoanode (Figure 12a).[223] Kinetic analysis found that methanol oxidation was independent of the band bending at the semiconductor-liquid junction, but was second order with respect to surface-accumulated holes on both hematite and titania photoanodes, while the rate constant for hematite is 2 orders of magnitude lower than that for titania.[223] The morphology of nanowire with tunable surface carrier dynamics may benefit such kind of carrier-dependent reactions.

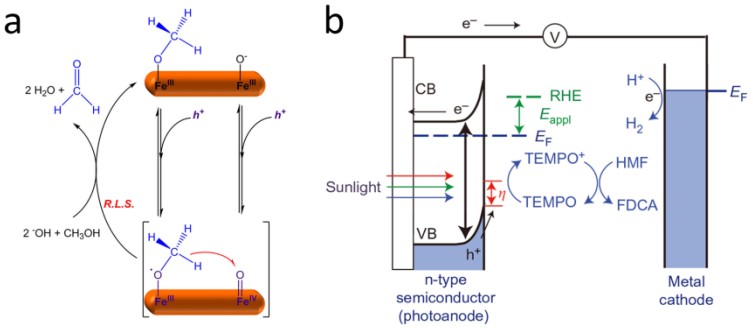

Figure 12. (a) Plausible mechanism of methanol oxidation on α-Fe_2O_3 photoanode. Reprinted with permission from ref[223]. Copyright 2017 American Chemical Society. (b) Schematic of the photoelectrochemical TEMPO-mediated organic oxidation. Reprinted with permission from ref[68]. Copyright 2015 Macmillan Publishers Limited.

Additionally, the efficient oxidation conversion of renewable biomass to valuable chemicals has attracted considerable attention in fundamental studies and for practical applications. Assisted by $BiVO_4$ photoanode, a 2,2,6,6-tetramethylpiperidine 1-oxyl (TEMPO)-mediated 5-hydroxymethylfurfural (HMF) oxidation into 2,5-furandicarboxylic acid (FDCA) was demonstrated by Choi *et al.* (Figure 12b).[68] The Faradaic efficiency of the TEMPO-mediated biomass conversion process can reach as high as 93%, suggesting that TEMPO oxidation is kinetically faster than water oxidation on $BiVO_4$. Without TEMPO medium, the HMF oxidation into FDCA was also completed by Sun *et al.* using Ni based electrocatalysts, and near-unity Faradaic efficiencies were achieved for the generation of hydrogen and FDCA.[224,225] Liu *et al.* developed a PEC system on porous $BiVO_4$ nanoarray photoanode for the selective oxidation of glycerol to value-added 1,3-dihydroxyacetone (DHA) without catalysts and redox mediator.[67] A photocurrent density of 3.7 mA cm^{-2} and an apparent quantum efficiency of the incident photons (η_{PEC}) of 25% for 400-nm photon at 1.2 V vs. RHE were achieved in acidic electrolyte. Meanwhile, this photoanode could produce 56 mmol $g_{catalyst}^{-1}$ h^{-1} of DHA with a DHA selectivity of 64 %. Faster reaction kinetics of PEC glycerol oxidation than water oxidation was demonstrated in this work. This nanoarray photoanode could produce DHA with higher rate and selectivity than thin-film photoanode. The authors attributed these features to the electrode's large surface area, abundant active sites, and probably the adequate mass transport (section 1.4).[67] By combining photovoltaics and catalytic reactions, they also established a biomass photo-reforming cell that is able to simultaneously produce hydrogen and chemical.[226] Nanowire photoanodes that have distinct advantages at charge kinetics and light absorption may be particularly useful for photoelectrochemical organic oxidation and biomass conversion.

3.2 Nanowire for reductive photoelectrochemistry

As the other half of the overall Z-scheme solar-to-fuel process, PEC cathodic reactions are equally important.[227-229] In a photocathodic process, the photo-generated electrons transport to the catalytic sites for chemical reactions at the interface between photocathode and electrolyte. A reasonably good photocathode should provide relatively large photovoltage given it band-gap, a

decent and stable photocurrent, and last but not least, high reaction selectivity of the desirable products under an acceptable overpotential.[230] Due to the unique structural, physical and chemical properties, photocathodes composed of semiconductor nanowires have demonstrated several advantages over planar ones, which have been summarized in previous section.[12] In the following section, we will review the recent research efforts in developing semiconductor nanowire photocathodes for PEC hydrogen evolution, CO_2 reduction and N_2 reduction, respectively.

3.2.1 Photoelectrochemical hydrogen evolution

PEC hydrogen production has attracted a lot of research interests since Fujishima and Honda demonstrated the first solar water splitting process with TiO_2 photoelectrode in 1972.[217] With the introduction of the Z-scheme dual-light-absorber design, relatively small-band-gap semiconductor materials such as Si and III-V group materials have been intensively investigated for photoelectrochemical hydrogen evolution.[230]

Si is widely considered a promising photocathode material for solar H_2 evolution, because it is earth-abundant, relatively stable, has suitable band gap for light absorption and conduction band edge for HER reaction.[231] However, as an indirect bandgap material, planar Si electrode typically suffers high reflection loss and requires a ~200 μm thickness to absorb the longer-wavelength light. On the other hand, Si wires decouple the light absorption and the charge carrier collection,[232] and at the same time bring the light trapping effect within the array, which significantly reduce the light reflection loss.[219] In addition, taking advantage of their large surface area, Si nanowire array photocathode allows the use of earth-abundant HER electrocatalyst instead of the precious noble metal electrocatalyst.[4] Oh *et al.* reported that *p*-type Si nanowires photocathode prepared via electroless etching yielded a photovoltage as high as 420 mV, and significantly outperformed the planar counterpart due to the reduced overpotential and light trapping effect.[69] P. Yang's group and D. Wang's group both reported that Pt can be deposited onto Si nanowire photocathode via the ALD method.[70,71] Precisely controlling the amount of Pt loading as low as ~10 ng cm^{-2} (Figure 13a), such approach represents a general method to minimize the cost of noble metal HER catalyst for efficient photoelectrochemical H_2 production (Figure 13b). Zhang *et al.* showed the integration

of earth-abundant MoS_2 HER electrocatalysts onto the high-surface area Si nanowire array photocathode.[72] A decent onset potential of ~0.3 V *vs.* RHE was obtained, owing to the reduced surface flux of electrons that can be handled by MoS_2 electrocatalysts.

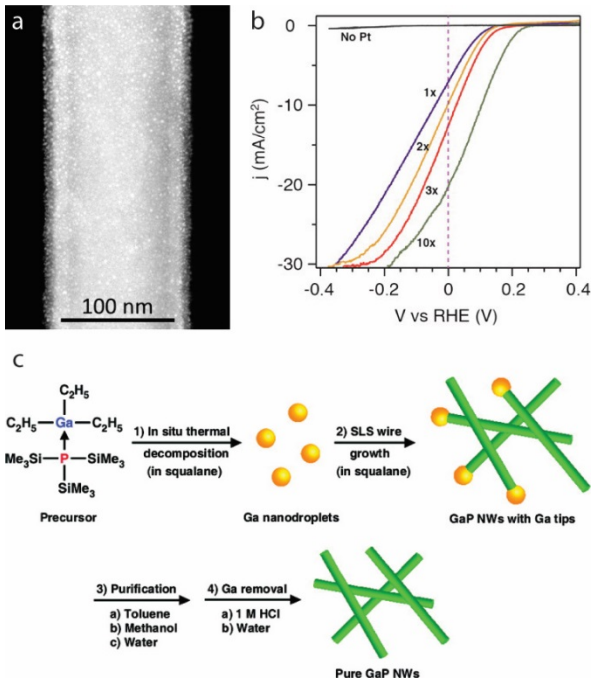

Figure 13. (a) Scanning transmission electron microscopy (STEM) image of Pt nanoparticles deposited on a Si nanowire by ALD. (b) HER performance of Si nanowire array photocathode with different ALD Pt loadings. (a-b) Reprinted with permission from ref[70]. Copyright 2013 American Chemical Society. (c) Schematics of synthesis and purification of colloidal GaP nanowires. Reprinted with permission from ref[178]. Copyright 2011 American Chemical Society.

The benefits obtained from Si nanowire are also applicable to photocathodes composed of III-V nanowires. Lee *et al.* reported that *p*-type InP nanopillars can dramatically increase the solar-to-hydrogen efficiency to 14%, compared with 9% of the planar counterpart.[42] Such enhancement results from the low reflection loss and efficient charge separation originated from the nanopilliar structure. It was also found that the InP nanopillars facilitate the desorption of H_2 bubbles, which in turn promote the H_2 evolution by reducing the reverse effect of local H_2 molecules. In addition, E. Bakkers's group used vapor-liquid-solid (VLS) method to grow vertically aligned *p*-type InP and GaP nanowire arrays with a small surface parking fraction.[73,74] Loaded with noble-metal-free

MoS_x HER electrocatalysts, these nanowire photocathodes can achieve higher energy conversion efficiency than planar analogues. Such high performance is attributed to the efficient charge separation in the high-quality III-V nanowires and the fast electron transfer at the nanowire/MoS_x interface. In addition to the benefits mentioned above, III-V nanowires also feature low-cost synthesis, compared to the expensive fabrication of planar III-V wafer. Sun *et al.* discovered that colloidal GaP nanowires can be synthesized via a low-cost solution-liquid-solid (SLS) method (Figure 13c).[178] These GaP nanowires can be conveniently drop-cast on a conductive substrate and carry out solar H_2 production for at least 12 hours. Furthermore, these GaP nanowires can be controllably doped by introducing Zn dopants during the SLS synthesis.[91] By optimizing the nanowire diameter and the Zn doping concentration, the doped GaP nanowires exhibit better absorbed photon-to-current efficiency (APCE) than planar GaP, with only 1/3000 of the amount of material used in the planar cathode. In addition, the nanowire geometry allows for the flexible multijunction design of III-V photocathode, which synergistically combines the advantages of III-V materials with different compositions. Fan *et al.* reported a monolithically integrated photocathode that is composed of *p*-InGaN/tunnel junction/*n*-GaN nanowire arrays on a planar n^+p Si substrate.[233] Such nanowire-based lateral multijunction circumvents the current mismatching issue typically present in conventional buried multijunction photocathode, and thus allows the photo-generated electrons at different segments to drive HER reaction at the same time. As a result, this system yielded an impressive 40 mA cm^{-2} photocurrent density, with a near-unity faraday efficiency of H_2.

In addition to Si and III-V materials, metal oxides, in particular Cu_2O and CuO, are also considered as promising photocathode for solar H_2 production, owing to their relatively small bandgap, suitable conduction band edge, earth abundance and simple synthesis procedure. However, because of the severe mismatch between the minority carrier diffusion length (20-200 nm) and the absorption depth (~2 μm), the planar copper oxide photocathode typically suffers low values of IPCE, especially at longer radiation wavelength. To solve such problem, Huang *et al*. prepared highly aligned Cu_2O nanowire arrays, and found that the photocurrent of Cu_2O nanowires

doubled that of the planar electrode, largely due to the efficient collection of photogenerated electrons along the nanowire's radial direction.[76] After protected by a CuO/TiO_2 shell, the resulting $Cu_2O/CuO/TiO_2$ core-shell nanowire structure gained 74% more photocurrent and 4.5 times higher stability. Moreover, Luo *et al*. developed a phase-controlled synthesis method to grow high-quality Cu_2O nanowire arrays with superior optoelectronic properties.[75] Such Cu_2O nanowire photocathode can achieve photocurrent as high as 10 mA cm^{-2}, and a better IPCE than planar counterpart for wavelength ranging from 350 nm to 650 nm.

3.2.2 Photoelectrochemical reduction of carbon dioxide

With the rise of CO_2 concentration in the atmosphere and the resulting climate issue, research in the field of catalytic CO_2 conversion has grown rapidly in the past decades.[234] Photoelectrochemical CO_2 reduction, where the dissolved CO_2 molecules are reduced at the photocathode/electrolyte interface, is considered a promising approach to realizing efficient CO_2 conversion.[235] However, photoelectrochemical CO_2 reduction on a planar photoelectrode typically suffers low energy-conversion efficiency, because the sluggish kinetics of CO_2 activation and conversion determines that typically a large overpotential is needed to drive the reaction.[236] In addition, the overall reaction process involves multiple proton coupled electron transfer steps, leading to a low selectivity of the desirable carbon products.[237] Photocathodes made of semiconductor nanowires provide opportunities to mitigate these challenges. In addition to the benefits regarding efficient charge transport and enhanced light absorption that observed in solar H_2 production process, the large surface area of the nanowire geometry in principle can gain more benefits in terms of the reduced overpotential for CO_2 reduction. Furthermore, the multifaceted nature of semiconductor nanowires and the unique mass transport of redox species within the nanowire arrays can also have an impact on the multi-step CO_2 reduction and thus bring further benefits to the CO_2 conversion efficiency. In this section, we will review the recent progress on photoelectrochemical CO_2 reduction using semiconductor nanowires as the light absorber. Based on the nature of the catalytic reaction, both homogeneous and heterogeneous process will be briefly discussed.

In homogeneous photoelectrochemical CO_2 catalysis, the molecular catalysts typically bind with the photocathode through physical interaction or covalent bonding.[227,235] The photogenerated electrons are transferred to the molecular catalysts, while the reduced catalytic species bind with the CO_2 molecules and carry out the catalytic reaction to release the carbon product and regenerate the catalyst. D. Wang's group reported that Si nanowire can serve as an efficient photocathode to synthesize trisubstituted alkenes from CO_2 and alkyne catalyzed by $[Ni(bpy)_2]$ molecular catalyst.[78] Owing to the multifaceted nature of the Si nanowire that presumably facilitates the electron transfer process, the Si nanowire photocathode yielded a 240 mV more positive onset potential than the planar counterpart. Moreover, such multifaceted Si nanowire photocathode can also fix CO_2 into carboxylic acid without the assistance of a molecular catalyst, and obtained a 110 mV photovoltage benefits compared to the planar photocathode (Figure 14a).[79] B. Fabre's group reported that Mn-based complexes can be grafted on the Si nanowire surface to carry out photoelectrochemical CO_2 conversion into CO in CH_3CN + 5% v/v H_2O.[80] Three kinds of Mn-based molecular catalysts are tested, and for each case the Si nanowire photocathode exhibit better onset potential, fill factor and energy conversion efficiency than the planar counterpart, thanks to the large surface area, efficient charge separation and better semiconductor/liquid interface. Furthermore, Jin *et al.* showed that Re(I)-NHC complexes can be strongly absorbed on the Si nanowire's surface to carry out photoelectrochemical CO_2 reduction.[174] The diffuse reflectance infrared Fourier transformation spectroscopy (DRIFTS) showed that the faraday efficiency of CO is correlated with the binding strength between the molecular catalyst and the Si nanowire photocathode.

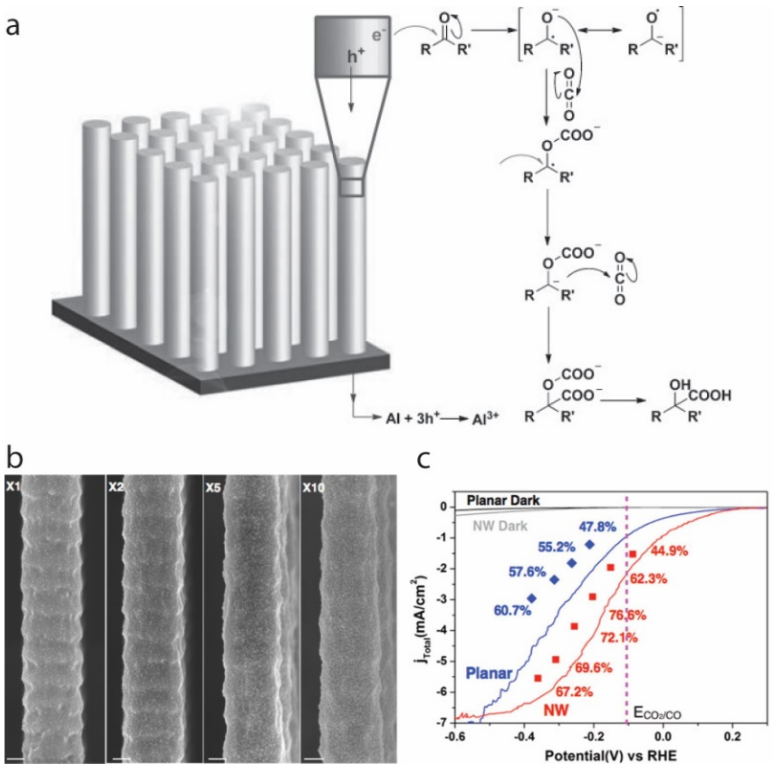

Figure 14. (a) Proposed mechanism of the solar-driven homogeneous CO_2 fixation with ketone as the substrate and Si nanowires as the light absorber. Reprinted with permission from ref[79]. Copyright 2012 John Wiley & Sons, Inc. (b) SEM images (scale bar 200 nm) of the uniformly deposited Au_3Cu nanoparticles on Si nanowires. Numbers indicate loading amounts that have been proportionally varied. (c) Comparison between Au_3Cu assembled planar photoelectrode and nanowire photoelectrode for photoelectrochemical CO_2 reduction. Solid lines show the linear sweep voltammetry. Each point indicates the total current density obtained from chronoamperometry and the numbers represent faraday efficiency toward CO. (b-c) Reprinted with permission from ref[81]. Copyright 2016 American Chemical Society.

Heterogeneous photoelectrochemical CO_2 reduction, where the CO_2 molecules are typically reduced at the interface between a metal-modified photocathode materials and the liquid electrolyte, has been intensively investigated in the past few decade.[227,229,235] While a lot of efforts have been focused on the design of metal catalyst, the introduction of the nanostructured photocathode, in particular nanowire morphology, has demonstrated substantial advantages. Choi and co-workers fabricated *p*-type Si nanowire arrays, where Sn nanoparticles are deposited as catalysts to specifically convert CO_2 into formate.[77] Such photocathode displayed a 0.5 V more anodic onset potential, a significantly enhanced photocurrent, and a five times enhancement in

formate production in comparison with the planar counterpart, thanks to the reduced reflectance and efficient electron transfer along the radial direction of the Si nanowire. Kong *et al.* reported that the Si nanowire arrays can guide the uniform spatial arrangement of Au_3Cu nanoparticles on the nanowire's surface (Figure 14b), while the nanoparticles tend to form isolated islands on a planar Si electrode.[81] A reduced overpotential of 120 mV compared to the planar counterpart was observed originated from the well-dispersed assembly of nanoparticles on the nanowire's surface (Figure 14c). Such well-defined semiconductor-catalyst interface enables efficient photoelectrochemical CO_2 reduction to CO, with the faraday efficiency close to 80% at –0.2 V *vs.* RHE. Efforts have also been put to investigate photoelectrochemical CO_2 reduction on III-V nanowire materials. Qiu *et al*. claimed that TiO_2-passivated InP nanopillars can reduce CO_2 into methanol with a faraday efficiency of 4.79%.[179] It was suggested that the O vacancies at the TiO_2 surface can facilitate the formation of CO_2^- intermediate and thus serve as catalytically active sites in the CO_2 reduction process. Deposition of Cu nanoparticle catalysts on the InP nanopillar's surface can further enhance the methanol faraday efficiency up to 8.7%. Mi's group has actively studied photoelectrochemical CO_2 reduction on GaN nanowires that modified by different metal nanoparticles. Taking advantage of the low defect density and high surface area of the GaN nanowires, it was shown that the as-grown nanowires can photocatalytically reduce CO_2 into CO, while the introduction of the Pt catalyst significantly enhances the CH_4 production by nearly one order of magnitude.[83] Such enhancement is attributed to the effective separation of the hot carriers and the reduction of CO_2 activation barrier by Pt nanoparticles. Furthermore, it was shown that deposition of metal catalyst on the oxide-passivated GaN nanowires can photoelectrochemically produce syngas with tunable ratio between CO and H_2. Specifically, Chu *et al*. fabricated a Cu/ZnO/GaN nanowire structure and obtained syngas products with CO/H_2 ratio ranging from 2:1 to 1:4.[82] Impressively, a high faraday efficiency of 70% for CO was observed at overpotential as low as 180 mV. It was suggested that such efficient syngas production is attributed to the synergistic co-catalytic effect between ZnO and Cu. Chu *et al*. further improved the photoelectrochemical syngas production by sequential deposition of Pt nanoparticles and ultrathin

TiO_2 on the GaN nanowires.[84] As the Pt/TiO_2 interface provides multifunctional sites for CO_2 activation and conversion, the resulting structure yielded a solar-to-syngas efficiency of 0.87%, a high turnover number of 24800 and a wide-range CO/H_2 ratio between 4:1 and 1:6. In order to circumvent the use of noble-metal catalyst, Rajeshwar and co-workers developed a two-step approach to synthesize the CuO/Cu_2O core-shell nanorod array photocathode.[85] An impressive faraday efficiency of 95% toward methanol can be realized at an underpotential greater than 150 mV. Such efficient CO_2 conversion is attributed to double electron transfer pathway from both the CuO core and the Cu_2O shell to the CO_2 molecules in the electrolyte. Taking advantage of the superior activity and product selectivity, biological catalysts recently have been integrated with semiconductor materials for solar-driven CO_2 conversion. Liu *et al*. reported that Si nanowires can serve as a bio-compatible photocathode to interface with *Sporomusa Ovata* to specifically convert CO_2 into acetic acid.[34] Compare to the planar counterpart, the unique nanowire geometry prevents the diffusion of the O_2 molecules, and thus provide an O_2-free local environment for the anaerobic bacteria to live and function.

3.2.3 Photoelectrochemical and photocatalytic reduction of dinitrogen

Ammonia (NH_3) is essential in agriculture and many industry processes. The invention of Haber-Bosch process to synthesize NH_3 from N_2 and H_2 has greatly changed the way that the food is produced, and contributed ~50% of the N atoms in humans today.[176] However, as high temperature (~700 K) and high pressure (~100 atm) are both required in the Haber-Bosch process, it is very energy-intensive and consumes nearly 2% of the annual energy output in the world. As a result, great efforts have been made to search for alternative approaches to synthesizing NH_3 at mild conditions. Photoelectrochemical/photocatalytic N_2 reduction, where N_2 molecules are reduced at the semiconductor/liquid electrolyte interface with solar energy as the reaction driving force, represents a sustainable strategy for NH_3 synthesis.[228] However, the inertness of N≡N triple-bond, the sluggish reaction kinetics and the lack of efficient catalyst lead to major challenges for this reaction, especially the high overpotential and the poor selectivity of NH_3 over H_2.[238,239] Nanostructuring the semiconductor light absorber, particularly into a 1D nanowire/nanorod

morphology, can mitigate these issues by introducing several benefits as following: i) the high surface area of nanowire geometry allows more catalyst loading and promote the interaction between the light absorber and catalyst; ii) the flexible modification/functionalization of the nanowire's surface properties allows the stabilization the intermediate species of the multi-step N_2 reduction reaction; iii) the strong light trapping effect within nanowire array is favorable to generate the plasmonic effect for hot carrier injection.

Recently, Ali *et al*. demonstrated a plasmon-enhanced photoelectrochemical N_2-reducing platform, where black Si (bSi), Au nanoparticle (GNP) and Chromium (Cr) are used as the light absorber, catalyst and hole scavenger, respectively.[86] The Si nanowires provide a large surface area for a high loading of GNP (Figure 15a-b), and a strong light absorption and scattering environment where GNPs induce the plasmon-enhanced N_2 reduction. The resulting ammonia production scales linearly with the N_2 partial pressure, and a highest ammonia yield of 60 mg m^{-2} h^{-1} was observed at 7 atmosphere pressure (Figure 15c). Li and co-workers reported a photocatalytic N_2 fixation approach using Re cluster-decorated III-V nanowires.[87] It was suggested that the Re nanoclusters can be firmly and homogeneously anchored on the surface of GaN nanowires with a 5 wt% high loading. The Re/GaN interfacial Schottky junction with a 0.94 eV barrier height facilitates the photo-generated electron transfer to Re clusters, resulting in negatively-charged Re species to promote the cleavage of N≡N triple-bond. The incorporation of In element into GaN nanowires allows for the photoelectrochemical N_2 reduction under visible light regime. In addition, S. Wang *et al.* showed that the synthesized Bi_5O_7Br nanotubes can be used for solar-driven N_2 fixation in pure water, thanks to the light-switchable oxygen-vacancy on the surface of nanotubes.[41] It was indicated that the light-induced oxygen-vacancies serve as the catalytic sites that can trap and subsequently inject the photogenerated electrons to the absorbed N_2 molecules. The NH_3 generation rate of these nanotubes was 1.38 mmol h^{-1} g^{-1} (2.5 times higher than nanosheet counterpart), with a quantum efficiency of 2.3% under 420 nm illumination. β-Ga_2O_3 nanorod was used as photocatalyst for N_2 photofixation by Zhao *et al*.[240] The photoactivity of β-Ga_2O_3 nanorod was promoted by using alcohols (methanol, ethanol, *n*-propanol and *n*-butanol)

as hole scavengers. The highest quantum yield of 36.1% was observed when butanol was used, attributed to the *in-situ* formed indirect electronic transmitter $^{\bullet}CO_2^-$. Brown *et al*. designed a biomimetic CdS/MoFe protein hybrid system for solar-driven N_2 reduction.[88] In such bio-inorganic hybrid design, the CdS nanorod serves as a photosensitizer to provide photogenerated electrons to nitrogenase MoFe protein, where the enzymatic reduction of N_2 to NH_3 is carried out (Figure 15d). This system shows a turnover rate of 75 per minute (Figure 15e), which is comparable with the ATP-coupled reaction rate for the nitrogenase complex. It was suggested that the high performance may be attributed to the strong binding between the CdS nanorod and the protein, which could induce the protein conformation changes necessary for N_2 reduction that normally occur in biological systems.

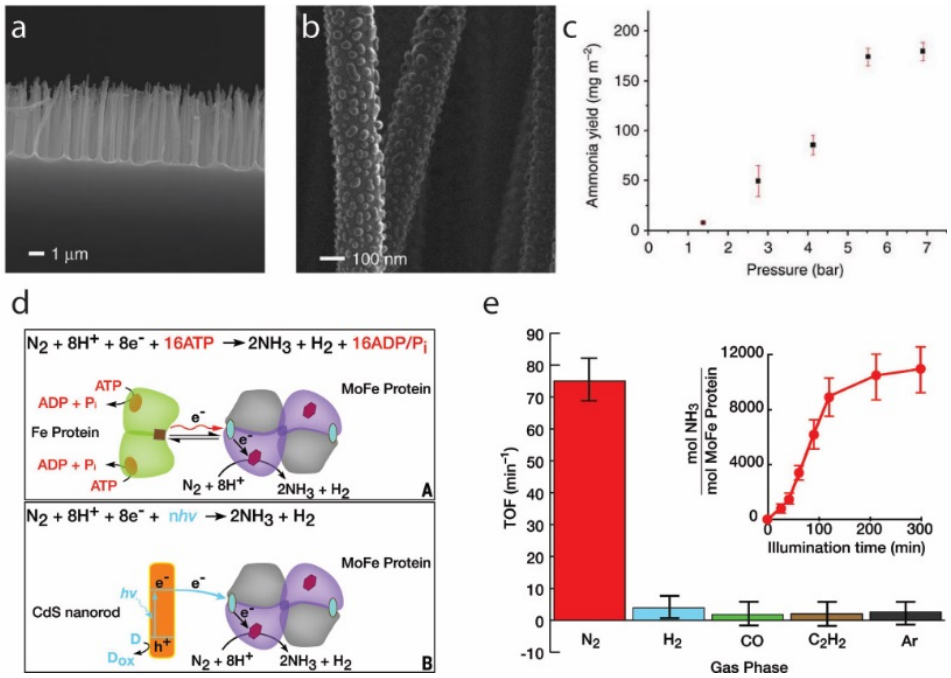

Figure 15. (a) Cross-sectional and (b) magnified SEM images of the GNP-coated bSi for photoelectrochemical N_2 reduction. (c) Ammonia production of GNP/bSi/Cr photoelectrochemical cell as a function of nitrogen gas pressure. (a-c) Reprinted with permission from ref[86]. Copyright 2016 Nature Publishing Group. (d) Reaction scheme of N_2 reduction by nitrogenase (upper) and the CdS:MoFe protein bio-inorganic hybrid system (lower). (e) Evaluation of N_2-reducing activity by the CdS:MoFe protein bio-inorganic hybrid system. (d-e) Reprinted with permission from ref[88]. Copyright 2016 American Association for the Advancement of Science.

4. Fundamentals of photoelectrochemistry at single-nanowire level

Although considerable research efforts have been focused on studying nanowire array photoelectrode, the heterogeneity in geometry, doping, defects density and catalyst loading typically present in such arrays can obscure the link between these properties and the photoelectrochemical performance of the nanowires, and correlating performance with the specific properties of individual nanowires is difficult because of the ensemble averaging.[241,242] In addition, the physical and chemical interactions between individual nanowires within the arrays, such as the light scattering and the diffusion of redox species, can significantly convolute our understanding on the nanowire's native properties and the fundamental reaction mechanisms.[243]

By overcoming the inhomogeneity found in arrays of nanowires, a single semiconductor nanowire device can provide a more precise link between the nanowire's properties and its photoelectrochemical/photocatalytic performance. By comparing the performance of individual nanowires with that of the ensemble arrays, we can in turn understand the impact of the inhomogeneity on the ensemble systems. In addition, controlling a single nanowire's properties, such as its geometry relative to the characteristic length scales of many fundamental processes that occur on the nano- and microscale, enables systematic investigations to determine the intrinsic limits of performance and optimal design of nanowire photoelectrodes. Moreover, a single-nanowire device can be flexibly coupled with other advanced characterization techniques, such as single-molecule fluorescence spectroscopy,[244,245] to understand the electron transport process and uncover the reaction mechanisms at the semiconductor/electrolyte interface. In this section, we will first discuss the state-of-art single-nanowire devices for photoelectrochemical characterizations beyond the ensemble averaging. In addition, we will also review the progress of single-molecule, single-particle fluorescence spectroscopy that can be used to uncover the reaction mechanisms during the photo(electro)catalytic process.

4.1 Single-nanowire photoelectrochemistry

A device composed of a single nanowire, a well-defined platform suitable for studying basic physical and chemical processes at the nanoscopic level, has been applied in electronics,[35] bio-

probing,[246] photovoltaics,[247,248] thermoelectrics[249] and electrochemistry.[250] Single-nanowire photoelectrochemistry is particularly challenging, because it requires the sophisticated manipulation of the device structure in order to avoid the interaction between individual nanowires and the contribution from the substrate. Recently, the Yang's group reported a unique single-nanowire photoelectrode platform (Figure 16a), which can reliably probe the photoelectrochemical behavior of individual nanowires.[251] Via the VLS approach, the single Si nanowires are vertically grown on electrically isolated Si electrodes, enabling the characterization of each nanowire individually (Figure 16b). The *J-V* characteristics yielded decent photoelectrochemical behavior with picoampere photocurrent sensitivity and tunable photovoltage output for devices with different doping profiles. In contrast to the inhomogeneity present in nanowire arrays, the well-defined geometry of a single nanowire in this study allows for the quantification of the photogenerated electron flux over the nanowire's surface, and provides quantitative information on the reduced overpotential owing to the nanowire's large surface area (Figure 16d). In addition, the authors observed that the photovoltage of the nanowire array devices is comparable with the lowest photovoltage of single nanowires (Figure 16c), indicating that the performance of ensemble array photoelectrode is largely affected by the worst performing individual nanowires within the array. This observation highlights the importance of controlling the homogeneity of the nanomaterials' quality, in order to produce efficient nanowire-based solar-to-fuel devices. Recently, Zhang *et al.* also reported single-nanowire photoelectrode device that is fabricated horizontally on the substrate.[92] By systematically tuning the diameter of the individual nanowires from 200 nm to 2000 nm, it was suggested that the diameter of 1415 nm yielded the highest solar energy conversion efficiency. The wavelength-dependent IPCE measurements suggested that the efficiency of single-nanowire photoelectrodes is determined by the diameter-dependent light absorption. Moreover, the photoelectrochemical behavior of individual nanowires can also be used to modulate the cellular activity. The Tian's group recently reported that the photocathodic effect generated by coaxial single nanowires can be harnessed to elicit action potentials in neuronal cells.[207] Taking advantage of patch-clamp setup, the photocurrent of free-standing individual

nanowires can be recorded. When the free-standing nanowire is interface with rat neuron cells, the photocurrent can induce action potentials with a minimum laser energy threshold. Furthermore, it was shown that the nanowires with atomic surface Au yield significantly enhanced photoelectrochemical current, in comparison to the Au-free counterpart. This result suggests that the atomic Au at the nanowire's surface is critical for the catalytic photoelectrochemical reaction and the generation of action potential in neurons. This approach opens up opportunities to optically control the cellular membrane potentials, which may be useful for advanced bioelectronics studies and photoresponsive therapeutics in the future.

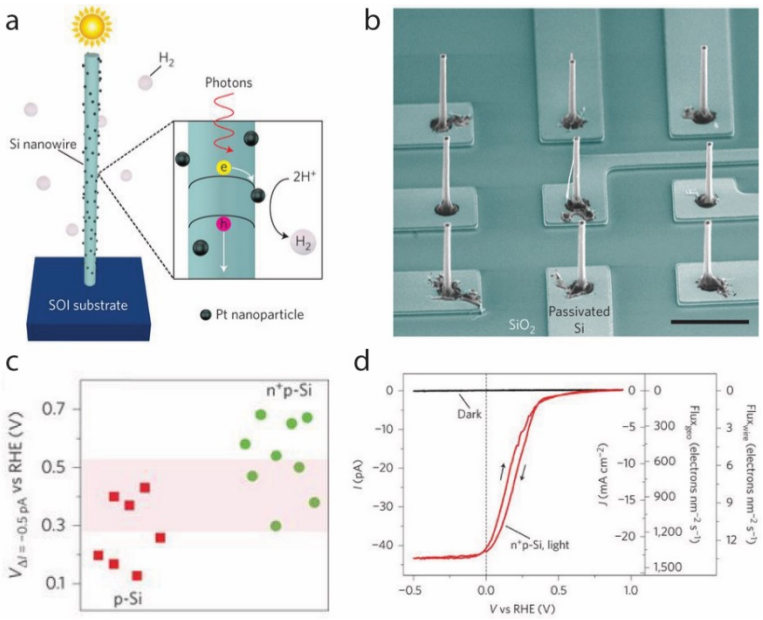

Figure 16. (a) Schematic of the single-nanowire device for photoelectrochemistry. (b) SEM image of the single-nanowire photoelectrodes. (c) Statistical analysis of onset potentials for single-nanowire photoelectrodes with *p* and n^+p doping profiles. (d) Photoelectrochemical behavior of a representative single-nanowire photoelectrode. (a-d) Reprinted with permission from ref[251]. Copyright 2016 Nature Publishing Group.

Single-nanowire photoelectrode platform can be also combined with other techniques to study the charge transfer fundamentals during photoelectrochemical processes. Liu *et al*. used Kelvin probe force microscopy (KPFM) to probe the transport of photogenerated electrons and holes within a single asymmetric Si/TiO_2 nanowire.[252] In their study, a *p*-Si/*n*-TiO_2 core-shell nanowire

is designed to explore the feasibility for direct solar water splitting, where the *n*-type TiO_2 and *p*-Si are proposed to behave as photoanode and photocathode, respective. Under illumination, KPFM observed higher surface potential on the *n*-TiO_2 shell, relative to the potential of the *p*-Si nanowire. This result suggests that the photogenerated holes and electrons tend to accumulate at *n*-TiO_2 and *p*-Si, respectively, with the recombination of majority carrier at the Si/TiO_2 interface. The efficient charge separation and transport indicate that the *p*-Si/*n*-TiO_2 core-shell nanowire is a promising building block for unassisted tandem solar water splitting. Spectroscopic techniques have also been employed to quantitatively investigate the photoinduced charge separation within a single-nanowire photo(electro)catalyst. In 2009, the Majima's group studied the behavior of photogenerated charge carriers in individual TiO_2 nanowires using photoluminescence (PL) spectroscopy.[253] The time trajectory of the PL intensity showed numerous burst-like features, which is believed to originate from the radiative recombination of electrons and holes at the color centers, such as the oxygen vacancies in TiO_2 nanowires. The quenching of the burst-like PL phenomenon with increased O_2 concentration suggests that the free electrons are quenched by the absorbed O_2 molecules following a Langmuir-Hinshelwood model. The potential-dependent PL spectra further revealed that the trapping sites are involved in the potential-induced PL process, and the energy level of the trapped electrons is considered to be –0.1 V to –0.3V *vs.* SHE. Moreover, the detection of the remote PL indicates long-distance transport of charge carriers, which can be explained by a trapping-detrapping model.

In addition to the representative techniques mentioned above, other characterization approaches including scanning electrochemical microscopy,[254] scanning photocurrent microscopy[255] and ultrafast transient absorption spectroscopy[256] have been widely applied to study the photoelectrochemical behavior on planar and nanowire array photoelectrodes. The integration between the state-of-art single-nanowire photo(electro)catalyst with these advanced characterization techniques may open up new opportunities to obtain further deep insights into the photoelectrochemical process.

4.2 Single-molecule, single-particle fluorescence spectroscopy

Although the single-nanowire photoelectrode platform is capable of obtaining nanoscopic insights that beyond the ensemble averaging, it can't provide comprehensive information regarding the photo(electro)catalytic reaction mechanisms. In addition, the heterogeneous distribution of defect and active sites within a single nanowire can blur our understanding on the defect/active site-dependent electron transfer process.[257] On the other hand, single molecule fluorescence spectroscopy is a powerful tool to image the fundamental photoelectrochemical/photochemical process with down to nanometer spatial resolution.[244,245] As a result, the combination of single-molecule fluorescence imaging with single-nanowire photoelectrode platform represents an intriguing approach to study the charge carrier activities of the photo(electro)catalysts with the highest possible sensitivity and spatial resolution. Here, we will give a brief review on the recent progress of single-molecule, single-particle fluorescence spectroscopy, with the focus on the one-dimensional TiO_2 photo(electro)catalysts.

In 2009, the Majima's group first reported the single-molecule imaging of photocatalytic reactions on a one-dimensional TiO_2 nanotube photocatalyst (Figure 17a).[258] A specific fluorescence probe, aminophenyl fluorescein (APF), was used to detect the hydroxyl radicals ($^{\bullet}OH$) generated during the photocatalytic process. When DMSO is added as a $^{\bullet}OH$ quencher, the fluorescence intensity is completely suppressed (Figure 17b). Distinguishable fluorescence time trajectories were observed for fluorescein products present in macropores and mesopores, indicating the positive correlation between the product diffusion rate and the pore size. In addition, the spatial-resolved fluorescence intensity on a single TiO_2 nanotube suggests a heterogeneous distribution of the active sites, which may be attributed to the intrinsic distribution of surface defects such as oxygen vacancies during the sample preparation. Single-molecule fluorescence imaging has widely been used to study the photocatalytic reaction mechanisms, particularly on individual TiO_2 nanorod photo(electro)catalyst. In 2012, Xu *et al*. found that the trapped holes and electrons on individual TiO_2 nanorod can both serve as active sites to produce the fluorescent molecules, while the trapped holes show relatively higher activity.[259] Specifically, the photogenerated electrons and hole can react with absorbed O_2 and H_2O molecules to yield $O_2^{-\bullet}$ and

$OH^{\bullet}$ radicals, respectively, which can both react with non-fluorescent amplex red to form the fluorescent product resorufin. By quenching one kind radical while keeping the other active, the activity of each radical can be separately identified. The fluorescence trajectory, coupled with the Langmuir-Hinshelwood model, quantitatively revealed that the absorption coefficient and net reactivity for reactions with $OH^{\bullet}$ as the oxidant have higher values than those with $O_2^{-\bullet}$ as the oxidant. These results can be explained by the positively-charged microenvironment around the trapped holes, which significantly enhance the absorption of the negatively-charged substrate molecules. In 2016, the Chen's group designed a single-TiO_2-nanorod photoanode platform, where the photoelectrooxidation mechanisms can be identified with single-molecule fluorescence.[260] By quantitatively characterizing the substrate oxidation rate as a function of the applied potential and light intensity, it was found that the oxidation rate scales with $(I_0)^{1/2}$ and $(E)^{1/4}$. Such correlation is consistent with the Gärtner model, and suggests that the organic substrate was oxidized indirectly via $OH^{\bullet}$ radicals instead of directly by photogenerated holes. Furthermore, Sambur *et al.* reported that the single-molecule fluorescence imaging can provide guidance for rational engineering the catalysts on the surface of the TiO_2 photoanode.[261] Taking advantage of the super-resolution imaging, the authors statistically analyzed the surface reaction rates along individual TiO_2 nanorod under different applied potentials (Figure 17c). By detecting the number of local fluorescence products in a certain period, it was found that the sites with high hole-induced reaction rates at more positive potentials also show high electron-induced reaction rates at more negative potentials. This result suggests that the photogenerated holes and electrons tend to reach the same sites on the TiO_2 nanorod surface, and thus the most active sites for water oxidation may also promote the electron-hole recombination. Furthermore, in order to quantify the benefits of the catalysts, oxygen evolution catalyst (OEC) was photoelectrochemically deposited onto either high- or low-activity sites that have been identified. By characterizing the onset potential and absorbed-photon-to-current efficiency (η) before and after the OEC deposition on a specific site, it was suggested that the locations with lowest initial activities achieve the most photocurrent enhancement or most reduced onset potentials from the OEC deposition. And the enhancement in photocurrent is not

necessarily accompanied by the negative shift in onset potential for the same OEC deposition site. These findings suggest a strategy to improve the performance of photoelectrodes by depositing catalysts onto selective positions.

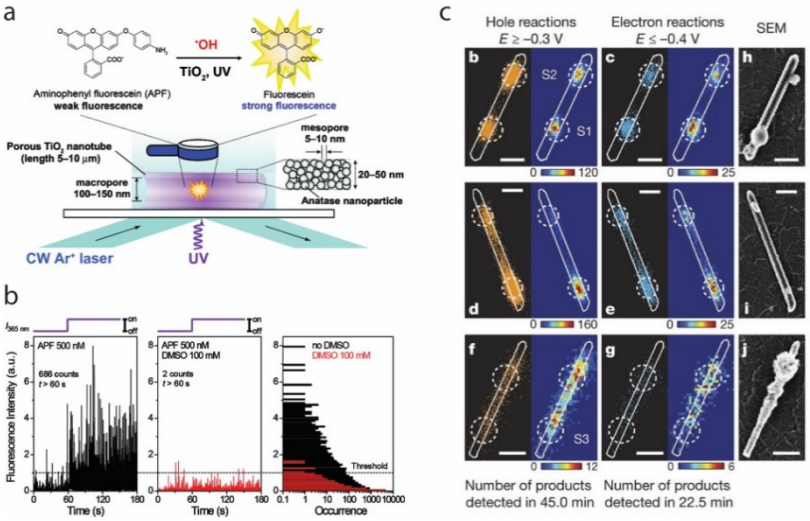

Figure 17. (a) Schematic illustration of the single-molecule fluorescence experiment to study the photocatalytic reaction in a single TiO_2 nanotube. (b) Time trajectories of the fluorescence intensity of the entire single TiO_2 nanotube in the absence (left) and presence (middle) of DMSO. The histograms of the fluorescence intensity are also shown (right). (a-b) Reprinted with permission from ref[258]. Copyright 2009 American Chemical Society. (c) Super-resolution mapping of the electron- and hole-induced reactions on the surface of individual TiO_2 nanorods. Reprinted with permission from ref[261]. Copyright 2016 Nature Publishing Group.

5. Integrated nanosystems for a closed cycle

5.1 Mimicking the microscopic assembly of natural photosynthesis

A completed solar-to-chemical cycle requires the participation of both oxidative and reduction half-reactions. In addition to the thermodynamic redox voltages set by the nature of chemical reactions, additional driving force in the form of photovoltages are needed in order to overcome the kinetic barriers and maintain a rate of reaction turnover.[10,262] This sets a quite restrictive limit on the choice of materials that can be applied. When only one light-absorber was considered in the process, only semiconductors of wide band-gap have been reported for a complete solar-to-fuel process, but the overall efficiency of the process was limited by the scarcity of high-energy photons

available in the solar spectrum.[263] Mimicking the "Z-scheme" in natural photosynthesis,[264,265] an integrated device for artificial photosynthesis requires the integration of two light-absorbers, commonly two semiconductor materials with well positioned band alignment, in order to carry out the photoanodic and photocathodic reactions with the eventual target of storing solar energy in chemical bonds in the absence of any additional energy supply.[12,13,22] Here, one semiconductor acts as photoanode for oxidation while the other one acts as photocathode for reduction, while an ohmic contact is established between these two semiconductor materials (Figure 18a). Under sunlight irradiation, photo-excited minority carriers move to the electrode/electrolyte interface for catalytic reactions, whereas the majority carriers recombine at the ohmic contact in order to complete the circuit (Figure 18a).[3,266-268] Depending on the exact configuration of the design, the nature of the ohmic contact could be metallic materials or a specific redox couple, termed as redox mediators, that shuttles between two semiconductors.[8,13,267] The possibility of integrating two semiconductor light-absorbers can be roughly evaluated based on their individual *I-V* curves when functioning as photocathode and photoanode. Taking water splitting as an example (Figure 18b), the intersection of the two independent curves suggests the maximum operating current density (J_{op}) for the overall water splitting. The maximum power generated for each component of the integrated system is illustrated by the red shaded area, while the power generated at the maximum operating current density is indicated by the blue shaded area (Figure 18b). When the points of J_{op} are close to their individual maximum power points (P_{PC} for photocathode and P_{PA} for photoanode), the highest solar-to-hydrogen efficiency could be obtained (Figure 18b). Inversely, if the $J_{op} \leq 0$, *i.e.* no crossover between the two curves, the directly serial combination of the two electrodes will not drive a water photo-electrolysis without additional energy input. Considering the steep increase of operating photocurrent density can be induced by a small change in the fill factor,[9,269,270] one way to dramatically enhance the solar-to-hydrogen efficiency is by increasing the *FF* and V_{oc} for one or both photoelectrodes.

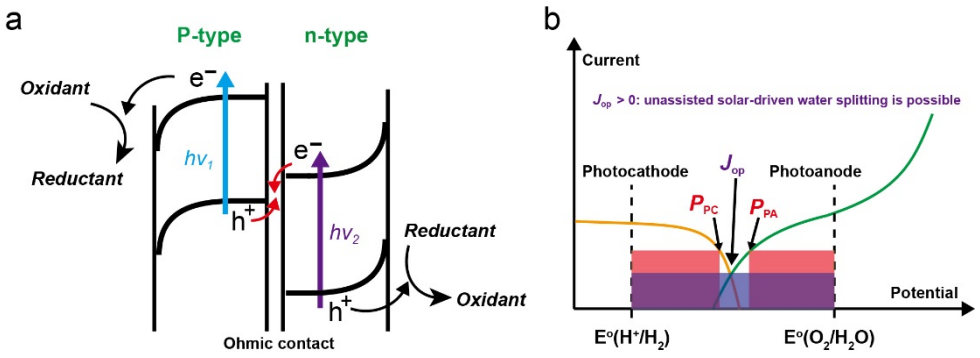

Figure 18. (a) Illustration of the "Z-scheme" by using two kinds of semiconductors with different band gaps. The photogenerated minority carriers move to the surface to drive a reduction (left) or oxidation (right) reaction, while the majority carriers recombine at the interface that linking the two semiconductors. (b) Compositive current-potential curves for both photocathode and photoanode with water splitting as an example. Thermodynamic potentials for H^+/H_2 and O_2/H_2O are presented as the dashed lines. J_{op} stands for the maximum operating current density, P_{PC} and P_{PA} stand for the individual maximum power points of photocathode and photoanode, respectively. Red shaded areas highlight the maximum power generated for each component of the integrated system, while blue shaded area highlights the power generated at the maximum operating current density.

The first report that mimics the "Z-scheme" concept for artificial photosynthesis is proposed by Art Nozik in the 1970s.[271] The central concept is to construct a photochemical diode by coupled two small bandgap materials as photocathode and photoanode, mimicking photosystems I and II in natural photosynthesis, for unassisted solar water splitting. The increased photocurrent as compared to the case of a single semicondutor,[21,47] promises spontaneous solar water splitting with high energy efficiencies. Such a design has inspired researchers in the passing decades and here we would like to provide some updates about the cases that nanowire photoelectrochemistry was applied.

5.2 Integrated artificial photosynthesis and its design principle

In the integrated "Z-scheme", charge carriers travel through both semiconductors in a tandem fashion. Therefore at working conditions the photocurrent flux from the photoanode and photocathode is the same. This indicates that an optimized device of high energy efficiency should have suitable band gaps and band alignments for both materials. Theoretical calculations have predicted that a pair of photoelectrodes with band gaps of approximately 1.1 and 1.7 eV should be

optimal for high efficiency when the factors of overpotentials and other losses are taken into consideration.[272,273] However, in practice the possible options of binary semiconductors with band gaps between 1.5 and 2.0 eV are limited (Figure 19a), not to mention the additional requirements of band alignment for optimal photovoltage output as well as fast charge transfer kinetics on the photoelectrodes' surface.[274] We posit that nanowire morphology can contribute to alleviate the challenges present above. With limited material options, nanowire morphology can help to reduce the overpotential for the charge transfer at the surface, which has been quantitatively illustrated in Figure 19b.[12] Such a reduction of overpotential will help increase *FF* and V_{oc} for the photoelectrodes. Since the J_{op} of the integrated "Z-scheme" system is quite sensitive to the overlap of *I-V* curves for photoelectrodes, the use of nanowires can help to increase J_{op} and subsequently energy efficiency in the "Z-scheme".

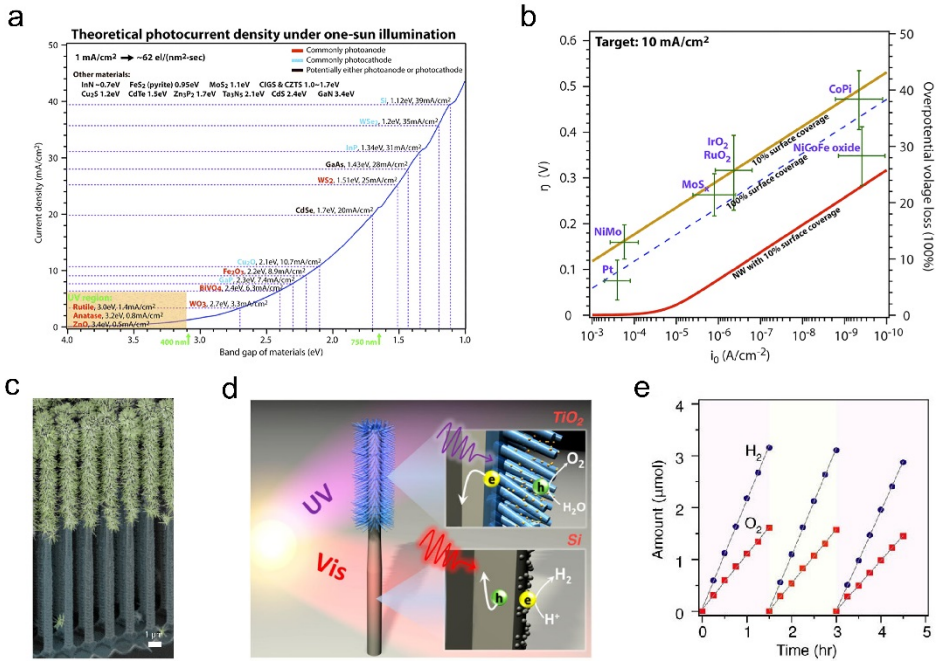

Figure 19. (a) Theoretical photocurrent densities versus the band gaps of semiconductors under one-sun illumination. Arrows at the bottom indicate the ultraviolet (below 400 nm), visible (400–750 nm), and infrared (beyond 750 nm) regions of the spectrum. Reprinted with permission from ref[4]. Copyright 2014 American Chemical Society. (b) Required overpotentials (η) to reach 10 mA cm^{-2} versus the exchange current densities (i_0) of planar electrodes loaded with various catalysts. Right y-axis shows the percentage of voltage lost, relative to the 1.23 V required thermodynamically to split water. The dashed blue curve is a calculation for 100% surface

coverage of the catalyst, while the yellow curve assumes only 10% surface coverage. The solid red curve indicates that a nanowire electrode with a roughness factor of 1000 and 10% catalyst coverage can significantly reduce the overpotential required to achieve the target current density. Reprinted with permission from ref[12]. Copyright 2015 The Royal Society of Chemistry. (c) A false-color SEM image of the asymmetric nanoscale tree-like heterostructures. (d) Schematics of the nanotrees used for solar-driven water splitting. The small diameter TiO_2 nanowires (blue) were grown on the upper half of a Si nanowire (gray), and the two semiconductors absorb different regions of the solar spectrum. The two insets display the photoexcited electron-hole pairs that are separated at the semiconductor-electrolyte interface to carry out water splitting with the help of cocatalysts (yellow and gray dots on the surface). (e) The nanotrees perform unbiased solar water splitting, producing a 2 to 1 ratio of hydrogen and oxygen. (c-e) Reprinted with permission from ref[17]. Copyright 2013 American Chemical Society.

An asymmetric nanowire composed of silicon core and TiO_2 shell (Si/TiO_2) was built to demonstrate the validity of charge separation within the integrated system.[252] KPFM was adopted to detect the local change of photovoltage on the asymmetric nanowire. Under illumination, higher surface potential was observed on TiO_2 side relative to the potential of Si side, due to the buildup of holes at TiO_2/electrolyte interface and electrons at Si/electrolyte interface. This indicates that an integrated nanostructure of Si/TiO_2 is feasible for unassisted solar-driven water-splitting.[252] Therefore, as a proof-of-concept, a solar-to-fuel device of Si and TiO_2 nanowires was integrated for solar water-splitting (Figure 19c-e).[17] Analogous with the natural photosynthesis, carefully designed at a microscopic scale in the tree-shaped Si/TiO_2 nanosystem was carried out by taking light-absorption, charge separation and chemical reactions all into consideration (Figure 19d).[17] The constructed nanosystem was at least one order of magnitude more active than the same composite without tree-shaped structure, and was capable of realizing comparable energy conversion efficiency to that of natural photosynthesis, even though TiO_2 photoanode remains as the bottleneck of overall performance.[17] Other combinations of redox reactions were also demonstrated on Si/TiO_2 nanotree structure.[275] With the use of hydrogen peroxide (H_2O_2) and 1,4-benzoquinone/hydroquinone (Q/QH_2) as the two redox reactions of interests, asymmetric Si/TiO_2 nanotree structure was developed as an artificial microswimmer. By controlling the zeta potential

of nanotree through chemical modification, the microswimmers with positive or negative phototaxis can be both successfully programmed.[275,276]

Materials combination other than Si and TiO_2 has been reported for unassisted solar water-splitting. Indium phosphide (InP) has been considered as a promising alternative to Si because of its relatively narrow bandgap (1.35-1.42 eV),[42,73] while bismuth vanadate ($BiVO_4$) shows advantages as photoanode materials with a relatively small band-gap.[17] InP nanowires have been integrated with nanoporous $BiVO_4$ for an overall reaction of water splitting at neutral pH.[277] The system generated 0.82 ± 0.04 mA per two electrodes with an area of 1 cm^2 each, corresponding to a solar-to-fuel efficiency of 0.5% for water splitting.[277]

A concept of bilayer nanowire fabrics was purposed in order to construct a low-cost and flexible PEC integrated system with facile production separation (Figure 20a).[21,47] In this design, the photoanode and photocathode, both made of nanowire meshes with high surface area, are physically connected for an ohmic contact. A proton transport medium will be placed between these two electrodes, and matching of current density is demanded to efficiently utilize the solar spectrum. A bilayer Ru/Rh-$SrTiO_3$ and $BiVO_4$ nanowire mesh film for unassisted solar overall water splitting was constructed as a proof of concept (Figure 20b-c). By employing such a bilayer nanowire mesh, it is possible to achieve simultaneous production and separation of H_2 an O_2 at the Ru/Rh-$SrTiO_3$ side and $BiVO_4$ side, respectively.[48] The Ru/Rh-$SrTiO_3$-$BiVO_4$ interface and the balance in light absorption by each nanowire mesh are both important for the H_2/O_2 evolution.[48] Additional effort such as the use of other semiconductor materials or the addition of conductive additives including graphene sheets and metallic carbon nanotubes, will potentially increase the overall reactivity of the integrated nanowire systems.[48]

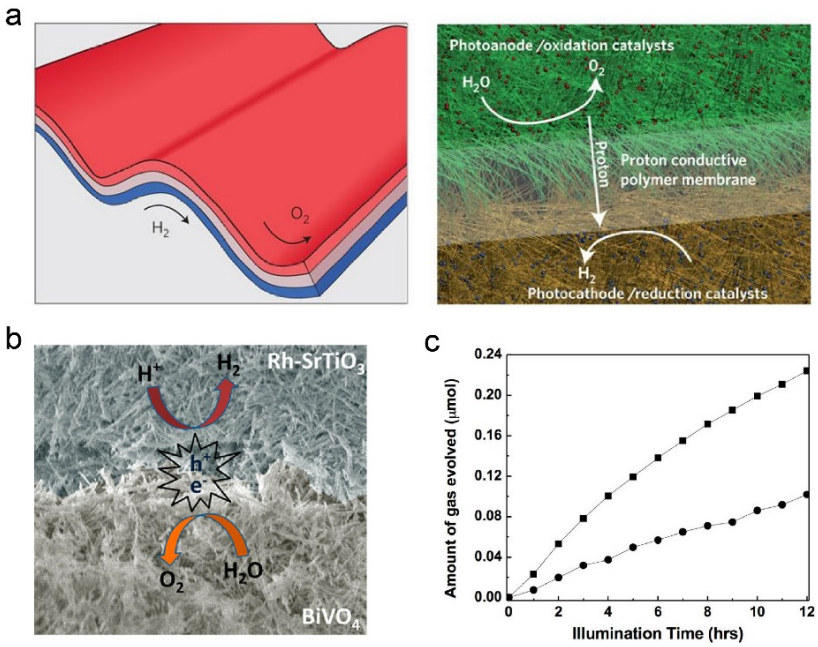

Figure 20. (a) Schematic illustration (left) and a zoomed-in view (right) of a bilayer nanowire fabric-based composite membrane for direct solar water-splitting. The top layer is a high-surface-area nanowire mesh decorated with oxidation catalysts. This part serves as a photoanode responsible for water oxidation; the bottom layer is a high-surface-area nanowire mesh decorated with reduction catalysts. This is the photocathode responsible for water reduction. Reprinted with permission from ref[47]. Copyright 2012 Nature Publishing Group. (b) Cross-sectional SEM image of bilayer Rh-$SrTiO_3$ and $BiVO_4$ nanowire mesh interface with illustration of the overall water splitting process. (c) Overall water splitting into hydrogen (■) and oxygen (●) using bilayer Ru/Rh-$SrTiO_3$ and $BiVO_4$ nanowire mesh film. (b-c) Reprinted with permission from ref[48]. Copyright 2014 American Chemical Society.

6. Conclusion and outlooks

The above discussions provide a summary of nanowire photoelectrochemistry. We examined the potential benefits of nanowires in photoelectrochemistry, different strategies that have been adopted when interfacing nanowires with other building blocks in artificial photosynthesis, and the current development of utilizing nanowires for a solar-powered chemical transformation. Since the inception of applying nanowires for photoelectrochemistry in 2002,[18] significant advances have taken place both at fundamental level and for practical applications. With so many excellent works that have been done, the question that we are now facing is: what's the next? In this section, we will not rephrase the benefits and achievements that have been discovered. Instead we strive to

provide a futuristic picture for the development of nanowires in photoelectrochemistry, by pointing out some of the exciting directions that this field may move towards. We hope that such a perspective will inspire new ideas of using nanowires, and motivate researchers in photoelectrochemistry and nanomaterials at large.

At fundamental level, our knowledge of the PEC process at the materials/liquid interface remains somewhat elusive. While the classic model of band-bending and the subsequent optoelectronic response is working well at macroscopic scale, the model per se neglects the possible heterogeneity on the materials' surface and there lacks a refined model at nanoscopic scale. For example, when nanoparticle catalyst is loaded at the interface between the semiconductors and electrolyte, it seems unclear how the presence of catalyst may affect the local band-bending. In literature people have applied different, sometimes contradicting, models to explain the experimental data. It is also intriguing to wonder what is the optimal distance among the loaded catalyst nanoparticles on the surface so that charge transfer of redox reactions can have high turnover rate yet the loaded catalyst won't perturb the band-bending significantly. We posit that a refined model of photoelectrochemistry at nanoscale can help to address some of the questions listed here. Nanowire morphology is a suitable well-defined platform to help develop such a nanoscopic model and current advances of studies at single-nanowire level is welcoming in such a context.

The range of chemical transformations and the entity that nanowires can interface with should be expanded. While the recent interests in photoelectrochemistry was largely inspired by the concept of artificial photosynthesis and the development of a solar-to-chemical process, the underlying principle of photoelectrochemistry does not restrict the interfacial redox reactions to these fuel-forming ones such as water splitting and the reduction of CO_2/N_2. We posit that it is possible to apply the PEC effect to other interesting chemical transformations that will be interesting to our society. Recent advances of electrochemically driven organic transformations[278,279] as well as the development of electricity-driven biochemical processes[280,281] illustrate some of the areas that photoelectrochemistry can contribute. The underlying hypothesis

is that unique chemical reactivities can arise from the band-bending and charge transfer processes in photoelectrochemistry, which is not available in other possible alternatives. Nanowire should gain a prominent role in the development of these PEC systems, as the large surface area of nanowires can magnify these proposed unique reactivities. In order to facilitate these proposed chemical transformations, a broader range of building blocks should be interfaced on the nanowire with a higher level of control at various length scales. While current research has demonstrated the interaction between nanowires with catalytic molecules, inorganic nanomaterials, and biocatalysts, there remains much room of advancement to fine-tune the interfacial interaction between them.

Last, sophisticated engineering and fabrication should continuously be devoted for a functional device. The natural photosynthetic system not only has the "Z-scheme" design that captures sunlight and yield energy-rich chemicals, but also contains the membrane that spatially separate the oxidation and reduction products. While a similar design has been envisioned for a while,[2,3] there haven't been a nanowire-based system that fully mimic both the solar chemistry and membrane-based separation of chemical products. The integration of nanowire building for a closed cycle in artificial photosynthesis has achieved much advance, yet additional efforts should be direct for a functional device. More broadly speaking, such an engineering effort at a system level[47] should not be limited only to the application of artificial photosynthesis, as any practical applications rely on the detailed design and system optimization.

Overall, even though here we present a "review" on the topic of nanowires in photoelectrochemistry, this article should not be a mere summary but a cornerstone for the scientific discoveries and breakthroughs in the future. The unique properties of nanowire photoelectrochemistry remain to be further explored. As Richard Feynman said, "there is plenty of room at the bottom", we posit that there is plenty of room for nanowire photoelectrochemistry so that this can be one of the tools that our society will wield against the challenges in energy, environment, and sustainability.

Author information

Corresponding authors

Emails: pyang@berkeley.edu (P. Y.); liubin@ntu.edu.sg (B. L.); chongliu@chem.ucla.edu (C. L.)

ORCID

Jiao Deng: 0000-0003-1008-6795

Yude Su: 0000-0002-3553-9458

Dong Liu: 0000-0002-3588-8762

Peidong Yang: 0000-0003-4799-1684

Bin Liu: 0000-0002-4685-2052

Chong Liu: 0000-0001-5546-3852

Present address

§ (Y. S.) Department of Chemistry, University of California, Santa Barbara

Notes

The authors declare no competing financial interests.

Biographies

Dr. Jiao Deng received his B. S. in Chemistry from Sichuan University, China in 2010. Under the supervision of Prof. Xinhe Bao and Prof. Dehui Deng, he obtained his Ph. D. degree in Physical chemistry in 2015 at Dalian Institute of Chemical Physics, Chinese Academy of Sciences. His PhD thesis focused on two-dimensional materials for renewable catalysis. After a short tenure as an *i*ChEM postdoctoral fellow at Xiamen University, Dr. Deng joined at 2017 as a postdoctoral fellow in Prof. Chong Liu's lab at the University of California, Los Angeles. His current research focuses on the electrocatalytic activation and conversion of small molecules.

Dr. Yude Su earned his bachelor's degree in Chemistry from University of Science and Technology of China in 2012. He joined Professor Peidong Yang's group and received his Ph.D. degree from the Department of Chemistry at U.C. Berkeley in 2017. He is currently a postdoctoral scholar working with Professor Guillermo Bazan in Center for Polymer and Organic Solids at U.C. Santa Barbara. His research interests include development of novel inorganic-biological hybrid systems for energy-conversion and energy-storage applications.

Dr. Dong Liu received his B.S. in chemistry (Special Class for the Gifted Young) in 2012, and Ph.D. in inorganic chemistry (Hefei National Laboratory for Physical Sciences at the Microscale) in 2017 from the University of Science and Technology of China. He is currently a research fellow in Prof. Bin Liu's research group at Nanyang Technological University. His research interests focus on developing solar-driven catalysis for valuable fuels and chemicals based on low-dimensional nanostructures.

Prof. Peidong Yang received a B.S. in chemistry from University of Science and Technology of China in 1993 and a Ph.D. in chemistry from Harvard University in 1997. He did postdoctoral research at University of California, Santa Barbara before joining the faculty in the Department of Chemistry at the University of California, Berkeley in 1999. He is currently professor in the

Department of Chemistry, Materials Science and Engineering and a senior faculty scientist at the Lawrence Berkeley National Laboratory. He is S. K. and Angela Chan Distinguished Chair Professor in Energy. He is the director for California Research Alliance by BASF and the Kavli Energy Nanoscience Institute.

Prof. Bin Liu received his B.Eng. (1st Class Honors) and M.Eng. degrees in Chemical Engineering from the National University of Singapore, and obtained his Ph.D. degree in Chemical Engineering from University of Minnesota in 2011. Thereafter, he moved to University of California, Berkeley and worked as a postdoctoral researcher under the supervision of Prof. Peidong Yang in Department of Chemistry during 2011 – 2012, before joining School of Chemical and Biomedical Engineering at Nanyang Technological University as an Assistant Professor in 2012. He is now an Associate Professor at NTU. His main research interests are electrocatalysis, photovoltaics and photoelectrochemistry.

Prof. Chong Liu received his B. S. in Chemistry in 2008 at Fudan University, China, during which he worked on mesoporous materials in the group of Prof. Dongyuan Zhao. Then he obtained his Ph. D. in Chemistry in 2014 under the supervision of Prof. Peidong Yang at University of California, Berkeley. His graduate research focused on the topic of artificial photosynthesis with semiconductor nanowires. During 2015 – 2017, He was a postdoctoral fellow in the group of Prof. Daniel Nocera at Harvard University, working on hybrid biological | inorganic systems for electricity-driven CO_2 and N_2 fixation. Since 2017, Dr. Liu has been working as an assistant professor at the University of California, Los Angeles. His research group focuses on the electrochemical activation of small molecules with a plethora of building blocks including organometallic complexes, nanomaterials, enzymes and microorganisms.

Acknowledgement

We would like to acknowledge Liwei Chang and Shuangmei Xue for the assistance of manuscript preparation. Y. S. acknowledges the graduate fellowship support from USTC-Suzhou Industrial Park; P. Y. acknowledges the U.S. Department of Energy, Office of Science, Basic Energy Sciences, Materials Sciences and Engineering Division under contract no. DE-AC02-05CH11231 (PChem KC3103). B. L. acknowledges funding support from Singapore Ministry of Education Academic Research Fund (AcRF): Tier 1: RG115/18, RG115/17 and RG9/17; Tier 2: MOE2016-T2-2-004. C. L. acknowledges the startup fund from the University of California, Los Angeles and the financial support of the Jeffery and Helo Zink Endowed Professional Development Term Chair.

References:

(1) Barber, J. Photosynthetic energy conversion: natural and artificial. *Chem. Soc. Rev.* **2009**, *38*, 185-196.

(2) Lewis, N. S.; Nocera, D. G. Powering the planet: chemical challenges in solar energy utilization. *Proc. Natl. Acad. Sci.* **2006**, *103*, 15729-15735.

(3) Gray, H. B. Powering the planet with solar fuel. *Nat. Chem.* **2009**, *1*, 7.

(4) Liu, C.; Dasgupta, N. P.; Yang, P. D. Semiconductor nanowires for artificial photosynthesis. *Chem. Mater.* **2014**, *26*, 415-422.

(5) Faunce, T. A.; Lubitz, W.; Rutherford, A. W.; MacFarlane, D.; Moore, G. F.; Yang, P.; Nocera, D. G.; Moore, T. A.; Gregory, D. H.; Fukuzumi, S. et al. Energy and environment policy case for a global project on artificial photosynthesis. *Energy Environ. Sci.* **2013**, *6*, 695-698.

(6) Faunce, T.; Styring, S.; Wasielewski, M. R.; Brudvig, G. W.; Rutherford, A. W.; Messinger, J.; Lee, A. F.; Hill, C. L.; Fontecave, M.; MacFarlane, D. R. Artificial photosynthesis as a frontier technology for energy sustainability. *Energy Environ. Sci.* **2013**, *6*, 1074-1076.

(7) Bequerel, E. Recherches sur les effects de la radiation chimique de la lumiere solaire, au moyen des courants electriques. *C. R. Acad. Sci.* **1839**, *9*, 145.

(8) Grätzel, M. Photoelectrochemical cells. *Nature* **2001**, *414*, 338-344.

(9) Walter, M. G.; Warren, E. L.; McKone, J. R.; Boettcher, S. W.; Mi, Q.; Santori, E. A.; Lewis, N. S. Solar water splitting cells. *Chem. Rev.* **2010**, *110*, 6446-6473.

(10) Tachibana, Y.; Vayssieres, L.; Durrant, J. R. Artificial photosynthesis for solar water-splitting. *Nat. Photon.* **2012**, *6*, 511-518.

(11) Licht, S. Multiple band gap semiconductor/electrolyte solar energy conversion. *J. Phys. Chem. B* **2001**, *105*, 6281-6294.

(12) Yang, P.; Brittman, S.; Liu, C. Semiconductor nanowires: from next-generation electronics to sustainable energy. Chapter 6. Nanowires for photovoltaics and artificial photosynthesis. *The Royal Society of Chemistry* **2015**, 277-311.

(13) Dasgupta, N. P.; Yang, P. Semiconductor nanowires for photovoltaic and photoelectrochemical energy conversion. *Front. Phys.* **2013**, *9*, 289-302.

(14) Yang, P.; Yan, R.; Fardy, M. Semiconductor nanowire: what's next? *Nano Lett.* **2010**, *10*, 1529-1536.

(15) Osterloh, F. E. Inorganic nanostructures for photoelectrochemical and photocatalytic water splitting. *Chem. Soc. Rev.* **2013**, *42*, 2294-2320.

(16) Hagfeldt, A.; Graetzel, M. Light-induced redox reactions in nanocrystalline systems. *Chem. Rev.* **1995**, *95*, 49-68.

(17) Liu, C.; Tang, J. Y.; Chen, H. M.; Liu, B.; Yang, P. D. A fully integrated nanosystem of semiconductor nanowires for direct solar water splitting. *Nano Lett.* **2013**, *13*, 2989-2992.

(18) Wu, Y. Y.; Yan, H. Q.; Yang, P. D. Semiconductor nanowire array: potential substrates for photocatalysis and photovoltaics. *Top. Catal.* **2002**, *19*, 197-202.

(19) Hochbaum, A. I.; Yang, P. Semiconductor nanowires for energy conversion. *Chem. Rev.*

2009, *110*, 527-546.
(20) Law, M.; Greene, L. E.; Johnson, J. C.; Saykally, R.; Yang, P. D. Nanowire dye-sensitized solar cells. *Nat. Mater.* **2005**, *4*, 455-459.
(21) Yang, P. Semiconductor nanowire building blocks: from flux line pinning to artificial photosynthesis. *Mrs. Bull.* **2012**, *37*, 806-813.
(22) Dasgupta, N. P.; Sun, J.; Liu, C.; Brittman, S.; Andrews, S. C.; Lim, J.; Gao, H.; Yan, R.; Yang, P. 25th anniversary article: semiconductor nanowires-synthesis, characterization, and applications. *Adv. Mater.* **2014**, *26*, 2137-2184.
(23) Xia, Y.; Yang, P.; Sun, Y.; Wu, Y.; Mayers, B.; Gates, B.; Yin, Y.; Kim, F.; Yan, H. One-dimensional nanostructures: synthesis, characterization, and applications. *Adv. Mater.* **2003**, *15*, 353-389.
(24) Yan, R.; Gargas, D.; Yang, P. Nanowire photonics. *Nat. Photon.* **2009**, *3*, 569-576.
(25) Law, M.; Goldberger, J.; Yang, P. Semiconductor nanowires and nanotubes. *Ann. Rev. Mater. Res.* **2004**, *34*, 83-122.
(26) Hu, J.; Odom, T. W.; Lieber, C. M. Chemistry and physics in one dimension: synthesis and properties of nanowires and nanotubes. *Acc. Chem. Res.* **1999**, *32*, 435-445.
(27) Alivisatos, A. P. Semiconductor clusters, nanocrystals, and quantum dots. *Science* **1996**, *271*, 933-937.
(28) Morales, A. M.; Lieber, C. M. A laser ablation method for the synthesis of crystalline semiconductor nanowires. *Science* **1998**, *279*, 208-211.
(29) Cui, Y.; Lieber, C. M. Functional nanoscale electronic devices assembled using silicon nanowire building blocks. *Science* **2001**, *291*, 851-853.
(30) Gudiksen, M. S.; Lauhon, L. J.; Wang, J.; Smith, D. C.; Lieber, C. M. Growth of nanowire superlattice structures for nanoscale photonics and electronics. *Nature* **2002**, *415*, 617-620.
(31) Duan, X.; Huang, Y.; Cui, Y.; Wang, J.; Lieber, C. M. Indium phosphide nanowires as building blocks for nanoscale electronic and optoelectronic devices. *Nature* **2001**, *409*, 66-69.
(32) Warren, E. L.; Atwater, H. A.; Lewis, N. S. Silicon microwire arrays for solar energy-conversion applications. *J. Phys. Chem. C* **2013**, *118*, 747-759.
(33) Sakimoto, K. K.; Kornienko, N.; Cestellos-Blanco, S.; Lim, J.; Liu, C.; Yang, P. Physical biology of the materials-microorganism interface. *J. Am. Chem. Soc.* **2018**, *140*, 1978-1985.
(34) Liu, C.; Gallagher, J. J.; Sakimoto, K. K.; Nichols, E. M.; Chang, C. J.; Chang, M. C.; Yang, P. Nanowire-bacteria hybrids for unassisted solar carbon dioxide fixation to value-added chemicals. *Nano Lett.* **2015**, *15*, 3634-3639.
(35) Cui, Y.; Wei, Q.; Park, H.; Lieber, C. M. Nanowire nanosensors for highly sensitive and selective detection of biological and chemical species. *Science* **2001**, *293*, 1289-1292.
(36) Bard, A. J.; Bocarsly, A. B.; Fan, F. R. F.; Walton, E. G.; Wrighton, M. S. The concept of Fermi level pinning at semiconductor-liquid junctions - consequences for energy-conversion efficiency and selection of useful solution redox couples in solar devices. *J. Am. Chem. Soc.* **1980**, *102*, 3671-3677.
(37) Chen, S.; Takata, T.; Domen, K. Particulate photocatalysts for overall water splitting. *Nat.*

Rev. Mater. **2017**, *2*, 17050.

(38) Hisatomi, T.; Kubota, J.; Domen, K. Recent advances in semiconductors for photocatalytic and photoelectrochemical water splitting. *Chem. Soc. Rev.* **2014**, *43*, 7520-7535.

(39) Foley, J. M.; Price, M. J.; Feldblyum, J. I.; Maldonado, S. Analysis of the operation of thin nanowire photoelectrodes for solar energy conversion. *Energy Environ. Sci.* **2012**, *5*, 5203-5220.

(40) Cho, I. S.; Chen, Z. B.; Forman, A. J.; Kim, D. R.; Rao, P. M.; Jaramillo, T. F.; Zheng, X. L. Branched TiO_2 nanorods for photoelectrochemical hydrogen Production. *Nano Lett.* **2011**, *11*, 4978-4984.

(41) Wang, S.; Hai, X.; Ding, X.; Chang, K.; Xiang, Y.; Meng, X.; Yang, Z.; Chen, H.; Ye, J. Light-switchable oxygen vacancies in ultrafine Bi_5O_7Br nanotubes for boosting solar-driven nitrogen fixation in pure water. *Adv. Mater.* **2017**, *29*, 1701774.

(42) Lee, M. H.; Takei, K.; Zhang, J.; Kapadia, R.; Zheng, M.; Chen, Y. Z.; Nah, J.; Matthews, T. S.; Chueh, Y. L.; Ager, J. W. et al. p-Type InP nanopillar photocathodes for efficient solar-driven hydrogen production. *Angew. Chem. Int. Ed.* **2012**, *51*, 10760-10764.

(43) Ding, Q.; Zhai, J. Y.; Caban-Acevedo, M.; Shearer, M. J.; Li, L. S.; Chang, H. C.; Tsai, M. L.; Ma, D. W.; Zhang, X. W.; Hamers, R. J. et al. Designing efficient solar-driven hydrogen evolution photocathodes using semitransparent MoQ_xCl_y (Q = S, Se) catalysts on Si micropyramids. *Adv. Mater.* **2015**, *27*, 6511-6518.

(44) Caban-Acevedo, M.; Stone, M. L.; Schmidt, J. R.; Thomas, J. G.; Ding, Q.; Chang, H. C.; Tsai, M. L.; He, J. H.; Jin, S. Efficient hydrogen evolution catalysis using ternary pyrite-type cobalt phosphosulphide. *Nat. Mater.* **2015**, *14*, 1245-1251.

(45) Han, S. E.; Chen, G. Optical absorption enhancement in silicon nanohole arrays for solar photovoltaics. *Nano Lett.* **2010**, *10*, 1012-1015.

(46) Li, L. S.; Yu, Y. H.; Meng, F.; Tan, Y. Z.; Hamers, R. J.; Jin, S. Facile solution synthesis of α-$FeF_3 \cdot 3H_2O$ nanowires and their conversion to α-Fe_2O_3 nanowires for photoelectrochemical application. *Nano Lett.* **2012**, *12*, 724-731.

(47) Yang, P. D.; Tarascon, J. M. Towards systems materials engineering. *Nat. Mater.* **2012**, *11*, 560-563.

(48) Liu, B.; Wu, C. H.; Miao, J. W.; Yang, P. D. All inorganic semiconductor nanowire mesh for direct solar water splitting. *ACS Nano* **2014**, *8*, 11739-11744.

(49) Xi, J. Q.; Schubert, M. F.; Kim, J. K.; Schubert, E. F.; Chen, M.; Lin, S.-Y.; Liu, W.; Smart, J. A. Optical thin-film materials with low refractive index for broadband elimination of Fresnel reflection. *Nat. Photon.* **2007**, *1*, 176-179.

(50) Huang, Y. F.; Chattopadhyay, S.; Jen, Y. J.; Peng, C. Y.; Liu, T. A.; Hsu, Y. K.; Pan, C. L.; Lo, H. C.; Hsu, C. H.; Chang, Y. H. et al. Improved broadband and quasi-omnidirectional anti-reflection properties with biomimetic silicon nanostructures. *Nat. Nanotechnol.* **2007**, *2*, 770-774.

(51) Sturmberg, B. C.; Dossou, K. B.; Botten, L. C.; Asatryan, A. A.; Poulton, C. G.; de Sterke, C. M.; McPhedran, R. C. Modal analysis of enhanced absorption in silicon nanowire arrays. *Opt. Express* **2011**, *19*, A1067-A1081.

(52) Kayes, B. M.; Atwater, H. A.; Lewis, N. S. Comparison of the device physics principles of planar and radial p-n junction nanorod solar cells. *J. Appl. Phys.* **2005**, *97*, 114302.
(53) Ling, Y. C.; Wang, G. M.; Wheeler, D. A.; Zhang, J. Z.; Li, Y. Sn-doped hematite nanostructures for photoelectrochemical water splitting. *Nano Lett.* **2011**, *11*, 2119-2125.
(54) Christesen, J. D.; Zhang, X.; Pinion, C. W.; Celano, T. A.; Flynn, C. J.; Cahoon, J. F. Design principles for photovoltaic devices based on Si nanowires with axial or radial p-n junctions. *Nano Lett.* **2012**, *12*, 6024-6029.
(55) Newman, J. S.; Tobias, C. W. Theoretical analysis of current distribution in porous electrodes. *J. Electrochem. Soc.* **1962**, *109*, 1183-1191.
(56) Lasia, A. Porous electrodes in the presence of a concentration gradient. *J. Electroanal. Chem.* **1997**, *428*, 155-164.
(57) Xiang, C. X.; Meng, A. C.; Lewis, N. S. Evaluation and optimization of mass transport of redox species in silicon microwire-array photoelectrodes. *Proc. Natl. Acad. Sci.* **2012**, *109*, 15622-15627.
(58) Liu, B.; Chen, H. M.; Liu, C.; Andrews, S. C.; Hahn, C.; Yang, P. Large-scale synthesis of transition-metal-doped TiO_2 nanowires with controllable overpotential. *J. Am. Chem. Soc.* **2013**, *135*, 9995-9998.
(59) Ai, G. J.; Li, H. X.; Liu, S. P.; Mo, R.; Zhong, J. X. Solar water splitting by TiO_2/CdS/Co-Pi nanowire array photoanode enhanced with Co-Pi as hole transfer relay and CdS as light absorber. *Adv. Funct. Mater.* **2015**, *25*, 5706-5713.
(60) Hwang, Y. J.; Hahn, C.; Liu, B.; Yang, P. Photoelectrochemical properties of TiO_2 nanowire arrays: a study of the dependence on length and atomic layer deposition coating. *ACS Nano* **2012**, *6*, 5060-5069.
(61) Chen, H. M.; Chen, C. K.; Chang, Y. C.; Tsai, C. W.; Liu, R. S.; Hu, S. F.; Chang, W. S.; Chen, K. H. Quantum dot monolayer sensitized ZnO nanowire-array photoelectrodes: true efficiency for water splitting. *Angew. Chem. Int. Ed.* **2010**, *49*, 5966-5969.
(62) Li, J.; Cushing, S. K.; Zheng, P.; Meng, F.; Chu, D.; Wu, N. Plasmon-induced photonic and energy-transfer enhancement of solar water splitting by a hematite nanorod array. *Nat. Commun.* **2013**, *4*, 2651.
(63) Mayer, M. T.; Du, C.; Wang, D. Hematite/Si nanowire dual-absorber system for photoelectrochemical water splitting at low applied potentials. *J. Am. Chem. Soc.* **2012**, *134*, 12406-12409.
(64) Rao, P. M.; Cai, L. L.; Liu, C.; Cho, I. S.; Lee, C. H.; Weisse, J. M.; Yang, P. D.; Zheng, X. L. Simultaneously efficient light absorption and charge separation in WO_3/$BiVO_4$ core/shell nanowire photoanode for photoelectrochemical water oxidation. *Nano Lett.* **2014**, *14*, 1099-1105.
(65) Li, Y. B.; Takata, T.; Cha, D.; Takanabe, K.; Minegishi, T.; Kubota, J.; Domen, K. Vertically aligned Ta_3N_5 nanorod arrays for solar-driven photoelectrochemical water splitting. *Adv. Mater.* **2013**, *25*, 125-131.
(66) Narkeviciute, I.; Chakthranont, P.; Mackus, A. J.; Hahn, C.; Pinaud, B. A.; Bent, S. F.; Jaramillo, T. F. Tandem core-shell Si-Ta_3N_5 photoanodes for photoelectrochemical water

splitting. *Nano Lett.* **2016**, *16*, 7565-7572.
(67) Liu, D.; Liu, J. C.; Cai, W. Z.; Ma, J.; Yang, H. B.; Xiao, H.; Li, J.; Xiong, Y. J.; Huang, Y. Q.; Liu, B. Selective photoelectrochemical oxidation of glycerol to high value-added dihydroxyacetone. *Nat. Commun.* **2019**, *10*, 1779.
(68) Cha, H. G.; Choi, K. S. Combined biomass valorization and hydrogen production in a photoelectrochemical cell. *Nat. Chem.* **2015**, *7*, 328-333.
(69) Oh, I.; Kye, J.; Hwang, S. Enhanced photoelectrochemical hydrogen production from silicon nanowire array photocathode. *Nano Lett.* **2012**, *12*, 298-302.
(70) Dasgupta, N. P.; Liu, C.; Andrews, S.; Prinz, F. B.; Yang, P. Atomic layer deposition of platinum catalysts on nanowire surfaces for photoelectrochemical water reduction. *J. Am. Chem. Soc.* **2013**, *135*, 12932-12935.
(71) Dai, P.; Xie, J.; Mayer, M. T.; Yang, X.; Zhan, J.; Wang, D. Solar hydrogen generation by silicon nanowires modified with platinum nanoparticle catalysts by atomic layer deposition. *Angew. Chem. Int. Ed.* **2013**, *52*, 11119-11123.
(72) Zhang, L.; Liu, C.; Wong, A. B.; Resasco, J.; Yang, P. MoS_2-wrapped silicon nanowires for photoelectrochemical water reduction. *Nano Res.* **2014**, *8*, 281-287.
(73) Gao, L.; Cui, Y.; Wang, J.; Cavalli, A.; Standing, A.; Vu, T. T.; Verheijen, M. A.; Haverkort, J. E.; Bakkers, E. P.; Notten, P. H. Photoelectrochemical hydrogen production on InP nanowire arrays with molybdenum sulfide electrocatalysts. *Nano Lett.* **2014**, *14*, 3715-3719.
(74) Standing, A.; Assali, S.; Gao, L.; Verheijen, M. A.; Van Dam, D.; Cui, Y.; Notten, P. H.; Haverkort, J. E.; Bakkers, E. P. Efficient water reduction with gallium phosphide nanowires. *Nat. Commun.* **2015**, *6*, 7824.
(75) Luo, J.; Steier, L.; Son, M.-K.; Schreier, M.; Mayer, M. T.; Grätzel, M. Cu_2O nanowire photocathodes for efficient and durable solar water splitting. *Nano Lett.* **2016**, *16*, 1848-1857.
(76) Huang, Q.; Kang, F.; Liu, H.; Li, Q.; Xiao, X. Highly aligned Cu_2O/CuO/TiO_2 core/shell nanowire arrays as photocathodes for water photoelectrolysis. *J. Mater. Chem. A* **2013**, *1*, 2418-2425.
(77) Choi, S. K.; Kang, U.; Lee, S.; Ham, D. J.; Ji, S. M.; Park, H. Sn-coupled p-Si nanowire arrays for solar formate production from CO_2. *Adv. Energy Mater.* **2014**, *4*, 1301614.
(78) Liu, R.; Stephani, C.; Han, J. J.; Tan, K. L.; Wang, D. Silicon nanowires show improved performance as photocathode for catalyzed carbon dioxide photofixation. *Angew. Chem. Int. Ed.* **2013**, *52*, 4225-4228.
(79) Liu, R.; Yuan, G.; Joe, C. L.; Lightburn, T. E.; Tan, K. L.; Wang, D. Silicon nanowires as photoelectrodes for carbon dioxide fixation. *Angew. Chem. Int. Ed.* **2012**, *124*, 6813-6816.
(80) Torralba-Peñalver, E.; Luo, Y.; Compain, J.-D.; Chardon-Noblat, S.; Fabre, B. Selective catalytic electroreduction of CO_2 at silicon nanowires (SiNWs) photocathodes using non-noble metal-based manganese carbonyl bipyridyl molecular catalysts in solution and grafted onto SiNWs. *ACS Catal.* **2015**, *5*, 6138-6147.
(81) Kong, Q.; Kim, D.; Liu, C.; Yu, Y.; Su, Y.; Li, Y.; Yang, P. Directed assembly of

nanoparticle catalysts on nanowire photoelectrodes for photoelectrochemical CO_2 reduction. *Nano Lett.* **2016**, *16*, 5675-5680.

(82) Chu, S.; Fan, S.; Wang, Y.; Rossouw, D.; Wang, Y.; Botton, G. A.; Mi, Z. Tunable syngas production from CO_2 and H_2O in an aqueous photoelectrochemical cell. *Angew. Chem. Int. Ed.* **2016**, *55*, 14262-14266.

(83) AlOtaibi, B.; Fan, S.; Wang, D.; Ye, J.; Mi, Z. Wafer-level artificial photosynthesis for CO_2 reduction into CH_4 and CO using GaN nanowires. *ACS Catal.* **2015**, *5*, 5342-5348.

(84) Chu, S.; Ou, P.; Ghamari, P.; Vanka, S.; Zhou, B.; Shih, I.; Song, J.; Mi, Z. Photoelectrochemical CO_2 reduction into syngas with the metal/oxide interface. *J. Am. Chem. Soc.* **2018**, *140*, 7869-7877.

(85) Ghadimkhani, G.; de Tacconi, N. R.; Chanmanee, W.; Janaky, C.; Rajeshwar, K. Efficient solar photoelectrosynthesis of methanol from carbon dioxide using hybrid CuO-Cu_2O semiconductor nanorod arrays. *Chem. Commun.* **2013**, *49*, 1297-1299.

(86) Ali, M.; Zhou, F.; Chen, K.; Kotzur, C.; Xiao, C.; Bourgeois, L.; Zhang, X.; MacFarlane, D. R. Nanostructured photoelectrochemical solar cell for nitrogen reduction using plasmon-enhanced black silicon. *Nat. Commun.* **2016**, *7*, 11335.

(87) Li, L.; Wang, Y.; Vanka, S.; Mu, X.; Mi, Z.; Li, C. J. Nitrogen photofixation over III-nitride nanowires assisted by ruthenium clusters of low atomicity. *Angew. Chem. Int. Ed.* **2017**, *56*, 8701-8705.

(88) Brown, K. A.; Harris, D. F.; Wilker, M. B.; Rasmussen, A.; Khadka, N.; Hamby, H.; Keable, S.; Dukovic, G.; Peters, J. W.; Seefeldt, L. C. Light-driven dinitrogen reduction catalyzed by a CdS: nitrogenase MoFe protein biohybrid. *Science* **2016**, *352*, 448-450.

(89) Hagedorn, K.; Forgacs, C.; Collins, S.; Maldonado, S. Design considerations for nanowire heterojunctions in solar energy conversion/storage applications. *J. Phys. Chem. C* **2010**, *114*, 12010-12017.

(90) Garnett, E.; Yang, P. Light trapping in silicon nanowire solar cells. *Nano Lett.* **2010**, *10*, 1082-1087.

(91) Liu, C.; Sun, J.; Tang, J.; Yang, P. Zn-doped p-type gallium phosphide nanowire photocathodes from a surfactant-free solution synthesis. *Nano Lett.* **2012**, *12*, 5407-5411.

(92) Zhang, B. C.; Wang, H.; He, L.; Duan, C. Y.; Li, F.; Ou, X. M.; Sun, B. Q.; Zhang, X. H. The diameter-dependent photoelectrochemical performance of silicon nanowires. *Chem. Commun.* **2016**, *52*, 1369-1372.

(93) Hu, L.; Chen, G. Analysis of optical absorption in silicon nanowire arrays for photovoltaic applications. *Nano Lett.* **2007**, *7*, 3249-3252.

(94) Retamal, J. R. D.; Chen, C. Y.; Lien, D. H.; Huang, M. R. S.; Lin, C. A.; Liu, C. P.; He, J. H. Concurrent improvement in photogain and speed of a metal oxide nanowire photodetector through enhancing surface band bending via incorporating a nanoscale heterojunction. *Acs Photonics* **2014**, *1*, 354-359.

(95) Chen, M. W.; Retamal, J. R. D.; Chen, C. Y.; He, J. H. Photocarrier relaxation behavior of a single ZnO nanowire UV photodetector: effect of surface band bending. *Ieee. Electr. Device. L* **2012**, *33*, 411-413.

(96) Varadhan, P.; Fu, H. C.; Priante, D.; Retamal, J. R. D.; Zhao, C.; Ebaid, M.; Ng, T. K.; Ajia, I.; Mitra, S.; Roqan, I. S. et al. Surface passivation of GaN nanowires for enhanced photoelectrochemical water-splitting. *Nano Lett.* **2017**, *17*, 1520-1528.

(97) Zhao, C.; Ng, T. K.; Prabaswara, A.; Conroy, M.; Jahangir, S.; Frost, T.; O'Connell, J.; Holmes, J. D.; Parbrook, P. J.; Bhattacharya, P. et al. An enhanced surface passivation effect in InGaN/GaN disk-in-nanowire light emitting diodes for mitigating Shockley-Read-Hall recombination. *Nanoscale* **2015**, *7*, 16658-16665.

(98) Li, S. P.; Zhang, P.; Song, X. F.; Gao, L. Photoelectrochemical hydrogen production of TiO_2 passivated Pt/Si-nanowire composite photocathode. *Acs Appl. Mater. Interfaces* **2015**, *7*, 18560-18565.

(99) Hu, S.; Shaner, M. R.; Beardslee, J. A.; Lichterman, M.; Brunschwig, B. S.; Lewis, N. S. Amorphous TiO_2 coatings stabilize Si, GaAs, and GaP photoanodes for efficient water oxidation. *Science* **2014**, *344*, 1005-1009.

(100) Kenney, M. J.; Gong, M.; Li, Y. G.; Wu, J. Z.; Feng, J.; Lanza, M.; Dai, H. J. High-performance silicon photoanodes passivated with ultrathin nickel films for water oxidation. *Science* **2013**, *342*, 836-840.

(101) Chen, Y. W.; Prange, J. D.; Duhnen, S.; Park, Y.; Gunji, M.; Chidsey, C. E. D.; McIntyre, P. C. Atomic layer-deposited tunnel oxide stabilizes silicon photoanodes for water oxidation. *Nat. Mater.* **2011**, *10*, 539-544.

(102) Shan, B.; Vanka, S.; Li, T. T.; Troian-Gautier, L.; Brennaman, M. K.; Mi, Z. T.; Meyer, T. J. Binary molecular-semiconductor p-n junctions for photoelectrocatalytic CO_2 reduction. *Nat. Energy* **2019**, *4*, 290-299.

(103) Zheng, J. Y.; Lyu, Y. H.; Wang, R. L.; Xie, C.; Zhou, H. J.; Jiang, S. P.; Wang, S. Y. Crystalline TiO_2 protective layer with graded oxygen defects for efficient and stable silicon-based photocathode. *Nat. Commun.* **2018**, *9*, 3572.

(104) Dasgupta, N. P.; Yang, P. Semiconductor nanowires for photovoltaic and photoelectrochemical energy conversion. *Front. Phys.* **2014**, *9*, 289-302.

(105) Hou, W.; Cronin, S. B. A review of surface plasmon resonance-enhanced photocatalysis. *Adv. Funct. Mater.* **2013**, *23*, 1612-1619.

(106) Lee, J. B.; Choi, S.; Kim, J.; Nam, Y. S. Plasmonically-assisted nanoarchitectures for solar water splitting: obstacles and breakthroughs. *Nano Today* **2017**, *16*, 61-81.

(107) Yang, J.; Wang, D.; Han, H.; Li, C. Roles of cocatalysts in photocatalysis and photoelectrocatalysis. *Acc. Chem. Res.* **2013**, *46*, 1900-1909.

(108) O'regan, B.; Grätzel, M. A low-cost, high-efficiency solar cell based on dye-sensitized colloidal TiO_2 films. *Nature* **1991**, *353*, 737-740.

(109) Youngblood, W. J.; Lee, S.-H. A.; Maeda, K.; Mallouk, T. E. Visible light water splitting using dye-sensitized oxide semiconductors. *Acc. Chem. Res.* **2009**, *42*, 1966-1973.

(110) Youngblood, W. J.; Lee, S.-H. A.; Kobayashi, Y.; Hernandez-Pagan, E. A.; Hoertz, P. G.; Moore, T. A.; Moore, A. L.; Gust, D.; Mallouk, T. E. Photoassisted overall water splitting in a visible light-absorbing dye-sensitized photoelectrochemical cell. *J. Am. Chem. Soc.* **2009**, *131*, 926-927.

(111) Swierk, J. R.; Mallouk, T. E. Design and development of photoanodes for water-splitting dye-sensitized photoelectrochemical cells. *Chem. Soc. Rev.* **2013**, *42*, 2357-2387.
(112) Alibabaei, L.; Sherman, B. D.; Norris, M. R.; Brennaman, M. K.; Meyer, T. J. Visible photoelectrochemical water splitting into H_2 and O_2 in a dye-sensitized photoelectrosynthesis cell. *Proc. Natl. Acad. Sci.* **2015**, *112*, 5899-5902.
(113) Xu, P.; Huang, T.; Huang, J.; Yan, Y.; Mallouk, T. E. Dye-sensitized photoelectrochemical water oxidation through a buried junction. *Proc. Natl. Acad. Sci.* **2018**, *115*, 6946-6951.
(114) Kibria, M. G.; Chowdhury, F. A.; Trudeau, M. L.; Guo, H.; Mi, Z. Dye-sensitized InGaN nanowire arrays for efficient hydrogen production under visible light irradiation. *Nanotechnology* **2015**, *26*, 285401.
(115) Dong, Y.-J.; Liao, J.-F.; Kong, Z.-C.; Xu, Y.-F.; Chen, Z.-J.; Chen, H.-Y.; Kuang, D.-B.; Fenske, D.; Su, C.-Y. Conformal coating of ultrathin metal-organic framework on semiconductor electrode for boosted photoelectrochemical water oxidation. *Appl. Catal. B* **2018**, *237*, 9-17.
(116) Zhang, L.; Cui, P.; Yang, H.; Chen, J.; Xiao, F.; Guo, Y.; Liu, Y.; Zhang, W.; Huo, F.; Liu, B. Metal-organic frameworks as promising photosensitizers for photoelectrochemical water splitting. *Adv. Sci.* **2016**, *3*, 1500243.
(117) Guo, C. X.; Dong, Y.; Yang, H. B.; Li, C. M. Graphene quantum dots as a green sensitizer to functionalize ZnO nanowire arrays on F-doped SnO_2 glass for enhanced photoelectrochemical water splitting. *Adv. Energy Mater.* **2013**, *3*, 997-1003.
(118) Fan, W.; Chen, C.; Bai, H.; Luo, B.; Shen, H.; Shi, W. Photosensitive polymer and semiconductors bridged by Au plasmon for photoelectrochemical water splitting. *Appl. Catal. B* **2016**, *195*, 9-15.
(119) Linic, S.; Christopher, P.; Ingram, D. B. Plasmonic-metal nanostructures for efficient conversion of solar to chemical energy. *Nat. Mater.* **2011**, *10*, 911-921.
(120) Chen, H. M.; Chen, C. K.; Chen, C.-J.; Cheng, L.-C.; Wu, P. C.; Cheng, B. H.; Ho, Y. Z.; Tseng, M. L.; Hsu, Y.-Y.; Chan, T.-S. Plasmon inducing effects for enhanced photoelectrochemical water splitting: X-ray absorption approach to electronic structures. *ACS Nano* **2012**, *6*, 7362-7372.
(121) Lin, Y.-G.; Hsu, Y.-K.; Chen, Y.-C.; Wang, S.-B.; Miller, J. T.; Chen, L.-C.; Chen, K.-H. Plasmonic $Ag@Ag_3(PO_4)_{1-x}$ nanoparticle photosensitized ZnO nanorod-array photoanodes for water oxidation. *Energy Environ. Sci.* **2012**, *5*, 8917.
(122) Li, J.; Cushing, S. K.; Zheng, P.; Senty, T.; Meng, F.; Bristow, A. D.; Manivannan, A.; Wu, N. Solar hydrogen generation by a CdS-Au-TiO_2 sandwich nanorod array enhanced with Au nanoparticle as electron relay and plasmonic photosensitizer. *J. Am. Chem. Soc.* **2014**, *136*, 8438-8449.
(123) Seh, Z. W.; Liu, S.; Low, M.; Zhang, S. Y.; Liu, Z.; Mlayah, A.; Han, M. Y. Janus Au-TiO_2 photocatalysts with strong localization of plasmonic near-fields for efficient visible-light hydrogen generation. *Adv. Mater.* **2012**, *24*, 2310-2314.
(124) Liu, D.; Yang, D.; Gao, Y.; Ma, J.; Long, R.; Wang, C.; Xiong, Y. Flexible near-infrared photovoltaic devices based on plasmonic hot-electron injection into silicon nanowire arrays.

Angew. Chem. Int. Ed. **2016**, *55*, 4577-4581.
(125) Li, S.; Zhang, J.; Kibria, M. G.; Mi, Z.; Chaker, M.; Ma, D.; Nechache, R.; Rosei, F. Remarkably enhanced photocatalytic activity of laser ablated Au nanoparticle decorated $BiFeO_3$ nanowires under visible-light. *Chem. Commun.* **2013**, *49*, 5856-5858.
(126) Xiao, F. X.; Hung, S. F.; Miao, J.; Wang, H. Y.; Yang, H.; Liu, B. Metal-cluster-decorated TiO_2 nanotube arrays: a composite heterostructure toward versatile photocatalytic and photoelectrochemical applications. *Small* **2015**, *11*, 554-567.
(127) Xiao, F. X.; Liu, B. In situ etching-induced self-assembly of metal cluster decorated one-dimensional semiconductors for solar-powered water splitting: unraveling cooperative synergy by photoelectrochemical investigations. *Nanoscale* **2017**, *9*, 17118-17132.
(128) Pu, Y. C.; Wang, G.; Chang, K. D.; Ling, Y.; Lin, Y. K.; Fitzmorris, B. C.; Liu, C. M.; Lu, X.; Tong, Y.; Zhang, J. Z. et al. Au nanostructure-decorated TiO_2 nanowires exhibiting photoactivity across entire UV-visible region for photoelectrochemical water splitting. *Nano Lett.* **2013**, *13*, 3817-3823.
(129) Wang, X.; Peng, K. Q.; Hu, Y.; Zhang, F. Q.; Hu, B.; Li, L.; Wang, M.; Meng, X. M.; Lee, S. T. Silicon/hematite core/shell nanowire array decorated with gold nanoparticles for unbiased solar water oxidation. *Nano Lett.* **2014**, *14*, 18-23.
(130) Wei, Y.; Kong, J.; Yang, L.; Ke, L.; Tan, H. R.; Liu, H.; Huang, Y.; Sun, X. W.; Lu, X.; Du, H. Polydopamine-assisted decoration of ZnO nanorods with Ag nanoparticles: an improved photoelectrochemical anode. *J. Mater. Chem. A* **2013**, *1*, 5045-5052.
(131) Wang, X.; Liow, C.; Qi, D.; Zhu, B.; Leow, W. R.; Wang, H.; Xue, C.; Chen, X.; Li, S. Programmable photo-electrochemical hydrogen evolution based on multi-segmented CdS-Au nanorod arrays. *Adv. Mater.* **2014**, *26*, 3506-3512.
(132) Shan, Z.; Clayton, D.; Pan, S.; Archana, P. S.; Gupta, A. Visible light driven photoelectrochemical properties of $Ti@TiO_2$ nanowire electrodes sensitized with core-shell $Ag@Ag_2S$ nanoparticles. *J. Phys. Chem. B* **2014**, *118*, 14037-14046.
(133) Zhang, X.; Liu, Y.; Kang, Z. H. 3D branched ZnO nanowire arrays decorated with plasmonic Au nanoparticles for high-performance photoelectrochemical water splitting. *Acs Appl. Mater. Interfaces* **2014**, *6*, 4480-4489.
(134) Duan, C.; Wang, H.; Ou, X.; Li, F.; Zhang, X. Efficient visible light photocatalyst fabricated by depositing plasmonic Ag nanoparticles on conductive polymer-protected Si nanowire arrays for photoelectrochemical hydrogen generation. *ACS Appl. Mater. Interfaces* **2014**, *6*, 9742-9750.
(135) DuChene, J. S.; Williams, B. P.; Johnston-Peck, A. C.; Qiu, J.; Gomes, M.; Amilhau, M.; Bejleri, D.; Weng, J.; Su, D.; Huo, F. et al. Elucidating the sole contribution from electromagnetic near-fields in plasmon-enhanced Cu_2O photocathodes. *Adv. Energy Mater.* **2016**, *6*, 1501250.
(136) Liu, Y.; Gu, Y.; Yan, X.; Kang, Z.; Lu, S.; Sun, Y.; Zhang, Y. Design of sandwich-structured ZnO/ZnS/Au photoanode for enhanced efficiency of photoelectrochemical water splitting. *Nano Res.* **2015**, *8*, 2891-2900.
(137) Wang, Y.; Fan, S.; AlOtaibi, B.; Wang, Y.; Li, L.; Mi, Z. A monolithically integrated

gallium nitride nanowire/silicon solar cell photocathode for selective carbon dioxide reduction to methane. *Chem. Eur. J.* **2016**, *22*, 8809-8813.

(138) Yang, X.; Li, H.; Zhang, W.; Sun, M.; Li, L.; Xu, N.; Wu, J.; Sun, J. High visible photoelectrochemical activity of Ag nanoparticle-sandwiched CdS/Ag/ZnO nanorods. *ACS Appl. Mater. Interfaces* **2017**, *9*, 658-667.

(139) Liu, Y.; Yan, X.; Kang, Z.; Li, Y.; Shen, Y.; Sun, Y.; Wang, L.; Zhang, Y. Synergistic effect of surface plasmonic particles and surface passivation layer on ZnO nanorods array for improved photoelectrochemical water splitting. *Sci. Rep.* **2016**, *6*, 29907.

(140) Li, H.; Li, Z.; Yu, Y.; Ma, Y.; Yang, W.; Wang, F.; Yin, X.; Wang, X. Surface-plasmon-resonance-enhanced photoelectrochemical water splitting from au-nanoparticle-decorated 3D TiO_2 nanorod architectures. *J. Phys. Chem. C* **2017**, *121*, 12071-12079.

(141) Kim, S.; Yu, Y.; Jeong, S. Y.; Lee, M. G.; Jeong, H. W.; Kwon, Y. M.; Baik, J. M.; Park, H.; Jang, H. W.; Lee, S. Plasmonic gold nanoparticle-decorated $BiVO_4$/ZnO nanowire heterostructure photoanodes for efficient water oxidation. *Catal. Sci. Technol.* **2018**, *8*, 3759-3766.

(142) Wang, L.; Wang, Y.; Schmuki, P.; Kment, S.; Zboril, R. Nanostar morphology of plasmonic particles strongly enhances photoelectrochemical water splitting of TiO_2 nanorods with superior incident photon-to-current conversion efficiency in visible/near-infrared region. *Electrochim. Acta* **2018**, *260*, 212-220.

(143) Wang, C.-C.; Chou, P.-H.; Yu, Y.-H.; Kei, C.-C. Deposition of Ni nanoparticles on black TiO_2 nanowire arrays for photoelectrochemical water splitting by atomic layer deposition. *Electrochim. Acta* **2018**, *284*, 211-219.

(144) Kumar, D.; Singh, S.; Khare, N. Plasmonic Ag nanoparticles decorated $NaNbO_3$ nanorods for efficient photoelectrochemical water splitting. *Int. J. Hydrogen Energy* **2018**, *43*, 8198-8205.

(145) Li, C.; Wang, P.; Li, H.; Wang, M.; Zhang, J.; Qi, G.; Jin, Y. Plasmon-driven water splitting enhancement on plasmonic metal-insulator-semiconductor hetero-nanostructures: unraveling the crucial role of interfacial engineering. *Nanoscale* **2018**, *10*, 14290-14297.

(146) Liu, D.; Ma, J.; Long, R.; Gao, C.; Xiong, Y. Silicon nanostructures for solar-driven catalytic applications. *Nano Today* **2017**, *17*, 96-116.

(147) Roger, I.; Shipman, M. A.; Symes, M. D. Earth-abundant catalysts for electrochemical and photoelectrochemical water splitting. *Nat. Rev. Chem.* **2017**, *1*, 0003.

(148) Bai, S.; Jiang, J.; Zhang, Q.; Xiong, Y. Steering charge kinetics in photocatalysis: intersection of materials syntheses, characterization techniques and theoretical simulations. *Chem. Soc. Rev.* **2015**, *44*, 2893-2939.

(149) Cao, S.; Yan, X.; Kang, Z.; Liang, Q.; Liao, X.; Zhang, Y. Band alignment engineering for improved performance and stability of $ZnFe_2O_4$ modified CdS/ZnO nanostructured photoanode for PEC water splitting. *Nano Energy* **2016**, *24*, 25-31.

(150) Yang, H. B.; Miao, J.; Hung, S.-F.; Huo, F.; Chen, H. M.; Liu, B. Stable quantum dot photoelectrolysis cell for unassisted visible light solar water splitting. *ACS Nano* **2014**, *8*, 10403-10413.

(151) Hensel, J.; Wang, G.; Li, Y.; Zhang, J. Z. Synergistic effect of CdSe quantum dot sensitization and nitrogen doping of TiO_2 nanostructures for photoelectrochemical solar hydrogen generation. *Nano Lett.* **2010**, *10*, 478-483.
(152) AlOtaibi, B.; Kong, X.; Vanka, S.; Woo, S. Y.; Pofelski, A.; Oudjedi, F.; Fan, S.; Kibria, M. G.; Botton, G. A.; Ji, W. et al. Photochemical carbon dioxide reduction on Mg-doped Ga(In)N nanowire arrays under visible light irradiation. *ACS Energy Lett.* **2016**, *1*, 246-252.
(153) Kibria, M. G.; Chowdhury, F. A.; Zhao, S.; AlOtaibi, B.; Trudeau, M. L.; Guo, H.; Mi, Z. Visible light-driven efficient overall water splitting using p-type metal-nitride nanowire arrays. *Nat. Commun.* **2015**, *6*, 6797.
(154) Wang, G.; Yang, X.; Qian, F.; Zhang, J. Z.; Li, Y. Double-sided CdS and CdSe quantum dot co-sensitized ZnO nanowire arrays for photoelectrochemical hydrogen generation. *Nano Lett.* **2010**, *10*, 1088-1092.
(155) Wang, H.; Bai, Y.; Zhang, H.; Zhang, Z.; Li, J.; Guo, L. CdS quantum dots-sensitized TiO_2 nanorod array on transparent conductive glass photoelectrodes. *J. Phys. Chem. C* **2010**, *114*, 16451-16455.
(156) Wang, H.; Wang, G.; Ling, Y.; Lepert, M.; Wang, C.; Zhang, J. Z.; Li, Y. Photoelectrochemical study of oxygen deficient TiO_2 nanowire arrays with CdS quantum dot sensitization. *Nanoscale* **2012**, *4*, 1463-1466.
(157) Wu, G.; Tian, M.; Chen, A. Synthesis of CdS quantum-dot sensitized TiO_2 nanowires with high photocatalytic activity for water splitting. *J. Photoch. Photobio A* **2012**, *233*, 65-71.
(158) Seol, M.; Jang, J.-W.; Cho, S.; Lee, J. S.; Yong, K. Highly efficient and stable cadmium chalcogenide quantum dot/ZnO nanowires for photoelectrochemical hydrogen generation. *Chem. Mater.* **2012**, *25*, 184-189.
(159) Shi, X.; Choi, I. Y.; Zhang, K.; Kwon, J.; Kim, D. Y.; Lee, J. K.; Oh, S. H.; Kim, J. K.; Park, J. H. Efficient photoelectrochemical hydrogen production from bismuth vanadate-decorated tungsten trioxide helix nanostructures. *Nat. Commun.* **2014**, *5*, 4775.
(160) Xiao, F. X.; Miao, J.; Wang, H. Y.; Yang, H.; Chen, J.; Liu, B. Electrochemical construction of hierarchically ordered CdSe-sensitized TiO_2 nanotube arrays: towards versatile photoelectrochemical water splitting and photoredox applications. *Nanoscale* **2014**, *6*, 6727-6237.
(161) Peng, Z.; Liu, Y.; Zhao, Y.; Chen, K.; Kovalev, V.; Chen, W. Photoelectrochemical behavior of TiO_2 nanorod arrays decorated with $CuInS_2$ quantum dots. *Appl. Surf. Sci.* **2014**, *292*, 514-519.
(162) Guo, C. X.; Xie, J.; Yang, H.; Li, C. M. Au@CdS core-shell nanoparticles-modified ZnO nanowires photoanode for efficient photoelectrochemical water splitting. *Adv. Sci.* **2015**, *2*, 1500135.
(163) Jin, B.; Jiao, Z.; Bi, Y. Efficient charge separation between Bi_2MoO_6 nanosheets and ZnO nanowires for enhanced photoelectrochemical properties. *J. Mater. Chem. A* **2015**, *3*, 19702-19705.
(164) Ning, F.; Shao, M.; Xu, S.; Fu, Y.; Zhang, R.; Wei, M.; Evans, D. G.; Duan, X.

TiO_2/graphene/NiFe-layered double hydroxide nanorod array photoanodes for efficient photoelectrochemical water splitting. *Energy Environ. Sci.* **2016**, *9*, 2633-2643.

(165) Zheng, X. L.; Dinh, C. T.; de Arquer, F. P.; Zhang, B.; Liu, M.; Voznyy, O.; Li, Y. Y.; Knight, G.; Hoogland, S.; Lu, Z. H. et al. $ZnFe_2O_4$ leaves grown on TiO_2 trees enhance photoelectrochemical water splitting. *Small* **2016**, *12*, 3181-3188.

(166) An, T.; Tang, J.; Zhang, Y.; Quan, Y.; Gong, X.; Al-Enizi, A. M.; Elzatahry, A. A.; Zhang, L.; Zheng, G. Photoelectrochemical conversion from graphitic C_3N_4 quantum dot decorated semiconductor nanowires. *ACS Appl. Mater. Interfaces* **2016**, *8*, 12772-12779.

(167) Mao, C.; Wang, Y.; Jiao, W.; Chen, X.; Lin, Q.; Deng, M.; Ling, Y.; Zhou, Y.; Bu, X.; Feng, P. Integrating zeolite-type chalcogenide with titanium dioxide nanowires for enhanced photoelectrochemical activity. *Langmuir* **2017**, *33*, 13634-13639.

(168) Pi, Y.; Li, Z.; Xu, D.; Liu, J.; Li, Y.; Zhang, F.; Zhang, G.; Peng, W.; Fan, X. 1T-phase MoS_2 nanosheets on TiO_2 nanorod arrays: 3D photoanode with extraordinary catalytic performance. *ACS Sustainable Chem. Eng.* **2017**, *5*, 5175-5182.

(169) Wang, M.; Han, K.; Zhang, S.; Sun, L. Integration of organometallic complexes with semiconductors and other nanomaterials for photocatalytic H_2 production. *Coord. Chem. Rev.* **2015**, *287*, 1-14.

(170) Hou, Y.; Abrams, B. L.; Vesborg, P. C.; Bjorketun, M. E.; Herbst, K.; Bech, L.; Setti, A. M.; Damsgaard, C. D.; Pedersen, T.; Hansen, O. et al. Bioinspired molecular co-catalysts bonded to a silicon photocathode for solar hydrogen evolution. *Nat. Mater.* **2011**, *10*, 434-438.

(171) Jiang, D.; Irfan, R. M.; Sun, Z.; Lu, D.; Du, P. Synergistic effect of a molecular cocatalyst and a heterojunction in a 1D semiconductor photocatalyst for robust and highly efficient solar hydrogen production. *ChemSusChem* **2016**, *9*, 3084-3092.

(172) Hou, Y.; Zhu, Z.; Xu, Y.; Guo, F.; Zhang, J.; Wang, X. Efficient photoelectrochemical hydrogen production over p-Si nanowire arrays coupled with molybdenum–sulfur clusters. *Int. J. Hydrogen Energy* **2017**, *42*, 2832-2838.

(173) Mange, Y. J.; Chandrasekaran, S.; Hollingsworth, N.; Voelcker, N. H.; Parkin, I. P.; Nann, T.; Macdonald, T. J. $\{Ni_4O_4\}$ cluster complex to enhance the reductive photocurrent response on silicon nanowire photocathodes. *Nanomaterials* **2017**, *7*, 33.

(174) Jin, T.; He, D.; Li, W.; Stanton, C. J.; Pantovich, S. A.; Majetich, G. F.; Schaefer, H. F.; Agarwal, J.; Wang, D.; Li, G. CO_2 reduction with Re(i)-NHC compounds: driving selective catalysis with a silicon nanowire photoelectrode. *Chem. Commun.* **2016**, *52*, 14258-14261.

(175) Seh, Z. W.; Kibsgaard, J.; Dickens, C. F.; Chorkendorff, I.; Norskov, J. K.; Jaramillo, T. F. Combining theory and experiment in electrocatalysis: insights into materials design. *Science* **2017**, *355*, eaad4998.

(176) Chen, J. G.; Crooks, R. M.; Seefeldt, L. C.; Bren, K. L.; Bullock, R. M.; Darensbourg, M. Y.; Holland, P. L.; Hoffman, B.; Janik, M. J.; Jones, A. K. et al. Beyond fossil fuel-driven nitrogen transformations. *Science* **2018**, *360*, eaar6611.

(177) Han, H. X.; Shi, C.; Zhang, N.; Yuan, L.; Sheng, G. P. Visible-light-enhanced Cr(VI) reduction at Pd-decorated silicon nanowire photocathode in photoelectrocatalytic

microbial fuel cell. *Sci. Total. Environ.* **2018**, *639*, 1512-1519.
(178) Sun, J.; Liu, C.; Yang, P. Surfactant-free, large-scale, solution-liquid-solid growth of gallium phosphide nanowires and their use for visible-light-driven hydrogen production from water reduction. *J. Am. Chem. Soc.* **2011**, *133*, 19306-19309.
(179) Qiu, J.; Zeng, G.; Ha, M. A.; Ge, M.; Lin, Y.; Hettick, M.; Hou, B.; Alexandrova, A. N.; Javey, A.; Cronin, S. B. Artificial photosynthesis on TiO_2-passivated InP nanopillars. *Nano Lett.* **2015**, *15*, 6177-6181.
(180) Sun, K.; Pang, X.; Shen, S.; Qian, X.; Cheung, J. S.; Wang, D. Metal oxide composite enabled nanotextured Si photoanode for efficient solar driven water oxidation. *Nano Lett.* **2013**, *13*, 2064-2072.
(181) Hu, D.; Xiang, J.; Zhou, Q.; Su, S.; Zhang, Z.; Wang, X.; Jin, M.; Nian, L.; Nozel, R.; Zhou, G. et al. One-step chemical vapor deposition of MoS_2 nanosheets on SiNWs as photocathodes for efficient and stable solar-driven hydrogen production. *Nanoscale* **2018**, *10*, 3518-3525.
(182) Tran, P. D.; Pramana, S. S.; Kale, V. S.; Nguyen, M.; Chiam, S. Y.; Batabyal, S. K.; Wong, L. H.; Barber, J.; Loo, J. Novel assembly of an MoS_2 electrocatalyst onto a silicon nanowire array electrode to construct a photocathode composed of elements abundant on the earth for hydrogen generation. *Chem. Eur. J* **2012**, *18*, 13994-13999.
(183) Long, L.-L.; Zhang, A.-Y.; Huang, Y.-X.; Zhang, X.; Yu, H.-Q. A robust cocatalyst Pd_4S uniformly anchored onto Bi_2S_3 nanorods for enhanced visible light photocatalysis. *J. Mater. Chem. A* **2015**, *3*, 4301-4306.
(184) Zhang, H.; Ding, Q.; He, D.; Liu, H.; Liu, W.; Li, Z.; Yang, B.; Zhang, X.; Lei, L.; Jin, S. A p-Si/NiCoSex core/shell nanopillar array photocathode for enhanced photoelectrochemical hydrogen production. *Energy Environ. Sci.* **2016**, *9*, 3113-3119.
(185) Bao, X. Q.; Fatima Cerqueira, M.; Alpuim, P.; Liu, L. Silicon nanowire arrays coupled with cobalt phosphide spheres as low-cost photocathodes for efficient solar hydrogen evolution. *Chem. Commun.* **2015**, *51*, 10742-10745.
(186) Huang, Z.; Chen, Z.; Chen, Z.; Lv, C.; Meng, H.; Zhang, C. $Ni_{12}P_5$ nanoparticles as an efficient catalyst for hydrogen generation via electrolysis and photoelectrolysis. *ACS Nano* **2014**, *8*, 8121-8129.
(187) Ai, G.; Mo, R.; Li, H.; Zhong, J. Cobalt phosphate modified TiO_2 nanowire arrays as co-catalysts for solar water splitting. *Nanoscale* **2015**, *7*, 6722-6728.
(188) Lv, C.; Chen, Z.; Chen, Z.; Zhang, B.; Qin, Y.; Huang, Z.; Zhang, C. Silicon nanowires loaded with iron phosphide for effective solar-driven hydrogen production. *J. Mater. Chem. A* **2015**, *3*, 17669-17675.
(189) Weng, B.; Wei, W.; Yiliguma, Y.; Wu, H.; Alenizi, A. M.; Zheng, G. Bifunctional CoP and CoN porous nanocatalysts derived from ZIF-67 in situ grown on nanowire photoelectrodes for efficient photoelectrochemical water splitting and CO_2 reduction. *J. Mater. Chem. A* **2016**, *4*, 15353-15360.
(190) Yang, Y.; Wang, M.; Zhang, P.; Wang, W.; Han, H.; Sun, L. Evident enhancement of photoelectrochemical hydrogen production by electroless deposition of M-B (M = Ni, Co)

catalysts on silicon nanowire arrays. *ACS Appl. Mater. Interfaces* **2016**, *8*, 30143-30151.
(191) Zhang, R.; Shao, M.; Xu, S.; Ning, F.; Zhou, L.; Wei, M. Photo-assisted synthesis of zinc-iron layered double hydroxides/TiO_2 nanoarrays toward highly-efficient photoelectrochemical water splitting. *Nano Energy* **2017**, *33*, 21-28.
(192) Sim, U.; Moon, J.; An, J.; Kang, J. H.; Jerng, S. E.; Moon, J.; Cho, S.-P.; Hong, B. H.; Nam, K. T. N-doped graphene quantum sheets on silicon nanowire photocathodes for hydrogen production. *Energy Environ. Sci.* **2015**, *8*, 1329-1338.
(193) Yang, K. D.; Ha, Y.; Sim, U.; An, J.; Lee, C. W.; Jin, K.; Kim, Y.; Park, J.; Hong, J. S.; Lee, J. H. et al. Graphene quantum sheet catalyzed silicon photocathode for selective CO_2 conversion to CO. *Adv. Funct. Mater.* **2016**, *26*, 233-242.
(194) Jin, J.; Yu, J.; Liu, G.; Wong, P. K. Single crystal CdS nanowires with high visible-light photocatalytic H_2-production performance. *J. Mater. Chem. A* **2013**, *1*, 10927-10934.
(195) Shen, M.; Yan, Z.; Yang, L.; Du, P.; Zhang, J.; Xiang, B. MoS_2 nanosheet/TiO_2 nanowire hybrid nanostructures for enhanced visible-light photocatalytic activities. *Chem. Commun.* **2014**, *50*, 15447-15449.
(196) Dai, D.; Xu, H.; Ge, L.; Han, C.; Gao, Y.; Li, S.; Lu, Y. In-situ synthesis of CoP co-catalyst decorated $Zn_{0.5}Cd_{0.5}S$ photocatalysts with enhanced photocatalytic hydrogen production activity under visible light irradiation. *Appl. Catal. B* **2017**, *217*, 429-436.
(197) Jang, J. S.; Joshi, U. A.; Lee, J. S. Solvothermal synthesis of CdS nanowires for photocatalytic hydrogen and electricity production. *J. Phys. Chem. C* **2007**, *111*, 13280-13287.
(198) Zhou, W.; Guan, Y.; Wang, D.; Zhang, X.; Liu, D.; Jiang, H.; Wang, J.; Liu, X.; Liu, H.; Chen, S. PdO/TiO_2 and Pd/TiO_2 heterostructured nanobelts with enhanced photocatalytic activity. *Chem. Asian J.* **2014**, *9*, 1648-1654.
(199) Xu, L.; Zhao, Y.; Owusu, K. A.; Zhuang, Z.; Liu, Q.; Wang, Z.; Li, Z.; Mai, L. Recent advances in nanowire-biosystem interfaces: from chemical conversion, energy production to electrophysiology. *Chem* **2018**, *4*, 1538-1559.
(200) Sakimoto, K. K.; Kornienko, N.; Yang, P. Cyborgian material design for solar fuel production: the emerging photosynthetic biohybrid systems. *Acc. Chem. Res.* **2017**, *50*, 476-481.
(201) Jeong, H. E.; Kim, I.; Karam, P.; Choi, H. J.; Yang, P. Bacterial recognition of silicon nanowire arrays. *Nano Lett.* **2013**, *13*, 2864-2869.
(202) Sakimoto, K. K.; Liu, C.; Lim, J.; Yang, P. Salt-induced self-assembly of bacteria on nanowire arrays. *Nano Lett.* **2014**, *14*, 5471-5476.
(203) Nevin, K. P.; Woodard, T. L.; Franks, A. E.; Summers, Z. M.; Lovley, D. R. Microbial electrosynthesis: feeding microbes electricity to convert carbon dioxide and water to multicarbon extracellular organic compounds. *Mbio* **2010**, *1*, e00103-10.
(204) Drake, H. L.; Gossner, A. S.; Daniel, S. L. Old acetogens, new light. *Ann. N. Y. Acda. Sci.* **2008**, *1125*, 100-128.
(205) Tang, J.; Zhang, Y. Y.; Kong, B.; Wang, Y. C.; Da, P. M.; Li, J.; Elzatahry, A. A.; Zhao, D. Y.; Gong, X. G.; Zheng, G. F. Solar-driven photoelectrochemical probing of

nanodot/nanowire/cell interface. *Nano Lett.* **2014**, *14*, 2702-2708.
(206) Zhu, Y. C.; Wang, Q.; Zhang, L. B.; Zhao, W. W.; Xu, J. J.; Chen, H. Y. Photoelectrochemical probing of cellular interfaces and evaluation of cellular H_2S production based on in situ-generated CdS-enhanced TiO_2 nanotube heterostructures. *Chemelectrochem* **2017**, *4*, 1011-1015.
(207) Parameswaran, R.; Carvalho-de-Souza, J. L.; Jiang, Y. W.; Burke, M. J.; Zimmerman, J. F.; Koehler, K.; Phillips, A. W.; Yi, J.; Adams, E. J.; Bezanilla, F. et al. Photoelectrochemical modulation of neuronal activity with free-standing coaxial silicon nanowires. *Nat. Nanotechnol.* **2018**, *13*, 260-266.
(208) Doyle, R. L.; Lyons, M. E. The oxygen evolution reaction: mechanistic concepts and catalyst design. In *Photoelectrochemical solar fuel production*. **2016**, 41-104.
(209) Dau, H.; Limberg, C.; Reier, T.; Risch, M.; Roggan, S.; Strasser, P. The mechanism of water oxidation: from electrolysis via homogeneous to biological catalysis. *ChemCatChem* **2010**, *2*, 724-761.
(210) Man, I. C.; Su, H.-Y.; Calle-Vallejo, F.; Hansen, H. A.; Martínez, J. I.; Inoglu, N. G.; Kitchin, J.; Jaramillo, T. F.; Nørskov, J. K.; Rossmeisl, J. Universality in oxygen evolution electrocatalysis on oxide surfaces. *ChemCatChem* **2011**, *3*, 1159-1165.
(211) Wang, H. Y.; Hung, S. F.; Chen, H. Y.; Chan, T. S.; Chen, H. M.; Liu, B. In operando identification of geometrical-site-dependent water oxidation activity of spinel Co_3O_4. *J. Am. Chem. Soc.* **2016**, *138*, 36-39.
(212) Wang, H. Y.; Hung, S. F.; Hsu, Y. Y.; Zhang, L.; Miao, J.; Chan, T. S.; Xiong, Q.; Liu, B. In situ spectroscopic identification of μ-OO bridging on spinel Co_3O_4 water oxidation electrocatalyst. *J. Phys. Chem. Lett.* **2016**, *7*, 4847-4853.
(213) Li, X.; Wang, H.-Y.; Yang, H.; Cai, W.; Liu, S.; Liu, B. In situ/operando characterization techniques to probe the electrochemical reactions for energy conversion. *Small Methods* **2018**, *2*, 1700395.
(214) Zandi, O.; Hamann, T. W. Determination of photoelectrochemical water oxidation intermediates on haematite electrode surfaces using operando infrared spectroscopy. *Nat. Chem.* **2016**, *8*, 778-783.
(215) Valdes, A.; Qu, Z.-W.; Kroes, G.-J.; Rossmeisl, J.; Nørskov, J. K. Oxidation and photo-oxidation of water on TiO_2 surface. *J. Phys. Chem. C* **2008**, *112*, 9872-9879.
(216) Tao, H. B.; Fang, L.; Chen, J.; Yang, H. B.; Gao, J.; Miao, J.; Chen, S.; Liu, B. Identification of surface reactivity descriptor for transition metal oxides in oxygen evolution reaction. *J. Am. Chem. Soc.* **2016**, *138*, 9978-9985.
(217) Fujishima, A.; Honda, K. Electrochemical photolysis of water at a semiconductor electrode. *Nature* **1972**, *238*, 37-38.
(218) Shankar, K.; Basham, J. I.; Allam, N. K.; Varghese, O. K.; Mor, G. K.; Feng, X.; Paulose, M.; Seabold, J. A.; Choi, K.-S.; Grimes, C. A. Recent advances in the use of TiO_2 nanotube and nanowire arrays for oxidative photoelectrochemistry. *J. Phys. Chem. C* **2009**, *113*, 6327-6359.
(219) Kelzenberg, M. D.; Boettcher, S. W.; Petykiewicz, J. A.; Turner-Evans, D. B.; Putnam, M.

C.; Warren, E. L.; Spurgeon, J. M.; Briggs, R. M.; Lewis, N. S.; Atwater, H. A. Enhanced absorption and carrier collection in Si wire arrays for photovoltaic applications. *Nat. Mater.* **2010**, *9*, 239-244.

(220) Palmisano, G.; Garcia-Lopez, E.; Marci, G.; Loddo, V.; Yurdakal, S.; Augugliaro, V.; Palmisano, L. Advances in selective conversions by heterogeneous photocatalysis. *Chem. Commun.* **2010**, *46*, 7074-7089.

(221) Hidaka, H.; Nagaoka, H.; Nohara, K.; Shimura, T.; Horikoshi, S.; Zhao, J.; Serpone, N. A mechanistic study of the photoelectrochemical oxidation of organic compounds on a TiO_2/TCO particulate film electrode assembly. *J. Photoch. Photobio., A* **1996**, *98*, 73-78.

(222) He, C.; Xiong, Y.; Chen, J.; Zha, C.; Zhu, X. Photoelectrochemical performance of Ag–TiO_2/ITO film and photoelectrocatalytic activity towards the oxidation of organic pollutants. *J. Photoch. Photobio., A* **2003**, *157*, 71-79.

(223) Mesa, C. A.; Kafizas, A.; Francas, L.; Pendlebury, S. R.; Pastor, E.; Ma, Y.; Le Formal, F.; Mayer, M. T.; Gratzel, M.; Durrant, J. R. Kinetics of photoelectrochemical oxidation of methanol on hematite photoanodes. *J. Am. Chem. Soc.* **2017**, *139*, 11537-11543.

(224) You, B.; Jiang, N.; Liu, X.; Sun, Y. Simultaneous H_2 generation and biomass upgrading in water by an efficient noble-metal-free bifunctional electrocatalyst. *Angew. Chem. Int. Ed.* **2016**, *55*, 9913-9917.

(225) Han, G.; Jin, Y. H.; Burgess, R. A.; Dickenson, N. E.; Cao, X. M.; Sun, Y. Visible-light-driven valorization of biomass intermediates integrated with H_2 production catalyzed by ultrathin Ni/CdS nanosheets. *J. Am. Chem. Soc.* **2017**, *139*, 15584-15587.

(226) Zhang, L.; Chen, R.; Luo, J.; Miao, J.; Gao, J.; Liu, B. Sustainable hydrogen and chemical production via photo-electrochemical reforming of biomass-derived alcohols. *Nano Res.* **2016**, *9*, 3388-3393.

(227) White, J. L.; Baruch, M. F.; Pander III, J. E.; Hu, Y.; Fortmeyer, I. C.; Park, J. E.; Zhang, T.; Liao, K.; Gu, J.; Yan, Y. Light-driven heterogeneous reduction of carbon dioxide: photocatalysts and photoelectrodes. *Chem. Rev.* **2015**, *115*, 12888-12935.

(228) Chen, X.; Li, N.; Kong, Z.; Ong, W.-J.; Zhao, X. Photocatalytic fixation of nitrogen to ammonia: state-of-the-art advancements and future prospects. *Mater. Horiz.* **2018**, *5*, 9-27.

(229) Zhang, N.; Long, R.; Gao, C.; Xiong, Y. Recent progress on advanced design for photoelectrochemical reduction of CO_2 to fuels. *Sci. China Mater.* **2018**, *61*, 771-805.

(230) Huang, Q.; Ye, Z.; Xiao, X. Recent progress in photocathodes for hydrogen evolution. *J. Mater. Chem. A* **2015**, *3*, 15824-15837.

(231) Boettcher, S. W.; Spurgeon, J. M.; Putnam, M. C.; Warren, E. L.; Turner-Evans, D. B.; Kelzenberg, M. D.; Maiolo, J. R.; Atwater, H. A.; Lewis, N. S. Energy-conversion properties of vapor-liquid-solid–grown silicon wire-array photocathodes. *Science* **2010**, *327*, 185-187.

(232) Goodey, A. P.; Eichfeld, S. M.; Lew, K.-K.; Redwing, J. M.; Mallouk, T. E. Silicon nanowire array photoelectrochemical cells. *J. Am. Chem. Soc.* **2007**, *129*, 12344-12345.

(233) Fan, S.; AlOtaibi, B.; Woo, S. Y.; Wang, Y.; Botton, G. A.; Mi, Z. High efficiency solar-to-hydrogen conversion on a monolithically integrated InGaN/GaN/Si adaptive tunnel

junction photocathode. *Nano Lett.* **2015**, *15*, 2721-2726.
(234) Appel, A. M.; Bercaw, J. E.; Bocarsly, A. B.; Dobbek, H.; DuBois, D. L.; Dupuis, M.; Ferry, J. G.; Fujita, E.; Hille, R.; Kenis, P. J. Frontiers, opportunities, and challenges in biochemical and chemical catalysis of CO_2 fixation. *Chem. Rev.* **2013**, *113*, 6621-6658.
(235) Kumar, B.; Llorente, M.; Froehlich, J.; Dang, T.; Sathrum, A.; Kubiak, C. P. Photochemical and photoelectrochemical reduction of CO_2. *Annu. Rev. Phys. Chem.* **2012**, *63*, 541-569.
(236) Kim, D.; Resasco, J.; Yu, Y.; Asiri, A. M.; Yang, P. Synergistic geometric and electronic effects for electrochemical reduction of carbon dioxide using gold–copper bimetallic nanoparticles. *Nat. Commun.* **2014**, *5*, 4948.
(237) Kuhl, K. P.; Hatsukade, T.; Cave, E. R.; Abram, D. N.; Kibsgaard, J.; Jaramillo, T. F. Electrocatalytic conversion of carbon dioxide to methane and methanol on transition metal surfaces. *J. Am. Chem. Soc.* **2014**, *136*, 14107-14113.
(238) Skulason, E.; Bligaard, T.; Gudmundsdottir, S.; Studt, F.; Rossmeisl, J.; Abild-Pedersen, F.; Vegge, T.; Jonsson, H.; Norskov, J. K. A theoretical evaluation of possible transition metal electro-catalysts for N_2 reduction. *Phys. Chem. Chem. Phys.* **2012**, *14*, 1235-1245.
(239) Montoya, J. H.; Tsai, C.; Vojvodic, A.; Norskov, J. K. The challenge of electrochemical ammonia synthesis: a new perspective on the role of nitrogen scaling relations. *ChemSusChem* **2015**, *8*, 2180-2186.
(240) Zhao, W.; Xi, H.; Zhang, M.; Li, Y.; Chen, J.; Zhang, J.; Zhu, X. Enhanced quantum yield of nitrogen fixation for hydrogen storage with in situ-formed carbonaceous radicals. *Chem. Commun.* **2015**, *51*, 4785-4788.
(241) Hwang, Y. J.; Boukai, A.; Yang, P. High density n-Si/n-TiO_2 core/shell nanowire arrays with enhanced photoactivity. *Nano Lett.* **2008**, *9*, 410-415.
(242) Hwang, Y. J.; Wu, C. H.; Hahn, C.; Jeong, H. E.; Yang, P. Si/InGaN core/shell hierarchical nanowire arrays and their photoelectrochemical properties. *Nano Lett.* **2012**, *12*, 1678-1682.
(243) Fountaine, K. T.; Whitney, W. S.; Atwater, H. A. Resonant absorption in semiconductor nanowires and nanowire arrays: relating leaky waveguide modes to Bloch photonic crystal modes. *J. Appl. Phys.* **2014**, *116*, 153106.
(244) Tachikawa, T.; Majima, T. Single-molecule, single-particle fluorescence imaging of TiO_2-based photocatalytic reactions. *Chem. Soc. Rev.* **2010**, *39*, 4802-4819.
(245) Hesari, M.; Mao, X.; Chen, P. Charge carrier activity on single-particle photo(electro)catalysts: toward function in solar energy conversion. *J. Am. Chem. Soc.* **2018**, *140*, 6729-6740.
(246) Yan, R.; Park, J. H.; Choi, Y.; Heo, C. J.; Yang, S. M.; Lee, L. P.; Yang, P. Nanowire-based single-cell endoscopy. *Nat. Nanotechnol.* **2011**, *7*, 191-196.
(247) Tian, B.; Kempa, T. J.; Lieber, C. M. Single nanowire photovoltaics. *Chem. Soc. Rev.* **2009**, *38*, 16-24.
(248) Tang, J.; Huo, Z.; Brittman, S.; Gao, H.; Yang, P. Solution-processed core-shell nanowires for efficient photovoltaic cells. *Nat. Nanotechnol.* **2011**, *6*, 568-572.
(249) Hochbaum, A. I.; Chen, R.; Delgado, R. D.; Liang, W.; Garnett, E. C.; Najarian, M.; Majumdar, A.; Yang, P. Enhanced thermoelectric performance of rough silicon nanowires.

Nature **2008**, *451*, 163-167.
(250) Cox, J. T.; Zhang, B. Nanoelectrodes: recent advances and new directions. *Annu. Rev. Anal. Chem.* **2012**, *5*, 253-272.
(251) Su, Y.; Liu, C.; Brittman, S.; Tang, J.; Fu, A.; Kornienko, N.; Kong, Q.; Yang, P. Single-nanowire photoelectrochemistry. *Nat. Nanotechnol.* **2016**, *11*, 609-612.
(252) Liu, C.; Hwang, Y. J.; Jeong, H. E.; Yang, P. Light-induced charge transport within a single asymmetric nanowire. *Nano Lett.* **2011**, *11*, 3755-3758.
(253) Tachikawa, T.; Majima, T. Exploring the spatial distribution and transport behavior of charge carriers in a single titania nanowire. *J. Am. Chem. Soc.* **2009**, *131*, 8485-8495.
(254) Simpson, B. H.; Rodriguez-Lopez, J. Electrochemical imaging and redox interrogation of surface defects on operating $SrTiO_3$ photoelectrodes. *J. Am. Chem. Soc.* **2015**, *137*, 14865-14868.
(255) Esposito, D. V.; Levin, I.; Moffat, T. P.; Talin, A. A. H_2 evolution at Si-based metal-insulator-semiconductor photoelectrodes enhanced by inversion channel charge collection and H spillover. *Nat. Mater.* **2013**, *12*, 562-568.
(256) Appavoo, K.; Liu, M.; Black, C. T.; Sfeir, M. Y. Quantifying bulk and surface recombination processes in nanostructured water splitting photocatalysts via in situ ultrafast spectroscopy. *Nano Lett.* **2015**, *15*, 1076-1082.
(257) Tachikawa, T.; Tojo, S.; Fujitsuka, M.; Sekino, T.; Majima, T. Photoinduced charge separation in titania nanotubes. *J. Phys. Chem. C* **2006**, *110*, 14055-14059.
(258) Naito, K.; Tachikawa, T.; Fujitsuka, M.; Majima, T. Single-molecule observation of photocatalytic reaction in TiO_2 nanotube: importance of molecular transport through porous structures. *J. Am. Chem. Soc.* **2009**, *131*, 934-936.
(259) Xu, W.; Jain, P. K.; Beberwyck, B. J.; Alivisatos, A. P. Probing redox photocatalysis of trapped electrons and holes on single Sb-doped titania nanorod surfaces. *J. Am. Chem. Soc.* **2012**, *134*, 3946-3949.
(260) Sambur, J. B.; Chen, P. Distinguishing direct and indirect photoelectrocatalytic oxidation mechanisms using quantitative single-molecule reaction imaging and photocurrent measurements. *J. Phys. Chem. C* **2016**, *120*, 20668-20676.
(261) Sambur, J. B.; Chen, T. Y.; Choudhary, E.; Chen, G.; Nissen, E. J.; Thomas, E. M.; Zou, N.; Chen, P. Sub-particle reaction and photocurrent mapping to optimize catalyst-modified photoanodes. *Nature* **2016**, *530*, 77-80.
(262) Bard, A. J. F., L. R. Electrochemical methods: fundamentals and applications. 2nd ed. *John Wiely & Sons, Inc. New York* **2001**.
(263) Bolton, J. R.; Strickler, S. J.; Connolly, J. S. Limiting and realizable efficiencies of solar photolysis of water. *Nature* **1985**, *316*, 495-500.
(264) Nocera, D. G. The artificial leaf. *Acc. Chem. Res.* **2012**, *45*, 767-776.
(265) Hall, D. O.; Rao, K. Photosynthesis, 6th ed. *Cambridge University Press* **1999**.
(266) Nozik, A. J. P-n Photoelectrolysis cells. *Appl. Phys. Lett.* **1976**, *29*, 150-153.
(267) Kudo, A. Z-scheme photocatalyst systems for water splitting under visible light irradiation.

Mrs. Bull. **2011**, *36*, 32-38.
(268) Maeda, K. Z-scheme water splitting using two different semiconductor photocatalysts. *ACS Catal.* **2013**, *3*, 1486-1503.
(269) Weber, M. F.; Dignam, M. J. Efficiency of splitting water with semiconducting photoelectrodes. *J. Am. Chem. Soc.* **1984**, *131*, 1258-1265.
(270) Kainthla, R.; Khan, S.; JO'M, B. The theory of electrode matching in photoelectrochemical cells for the production of hydrogen. *Int. J. Hydrogen Energy* **1987**, *12*, 381-392.
(271) Nozik, A. J. Photochemical diodes. *Appl. Phys. Lett.* **1977**, *30*, 567-569.
(272) Hu, S.; Xiang, C.; Haussener, S.; Berger, A. D.; Lewis, N. S. An analysis of the optimal band gaps of light absorbers in integrated tandem photoelectrochemical water-splitting systems. *Energy Environ. Sci.* **2013**, *6*, 2984.
(273) Pinaud, B. A.; Benck, J. D.; Seitz, L. C.; Forman, A. J.; Chen, Z.; Deutsch, T. G.; James, B. D.; Baum, K. N.; Baum, G. N.; Ardo, S. et al. Technical and economic feasibility of centralized facilities for solar hydrogen production via photocatalysis and photoelectrochemistry. *Energy Environ. Sci.* **2013**, *6*, 1983-2002.
(274) Madelung, O. Semiconductors: data handbook, 3rd ed. **2003**.
(275) Dai, B.; Wang, J.; Xiong, Z.; Zhan, X.; Dai, W.; Li, C. C.; Feng, S. P.; Tang, J. Programmable artificial phototactic microswimmer. *Nat. Nanotechnol.* **2016**, *11*, 1087-1092.
(276) Zheng, J.; Dai, B. H.; Wang, J. Z.; Xiong, Z.; Yang, Y.; Liu, J.; Zhan, X. J.; Wan, Z. H.; Tang, J. Y. Orthogonal navigation of multiple visible-light-driven artificial microswimmers. *Nat. Commun.* **2017**, *8*, 1438.
(277) Kornienko, N.; Gibson, N. A.; Zhang, H.; Eaton, S. W.; Yu, Y.; Aloni, S.; Leone, S. R.; Yang, P. D. Growth and photoelectrochemical energy conversion of wurtzite indium phosphide nanowire arrays. *ACS Nano* **2016**, *10*, 5525-5535.
(278) Mohle, S.; Zirbes, M.; Rodrigo, E.; Gieshoff, T.; Wiebe, A.; Waldvogel, S. R. Modern electrochemical aspects for the synthesis of value-added organic products. *Angew. Chem. Int. Ed.* **2018**, *57*, 6018-6041.
(279) Horn, E. J.; Rosen, B. R.; Baran, P. S. Synthetic organic electrochemistry: an enabling and innately sustainable method. *ACS Cent. Sci.* **2016**, *2*, 302-308.
(280) Kato, M.; Zhang, J. Z.; Paul, N.; Reisner, E. Protein film photoelectrochemistry of the water oxidation enzyme photosystem II. *Chem. Soc. Rev.* **2014**, *43*, 6485-6497.
(281) Milton, R. D.; Minteer, S. D. Direct enzymatic bioelectrocatalysis: differentiating between myth and reality. *J. R. Soc. Interface* **2017**, *14*, 20170253.

Table of contents in graphics